

# Electrochemical deposition of metal matrix composites

**Citation for published version (APA):**

Hovestad, A. (1997). *Electrochemical deposition of metal matrix composites*. [Phd Thesis 1 (Research TU/e / Graduation TU/e), Chemical Engineering and Chemistry]. Technische Universiteit Eindhoven.  
<https://doi.org/10.6100/IR504662>

**DOI:**

[10.6100/IR504662](https://doi.org/10.6100/IR504662)

**Document status and date:**

Published: 01/01/1997

**Document Version:**

Publisher's PDF, also known as Version of Record (includes final page, issue and volume numbers)

**Please check the document version of this publication:**

- A submitted manuscript is the version of the article upon submission and before peer-review. There can be important differences between the submitted version and the official published version of record. People interested in the research are advised to contact the author for the final version of the publication, or visit the DOI to the publisher's website.
- The final author version and the galley proof are versions of the publication after peer review.
- The final published version features the final layout of the paper including the volume, issue and page numbers.

[Link to publication](#)

**General rights**

Copyright and moral rights for the publications made accessible in the public portal are retained by the authors and/or other copyright owners and it is a condition of accessing publications that users recognise and abide by the legal requirements associated with these rights.

- Users may download and print one copy of any publication from the public portal for the purpose of private study or research.
- You may not further distribute the material or use it for any profit-making activity or commercial gain
- You may freely distribute the URL identifying the publication in the public portal.

If the publication is distributed under the terms of Article 25fa of the Dutch Copyright Act, indicated by the "Taverne" license above, please follow below link for the End User Agreement:

[www.tue.nl/taverne](http://www.tue.nl/taverne)

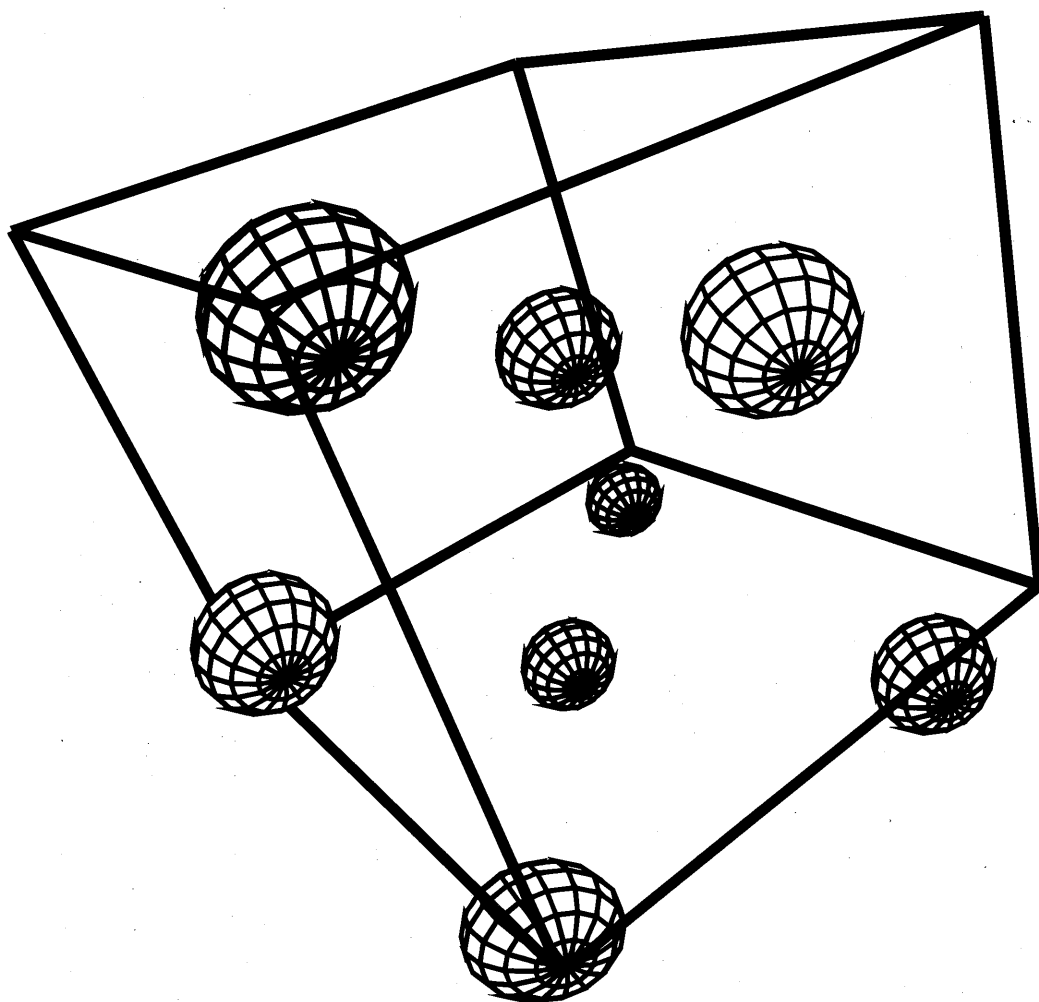
**Take down policy**

If you believe that this document breaches copyright please contact us at:

[openaccess@tue.nl](mailto:openaccess@tue.nl)

providing details and we will investigate your claim.

# Electrochemical Deposition of Metal Matrix Composites



Arjan Hovestad

# **Electrochemical deposition of metal matrix composites**

## **PROEFSCHRIFT**

ter verkrijging van de graad van doctor aan de  
Technische Universiteit Eindhoven, op gezag van de  
Rector Magnificus, prof.dr. M. Rem, voor een  
commissie aangewezen door het College voor  
Promoties in het openbaar te verdedigen  
op woensdag 10 december 1997 om 16.00 uur

door

Arjan Hovestad

geboren te Zevenaar

Dit proefschrift is goedgekeurd door de promotoren:

prof.dr.ir. F.M. Everaerts

en

prof.dr. F.J.J. van Loo

en de copromotor

dr. L.J.J. Janssen

Het in dit proefschrift beschreven onderzoek werd gefinancierd door Hoogovens Groep B.V, IJmuiden

*In effetti, il gioco con la palla costituisce una espressione di sviluppate qualità psichiche. Poiché la palla è una sfera, essa offre alla nostra carezza una superficie senza resistenze, senza ostacoli e senza sorprese. Il poterla maneggiare e controllare ci autorizza a ritenerci capaci di dominare la vita, di regolare ogni salita ed ogni caduta, di realizzare le nostre aspirazioni di sicurezza e persino di felicità. Ma accade pure che un rimbalzo irregolare o un colpo di vento facciano conservare al gioco della palla quel tanto di aleatorio che movimentata ogni esistenza.*

Eigenlijk vormt het spel met de bal een uiting van ontwikkelde mentale eigenschappen. Omdat de bal rond is, biedt hij onze streling een oppervlak zonder weerstand, zonder obstakels en zonder verrassingen. Hem kunnen hanteren en controleren staat ons toe om onszelf in staat te achten het leven te domineren, iedere stijging en iedere val te reguleren, ons streven naar veiligheid en zelfs geluk te realiseren. Maar het gebeurt toch dat een onregelmatige terugkaatsing of een windvlaag aan het spel met de bal dat beetje willekeur behoudt, dat ieder bestaan beïnvloedt.

*(Antonino Fugardi, 'Il calcio dalle origini ad oggi')*

*Voor mijn ouders*

Hoofdstuk 7 over de depositie van metaal-polymeercomposieten is niet opgenomen in dit proefschrift vanwege het vertrouwelijke karakter. De kerncommissie heeft dit hoofdstuk ter inzage gehad.

# Contents

## 1. General introduction

1.1	Introduction	1
1.2	Silicon-rich iron foil	2
1.3	Scope of this thesis	3
	References	4

## 2. Electrochemical codeposition of inert particles in a metallic matrix

2.1	Introduction	5
2.2	Applications	5
2.3	Experimental parameters	6
	2.3.1 Particle concentration, type, shape and size	6
	2.3.2 Bath constituents, additives and ageing	7
	2.3.3 Temperature, pH and current density	8
	2.3.4 Agitation and surfactants	9
	2.3.5 Surface charge	12
2.4	Mechanism and models	13
	2.4.1 Guglielmi's model	14
	2.4.2 Model of Buelens and Celis et. al.	16
	2.4.3 Recent models	18
2.5	Concluding remarks	23
	References	24

---

### **3. Electrochemical deposition and heat treatment of Fe-Fe<sub>x</sub>Si composites**

3.1	Introduction	27
3.2	Experimental details	28
3.3	Results	31
3.4	Discussion	36
3.5	Conclusions	40
	References	41

### **4. Iron deposition from a FeCl<sub>2</sub> solution containing suspended silicon particles**

4.1	Introduction	43
4.2	Experimental details	43
4.3	Results and discussion	46
	4.3.1 Conductivity and viscosity	46
	4.3.2 Particle type	47
	4.3.3 Mass transfer	48
	4.3.4 Current efficiency for Fe deposition	50
	4.3.5 Polarization behaviour	50
	4.3.6 Codeposition	54
	References	55

---



**5. Stability of suspensions of polystyrene particles in a zinc deposition electrolyte**

5.1	Introduction	57
5.2	Experimental details	58
5.3	Results	59
	5.3.1 Suspension rheology	59
	5.3.2 Conductivity	62
	5.3.3 Microscopical observation	64
5.4	Discussion	64
5.5	Conclusions	67
	References	68

**6. Effect of surfactants on the electrochemical codeposition of zinc and polystyrene particles**

6.1	Introduction	71
6.2	Experimental details	71
6.3	Results	74
	6.3.1 Surfactant adsorption	74
	6.3.2 Surfactant type and concentration	76
	6.3.3 Particle concentration	77
	6.3.4 Current density	78
	6.3.5 Electrode rotation speed	79
	6.3.6 Surface appearance and morphology	80
6.4	Discussion	84
6.5	Conclusions	90
	References	90

---

<b>List of symbols</b>	93
<b>Summary</b>	97
<b>Samenvatting</b>	99
<b>Curriculum Vitae</b>	101

---

# **1. General introduction**

## **1.1 Introduction**

It is well-known that insoluble substances present in an electroplating bath codeposit with the depositing metal [1]. The properties of the metal can be strongly affected by the incorporated substances. In conventional electroplating this is considered a nuisance and continuous filtering and anode bagging are employed to avoid it. In electrochemical composite plating inert particles are deliberately added to the plating bath to obtain metal matrix composites having improved properties compared to the plain metal [2,3]. Although Fink and Prince in 1928 [4] already investigated the possibility of using electrochemical composite plating to produce self-lubricating Cu-graphite coatings for use in car engines, until about thirty years ago little research was done in this field. In the early sixties the first investigations started and soon after this new industrial applications of electrodeposited composites were found.

There are other methods to produce metal matrix composites. The most widely used are powder metallurgy, metal spraying and internal oxidation or nitridation [5-7]. A major disadvantage of these methods is that they need to be performed at high temperatures. Since, electroplating is a very suitable method to produce thin metal coatings, electrochemical composite plating is a good alternative in the field of composite coatings.

Despite the extensive research done on electrochemical composite plating the process is only partly understood. Because there was an interest in the use of electrochemical composite plating on industrial scale, a study to gain more insight into this technique was initiated. As subject of this study the production of silicon-rich iron foil was chosen, because of its possible practical use. This constitutes the first part of the investigations presented in this thesis. In the course of the study the interests shifted towards the electrochemical deposition of zinc-polystyrene composites as a model system for certain applicable metal-polymer composites. Investigations related to this model system make up the remainder of the thesis. A chapter concerning the industrially applicable composites is not contained in the thesis for reasons of confidentiality.

## 1.2 Silicon-rich iron foil

Iron core transformers suffer appreciable magnetic energy losses due to eddy currents. Using iron foil alloyed with a few percent of Si as transformer sheet minimizes these losses. In Figure 1.1 the effect of Si on some properties of Fe-Si alloys, normalized with respect to Fe, are given. The advantage of using Fe-Si alloys results from the decrease in magnetocrystalline anisotropy, which causes an increase in permeability, and electrical conductivity with increasing Si content as shown in Figure 1.1. The beneficial effect of the reduction in conductivity follows from the fact that the energy losses due to eddy currents in a metal foil are proportional to:

$$\frac{d^2 f^2 \mathbf{B}^2 \kappa}{\rho} \quad (1.1)$$

where  $\kappa$  is the conductivity of the metal,  $\rho$  is its density,  $d$  is the thickness of the foil,  $f$  is the frequency and  $\mathbf{B}$  is the maximal induction [9].

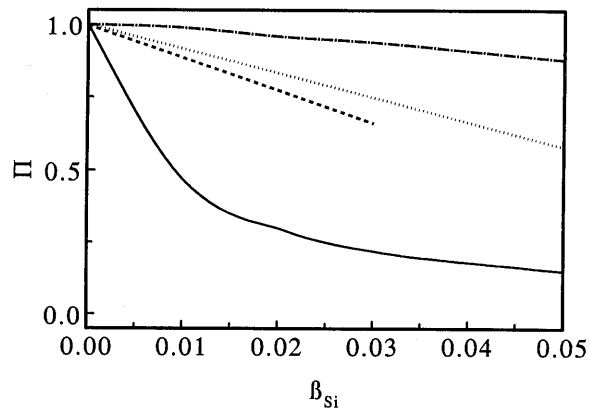


Figure 1.1: Conductivity (—), magnetocrystalline anisotropy (·····), saturation induction (---) and elongation percentage (-·-·-) of Fe-Si alloys normalized with respect to pure Fe against mass fraction Si [8].

A disadvantage of Si addition is the reduction in saturation induction with increasing Si content (Figure 1.1). Optimal properties are found for Fe alloyed with 5-7 wt% of Si. The presence of other elements, particularly carbon, should be avoided. Although Fe-Si alloys can be easily prepared, they are too brittle to be rolled to thin sheets. This is evidenced by the decrease in elongation percentage with the amount of alloyed Si (Figure 1.1). It follows from equation 1.1 that the thickness of the transformer sheet should be small, typically  $< 0.1$  mm. Since, electrodeposition allows the production of very thin sheets of high purity, electrochemical deposition of Fe-Si composites followed by a homogenizing heat treatment could be used to produce transformer sheet.

### 1.3 Scope of this thesis

It is the aim of this thesis to determine the feasibility of using electrochemical composite plating to produce the silicon-rich iron foil and the metal-polymer composite. The main requirements for successful application of these systems were investigated. For silicon-rich iron foil this concerns the deposition of composites containing approximately 6 wt% Si and the annealing of these composites to a homogeneous alloy. The metal-polymer composites should be deposited from a unaggregated electrolyte suspension at current densities of  $5 - 10 \text{ kA m}^{-2}$  and under turbulent flow conditions.

On the basis of these two systems a better understanding of the mechanism underlying composite plating was achieved. In the literature a possible effect of the metal deposition behaviour on particle codeposition is often neglected, although correlations between the metal deposition behaviour and particle codeposition have been reported. The relation between the physical and electrochemical behaviour of the composite deposition suspension and the codeposition of the particles was investigated.

Chapter 2 gives an overview of the open literature on electrochemical composite plating. Both the effect of various experimental parameters on composite composition and theoretical modeling of particle codeposition with a metal are discussed. In Chapter 3 the possibility of homogenizing Fe-Fe<sub>x</sub>Si composites is described. Chapter 4 shows the changes in the physical and

electrochemical properties of the iron deposition electrolyte on the addition of Si particles. The stability of polystyrene particles in the zinc deposition electrolyte is discussed Chapter 5. The codeposition of polystyrene particles with zinc is treated in Chapter 6. The effect of surfactant addition and of several experimental parameters is considered.

## References

- [1] E.H. Lyons Jr., in 'Modern Electroplating', 3rd edition, (edited by F.A. Lowenheim), J. Wiley & Sons, New York (1974) p. 38 - 40.
- [2] J.R. Roos, J.P. Celis, J. Fransaer and C. Buelens, *J. Metals* **42** (1990) 60.
- [3] J.P. Celis, J.R. Roos, C. Buelens and J. Fransaer, *Trans. Inst. Met. Finish.* **69** (1991) 133.
- [4] C.G. Fink and J.D. Prince, *Trans. Am. Electrochem. Soc.* **54** (1928) 315.
- [5] J. Fransaer, J.P. Celis and J.R. Roos, *Met. Finish.* **91** (1993) 97.
- [6] J.R. Roos and J.P. Celis, *Proceedings AESF'84*, New York (1984) 1.
- [7] J.R. Roos, *Proceedings INCEF'86*, Bangalore (1988) 382.
- [8] B.D. Cullity, 'Introduction to Magnetic Materials', Addison-Wesley Publishing Company Inc., Amsterdam (1972) 516.
- [9] S. Cedighian, 'Die Magnetischen Werkstoffe: Grundlagen, Eigenschaften und Anwendungen', VDI-Verlag GmbH, Düsseldorf (1973) 201.

## 2. Electrochemical codeposition of inert particles in a metallic matrix

(A. Hovestad and L.J.J. Janssen, *J. Appl. Electrochem.* **25** (1995) 519)

### 2.1 Introduction

Several excellent review papers concerning electrolytic composite plating have been published in recent years by Celis et. al. [1,2,3,4]. These papers mainly treat the uses and the mechanism and models of the codeposition process. The present chapter will include the most recent developments in these fields, but will also give an overview of the experimental facts reported in literature.

### 2.2 Applications

The main uses of electrodeposited composites are in wear resistance, corrosion resistance and lubrication [1,3]. Metals are dispersion hardened by the incorporation of oxide particles like  $\text{Al}_2\text{O}_3$  and  $\text{TiO}_2$  or fibres and whiskers [1,3,5]. These composites have a considerably higher yield strength and hardness than the pure metal [5,6]. By coating metals with a metal matrix composite containing particles of hard materials, like diamond, WC and SiC [7-9], they can be protected from abrasion. These hard materials are too brittle and have too weak adhesion to metal surfaces to be used as coatings themselves. Therefore, a metal matrix is used to hold the particles together and facilitate a good adhesion to the metal surface being coated. These types of coatings, especially the use Ni-SiC coatings in motor blocks of aluminium alloys, are the main cause of the growing interest in electrochemical codeposition [1,3,5,10].

The incorporation of submicron powders, like  $\text{Al}_2\text{O}_3$ ,  $\text{BaSO}_4$ ,  $\text{Si}_3\text{N}_4$ ,  $\text{V}_2\text{O}_5$  and  $\text{Cr}_2\text{O}_3$ , in a metal decreases the corrosion rate of the metal considerably [1,6,11,12]. A composite coating can also reduce the corrosion by enhancing the adhesion of a lacquer on a metal. The metal

matrix adheres strongly to the metal base and the occluded particles adhere strongly to the (organic) lacquer [1,3]. A different use of codeposition for corrosion protection is the production of an alloy coating through a homogenizing heat treatment of a Ni [13] or Fe-Ni [14] deposit containing Cr-particles.

Furthermore, electrodeposited composite coatings are used to increase the lifetime of metal surfaces that are in moving contact [1,3]. Particles of low friction materials like graphite, MoS<sub>2</sub> and PTFE in these coatings reduce the friction between the metal surfaces [15,16]. Again the metal matrix enables a better adhesion to the underlying metal surface. Apart from this dry lubrication a relatively new development in electrochemical codeposition also allows wet lubrication of metal surfaces. In this technique microcapsules containing a liquid lubricant are codeposited in a metal [1,3]. During use of such a coating the metal matrix and the occluded microcapsules slowly erode away, thereby releasing the liquid lubricant. Particularly in this method appears the advantage of electrochemical codeposition.

Finally, Keddani et al. [17] and Anani et al. [18] reported the use of codeposition in electrocatalysis. Electrodes are made by codeposition of particles of an electro-active material with a metal matrix. The behaviour of these electrodes was seen to be controlled by the embedded material.

## **2.3 Experimental parameters**

### **2.3.1 Particle concentration, type, shape and size**

Sautter [19] found that the volume percentage of Al<sub>2</sub>O<sub>3</sub> particles in a Ni-matrix increases, in decreasing rate, with increasing particle concentration in the bath. This behaviour was confirmed by all further investigators for a wide range of metal particle systems [5,7,9,12,16,20-30]. On the other hand, the absolute values of the particle content vary for different systems. For example, Greco and Baldauf [5] noticed that three times as much TiO<sub>2</sub> is built in a Ni matrix as Al<sub>2</sub>O<sub>3</sub> for the same plating conditions. Moreover, Celis [22] showed that  $\gamma$ -Al<sub>2</sub>O<sub>3</sub> codeposits with Cu in much smaller amounts than  $\alpha$ -Al<sub>2</sub>O<sub>3</sub>.



No investigations on the influence of the particle shape on codeposition are reported. However, the particle shape affects the adsorption of the particles on the cathode, the adsorption of ions on the particle surface and the suspension stability, which are factors that influence codeposition [31].

Regarding the effect of particle size on codeposition different results have been reported. For Ni-Al<sub>2</sub>O<sub>3</sub> [32] and Ni-Cr [21] an increase in the percentage of incorporated particles was reported, if the particle size was increased. It was shown quantitatively that the amount of P codeposited with Cu increases linearly with the median volume size of the particles [28]. In contrast to these results negligible influence of particle size for Ni-Al<sub>2</sub>O<sub>3</sub> [29] was observed and for Ag-Al<sub>2</sub>O<sub>3</sub> a lower deposition ratio for larger particles was reported [26]. Recently Berkh et. al. [33] and Bozzini et. al. [34] reported the occurrence of preferential codeposition. Due to particle crowding at the electrode surface only particles smaller than a certain size are able to codeposit. Consequently, a fraction of the particles, which depends on the deposition conditions, does not contribute to particle incorporation.

### **2.3.2 Bath constituents, additives and ageing**

The influence of the bath constituents on the codeposition of particles is evident. For different types of baths different incorporation rates are reported, when the same kind of particles are used. For example, Brandes and Goldthorpe [32] observed that Al<sub>2</sub>O<sub>3</sub> particles codeposit in Cu- and Ni-baths, but not in a chromate-bath. Furthermore, they were not able to produce good Cu-Al<sub>2</sub>O<sub>3</sub> deposits in a copper sulphate bath, while they obtain good deposits in a copper cyanide bath. In contrast to the extensive qualitative evidence for the effect of the bath constituents, there is little quantitative information regarding this effect. Williams and Martin [16] found that by increasing the CuCN concentration in a copper cyanide bath the density of codeposited silica fibres increases with decreasing rate. Experiments for Cr-graphite give similar results [24].

To standard plating baths often brighteners or wetting agents are added, which will affect codeposition from such baths. Tomaszewski et. al. [11] stated that different brighteners have a different effect, but generally they increase particle codeposition. Greco and Baldauf [5] confirmed this effect and named the use of wetting agents as one of the possibilities to increase the

---

number of occluded particles. On the other hand, some researchers [22,32] observed a decrease in particle content on addition of wetting agents.

According to Tomaszewski et. al. [35] the addition of small amounts of monovalent cations, like  $Tl^+$ ,  $Ce^+$ ,  $Rb^+$  and  $NH_4^+$ , or amines, like TEPA (tetra-ethylene pentamine), alanine and EDTA (ethylene diamine tetra-acetic acid) promote the codeposition of particles. The weight percentage of embedded  $BaSO_4$  particles in Cu increases from 0.5 to 4.5 by the addition of 25g/l EDTA. These promoting effects are confirmed by other authors [22,36,37].

Ageing of the codeposition bath seems to influence only certain metal particle systems. A decrease of  $Al_2O_3$ -content in Cu on ageing, which might be caused by impurities in the bath, was observed [38]. Narayan and Chattopadhyay [25] reported no ageing effect up to 18 days for Cr- $Al_2O_3$ . According to Buelens [39] codeposition of  $Al_2O_3$  particles with Ni, Au and Cu does not show ageing effects, while they observe a pronounced ageing effect for Cu-SiC codeposition.

### **2.3.3 Temperature, pH and current density**

The effect of the temperature seems to vary per codeposition system. For Ni- $Al_2O_3$  no effect of the temperature on the percentage of embedded particles was found [19,29]. On the other hand, the graphite content of a Cr-matrix was seen to increase with temperature up to 50°C [24], while for Cr- $Al_2O_3$  [25] exactly the reverse was reported, that is a decrease of particle content up to 50°C. In both cases no effect above this temperature, was found. For Ni- $V_2O_5$  a maximum particle content at 50°C was reported [12]. A continuous decrease of the weight percent embedded particles in Cu was observed by Tomaszewski et. al. [35].

Investigations concerning the effect of the pH give consistent results. Sautter [19] found no influence of the pH above pH 2 and a sharp decrease of occluded particles below this value for Ni- $Al_2O_3$ . This result was confirmed for different systems [9,11,22,29,32,35]. Recently, Yeh and Wan [40] noticed that the current efficiency of Ni reduction decreases markedly below pH 2 if SiC particles are present. Moreover, this pH corresponds to the point of zero charge of SiC particles in a NaCl solution. It is not clear if these effect are accompanied by a decrease of particle content below pH 2, because the SiC content of the deposits was not measured.

---

Together with the particle concentration the current density is probably the most extensively investigated parameter. Roughly two different current density dependencies can be distinguished. Firstly, some authors found little or no influence of the current density on the number of occluded particles [9,24,28]. Secondly, the current density versus particle content curve shows or suggests the presence of one or several maxima [7,16,18,22,23,25,27,29,41-43]. For Ni-TiO<sub>2</sub> a shift of the maximum to a higher current density for a higher agitation rate was observed. Similarly, for Cr-Al<sub>2</sub>O<sub>3</sub> a minimum was formed in the particle content versus current density curve when the particle concentration in the bath was increased [25].

Apart from the fact that the current density influences the codeposition, the current density itself is affected by the presence of particles. Several authors determined cathodic polarization curves for the codeposition plating bath with and without particles. Most of them [19,22,41,44,45] found a higher current density for the same cathode potential when particles were present, indicating a depolarization of the cathode. Suzuki et.al. [46] did an extensive research on the polarization behaviour of the cathode for Ag-Al<sub>2</sub>O<sub>3</sub>. According to them at low overvoltage the particles near the cathode suppress the reduction of the metal ion. At high overvoltage the transport of the metal ions to the cathode becomes an important factor and it is known that the addition of inert particles enhances this transport [47,48], which leads to a depolarization of the cathode.

Buelens [39,41] noticed that at the current density, where a maximum in the particle occlusion is found, a kink in the polarization curve for Cu-Al<sub>2</sub>O<sub>3</sub> and Au-Al<sub>2</sub>O<sub>3</sub> is present. Recently, Webb and Robertson [49] reported that apart from a large polarization of the cathode, the maximum is accompanied by a sharp decrease in the current efficiency. These results indicate a relation between particle incorporation and the metal deposition mechanism, which determines the polarization behaviour.

#### **2.3.4 Agitation and surfactants**

It is obvious that particles need to arrive at the cathode surface to be built in and therefore, have to be transported from the bulk to the cathode [31]. Greco and Baldauf [5] realised that agitation of the bath enhances the particle transport and stated that increasing the bath agitation results in

---

a larger amount of embedded particles. However, 4 years earlier Williams and Martin [16] reported that too much agitation leads to a decrease of particle codeposition, because the particles are swept away from the cathode surface before they are built in. Both these observations were confirmed by Lee and Wan [36], who found that the curve of particle content versus electrolyte flow rate shows a maximum.

For the effect of bath agitation by a RDE on particle incorporation, three different flow regimes can be distinguished: laminar, transition and turbulent flow [41]. In the laminar flow regime there is no influence of the rotating speed of the RDE. For the transition area a decrease followed by a large increase of the particle content is observed. In the turbulent flow regime a continuous decrease takes place. Furthermore, the particle content was found to decrease going from the centre to the edges of a RDE [36,50]. Correspondingly, Graydon and Kirk [51] were able to relate different zones of hydrodynamic flow to different zones of particle occlusion on the cathode for a channel electrode.

Apart from particle transportation agitation also serves to keep particles in suspension. Therefore, all researchers used some kind of bath agitation and sometimes [5,19] even blended the electrolyte and particles before the experiments to obtain a stable suspension. Both the bath agitation and the blending break up agglomerates of particles, which is necessary to obtain homogenous deposits containing a fine dispersion of particles.

The effects of some of the parameters on codeposition discussed earlier could be connected among others to the way they affect the suspension stability [31]. The suspension stability increases with decreasing settling speed of the particles, which for spherical particles is given by Stokes law:

$$v = \frac{2gr_p^2(\rho_p - \rho_c)}{9\mu} \quad (2.1)$$

The suspension stability directly depends on the particle size  $r_p$  and the particle density  $\rho_p$ , that is the particle type. Furthermore, the density  $\rho_c$  and viscosity  $\mu$  of the electrolyte are both determined by the bath constituents and temperature. The relative importance of the effect of these parameters on codeposition is difficult to assess.

Because their graphite particles agglomerated and precipitated Fink and Prince [15] needed another method, apart from bath agitation, to keep the particles suspended. They added the particles to the plating bath already in a suspension stabilized by surfactants, that is tannin and gelatine. Surfactants improve the stability of a suspension by increasing the wettability of the suspended particles by adsorbing on their surfaces. The wettability of (inorganic) particles is not a major problem in codeposition, but additional advantages are obtained if cationic surfactants are used [31]. These cationic surfactants confer a net positive charge on the particles, which prevents them from agglomerating and attracts them electrostatically to the cathode.

Helle [52,53] found that a combination of cationic and non-ionic surfactants produces a stable suspension of PTFE particles in a Ni-bath, which allows the plating of composites containing up to 70 volume percent PTFE. In this system the use of surfactants is particularly successful, because in comparison to inorganic particles the wettability of PTFE particles is more of a problem [31]. Furthermore, the affinity of the fluorocarbon surfactant to a fluoropolymer, like PTFE, is quite large. However, Helle also showed that these fluorocarbon surfactants produce a dramatic increase (up to 50%) in particle content for inorganic particles, like SiC and diamond. This increase in particle content is confirmed by Meguno et. al. [54], who found twice as much SiC particles embedded in a Ni-matrix if a non-ionic surfactant was used. By using a surfactant Chang and Lee [7] produced Ni deposits containing about 5 times as much Al<sub>2</sub>O<sub>3</sub> particles, while using particle concentration about ten times as low as in experiments without surfactants [5,19,29].

The disadvantage of using surfactants is that they are incorporated in the deposit [53]. Surfactant molecules adsorbed on a particle are embedded in the deposit together with the particle. Because of the relatively small amount of adsorbed surfactant, this hardly affects the deposit. However, free surfactant, that is surfactant molecules which are not adsorbed on a particle, codeposits with the metal, which leads to stressed and brittle deposits.

Brighteners and wetting agents also act as surfactants, which explains their effect on codeposition [5,11,22,32]. If they act as cationic surfactant, they will promote codeposition. Correspondingly, some wetting agents or brighteners will reduce codeposition by acting as an anionic surfactants, conferring a negative charge onto the particles [54].

Similar to the electrostatic interactions, magnetic interactions can be used to promote particle incorporation. Tacke et. al. [55] described a method, where Ni-particles are magnetically charged before being suspended in a Zn deposition electrolyte. The remanent magnetization of the Ni-particles attracts them to the steel cathode, where they codeposit with Zn. About three times as much magnetically charged particles are incorporated compared to uncharged particles.

### **2.3.5 Surface charge**

Many parameters discussed above influence the surface charge of the particles. Fink and Prince in 1928 [15] already realized the importance of the surface charge and stated that obviously a positive surface charge enhances codeposition, because the particles are electrostatically attracted by the cathode. This was confirmed by Tomaszewski et. al. [35], who found that the negatively charged silica particles move much more difficult to the cathode than the positively charged  $\text{Al}_2\text{O}_3$  particles. Furthermore, Narayan and Chattopadhyay [25] were able to solve the problem of codepositing  $\text{Al}_2\text{O}_3$  particles with Cr [32] by dry grinding them before an experiment, which changes their surface properties and enables them to obtain a positive surface charge.

In 1963 Tomaszewski et. al. [11] had suggested that particles obtain a positive surface charge by adsorption of metal ions and  $\text{H}^+$  ions. Kariapper and Foster [37] noticed that the amount of adsorbed metal ions increases with increasing metal ion concentration in the bath or the addition of  $\text{Ti}^+$ , TEPA or EDTA. Consequently, they assumed that the promoting effect on codeposition of these additives, is derived from the fact that they enhance metal ion adsorption. Celis et. al. [22,23] confirmed these results and found that the additives themselves are not adsorbed on the particles. The reverse effect was described by Lakshminarayanan et. al. [38], who noticed that  $\text{Cl}^-$  ions reduce codeposition of  $\text{Al}_2\text{O}_3$  with Cu. According to them  $\text{CuCl}$  is formed, which adsorbs onto the particle, thus inhibiting  $\text{Cu}^{2+}$  adsorption.

Meguno et. al. [54] confirmed the suggestions of the earlier researchers by measuring the  $\zeta$ -potential, which is a quantitative measure for the surface charge of particles [31]. The  $\zeta$ -potential of  $\alpha$ -SiC and  $\gamma$ -SiC is negative at high pH and it increases with decreasing pH. At low

pH it becomes positive, which disagrees with the generally observed decrease in particle incorporation at low pH as described in section 2.3.3. Lee and Wan [36] investigated the  $\zeta$ -potential of  $\text{Al}_2\text{O}_3$  particles in a dilute copper sulphate bath. Firstly, the  $\zeta$ -potential of  $\alpha\text{-Al}_2\text{O}_3$  increases with copper sulphate concentration and becomes positive, while that of  $\gamma\text{-Al}_2\text{O}_3$  becomes more negative. This explains why  $\alpha\text{-Al}_2\text{O}_3$  can be codeposited much easier than  $\gamma\text{-Al}_2\text{O}_3$ . Secondly, codeposition promoters like  $\text{Ti}^+$  and TEPA cause a large increase in the  $\zeta$ -potential to positive values, confirming the enhanced metal ion adsorption as found by Kariapper and Foster [37]. Similarly, the addition of even a small amount of  $\text{Cl}^-$  ions decreases the  $\zeta$ -potential of  $\alpha\text{-Al}_2\text{O}_3$  to a negative value, explaining their inhibitory effect.

Hayashi et. al. [30] determined the  $\zeta$ -potential of  $\alpha\text{-Al}_2\text{O}_3$  particles in more concentrated copper sulphate baths, that is comparable to standard plating baths. In contrast to all earlier investigations they observed that the  $\zeta$ -potential is negative and becomes more negative with decreasing pH. The amount of  $\text{SO}_4^{2-}$  adsorbed on the particles was about 7 times as high as the amount of adsorbed  $\text{Cu}^{2+}$ . So, they concluded that indeed  $\text{Cu}^{2+}$  and  $\text{H}^+$  ions are adsorbed on the  $\alpha\text{-Al}_2\text{O}_3$  particles, but that their positive charge is more than compensated for by the adsorption of  $\text{SO}_4^{2-}$  ions, resulting in a negative  $\zeta$ -potential.

Particles with a surface charge form more stable suspensions, because due to their mutual repulsion they do not agglomerate. By addition of a cationic surfactant to initially negatively charged particles, Bartlett [31] showed that the dispersion stability reaches a minimum when the  $\zeta$ -potential equals 0. Correspondingly, Helle [53] reported that codeposition is small when the  $\zeta$ -potential is negative, inhibited when it is zero and large when it is positive.

## 2.4 Mechanism and models

The first attempt to explain electrochemical codeposition was made by Whithers in 1962 [56]. He proposed that the particles with a positive surface charge are drawn to the cathode by electrophoresis. In 1964 Martin and Williams [16] suggested that the particles are also transported to the cathode by the agitation of the bath and are mechanically entrapped by the growing metal layer. In 1967 Brandes and Goldthorpe [32] rejected the idea of mechanical entrapment.

---

They suggested that there is some attractive force holding the particles at the cathode long enough to be incorporated by the growing metal layer. This force could be an electrostatic one. At present it is still difficult to assess the relative importance of these three mechanisms.

In 1968 Saifullin and Khalilova [57] were the first to present a model to calculate the weight percent of incorporated particles. This model was based on mechanical entrapment only and has to be rejected. Three years later Bazzard and Boden [21] proposed that particles collide with the cathode surface due to the bath agitation and that the particles should stay at the cathode surface a certain time to become occluded. They developed a simple equation to calculate the weight percent of embedded particles, but rightly stated that it lacked any physical significance.

#### **2.4.1 Guglielmi's model**

The model developed by Guglielmi in 1972 [20] presented an important contribution to the understanding of codeposition. He proposed a two-step mechanism taking into account electrophoresis and adsorption. In the first step, which is of a physical nature, particles approaching the cathode become loosely adsorbed on the cathode surface. These loosely adsorbed particles are still surrounded by a cloud of adsorbed ions. In the second step the particles lose this ionic cloud and become strongly adsorbed on the cathode. This step is thought to be of an electrochemical character, that is it depends on the electrical field at the cathode. Finally, the strongly adsorbed particles are occluded by the growing metal layer.

In the model the loose adsorption step is described by a Langmuir adsorption isotherm, taking into account the cathode area available for this loose adsorption:

$$\sigma = \frac{k\phi}{1+k\phi}(1-\theta) \quad (2.2)$$

where  $\sigma$  is the loose adsorption surface coverage,  $\theta$  the strong adsorption surface coverage and  $k$  depends on the intensity of the particle-cathode interaction. Obviously the second step depends on  $\sigma$  and this dependence is considered linear by Guglielmi. Together with a factor to describe its postulated dependence on the electrical field at the cathode, represented by the cathode overpotential ( $\eta$ ), the following formula for the strong adsorption rate was obtained:

$$V_p = \sigma v_0 e^{B\eta} \quad (2.3)$$



where  $v_0$  and B are constants. The deposition rate of the metal is found using Faraday's law:

$$V_M = \frac{M_M j}{nF\rho_M} \quad (2.4)$$

Taking into account the area of the cathode available for codeposition the current density is related to the overpotential by the Tafel equation:

$$j = (1 - \theta)j_0 e^{A\eta} \quad (2.5)$$

Assuming that the volume fraction of embedded particles  $\alpha \approx \theta \ll 1$  these expressions give:

$$\frac{\phi}{\alpha} = \frac{M_M j_0^{B/A}}{nF\rho_M v_0} j^{(1-B/A)} \left( \frac{1}{k} + \phi \right) \quad (2.6)$$

The constants  $k$ ,  $v_0$  and B depend on the particle-metal system considered and have to be determined from codeposition experiments, while the other parameters can be measured (A and  $j_0$ ) or are known constants. Hence, the model is not able to predict the codeposition rate for a particular system.

Using some experimental information it was successful in describing the codeposition behaviour of Ni-SiC, Ni-TiO<sub>2</sub> [20], Cu-Al<sub>2</sub>O<sub>3</sub> [23], Cr-C [24], Ag-Al<sub>2</sub>O<sub>3</sub> [26], Cu-SiC [27] and Cu-P [28]. However, it was not able to describe Cr-Al<sub>2</sub>O<sub>3</sub> codeposition [25]. The Langmuir isotherm and the Tafel equation seem to be incorrect descriptions to take into account respectively the particle concentration and the current density. It is obvious from equation (2.6) that using the Tafel equation the maximum in particle incorporation at low current density reported for various codeposition systems (section 2.3.3.) can not be described. Moreover, other parameters, like bath agitation, bath constituents and particle size and type are disregarded. They are inherently accounted for by the constants  $k$ ,  $v_0$  and B, but of course it is difficult to assess exactly how. Therefore, these constants have to be determined separately for every set of experimental conditions.

Regarding the role of the ionic cloud surrounding the particles some obscurity can be noted in Guglielmi's model [39]. Several authors already noted the importance of adsorption of ions on the particles in codeposition and in 1974 Kariapper and Foster [37] showed it quantitatively. They concluded that the adsorbed metal ions play a twofold role: they cause the particles to be

---

electrostatically attracted to the cathode and they are reduced at the cathode thus creating a physical bond between the cathode and the particle by their reduction. They also found a strong dependence of the codeposition rate on the bath agitation. The particle content versus current density curves exhibit a maximum, whose position depends on the agitation rate.

They proposed a model based on these observations, taking into account the effect of most experimental parameters. However, the factors used to describe these effects can hardly be measured or evaluated [39].

#### **2.4.2 Model of Buelens and Celis et.al.**

Celis et. al. [22,23,39,41] noticed that Guglielmi's model can not explain the maximum in the particle content versus current density curve of Cu-Al<sub>2</sub>O<sub>3</sub> codeposition. A comparison between this curve and the cathodic polarization curve, led to the suggestion that the particle deposition rate depends on the reduction rate of the Cu<sup>2+</sup> ions adsorbed on particles. It was concluded that two processes play a fundamental role in the codeposition mechanism:

- the adsorption of ions onto the particle.
- the reduction of these adsorbed ions at the cathode surface.

Based on these postulates and the pronounced effect of agitation on codeposition [41] Buelens [39,42] proposed a five step mechanism for codeposition. In the first step particles in the bulk of the solution obtain an ionic cloud by adsorbing ions from the solution. Then, in the second and third step the particles are transported by bath agitation to the hydrodynamic boundary layer and by diffusion to the diffusion layer, respectively to the cathode surface. Finally, similar to Guglielmi's model the particles are incorporated in two steps. They are adsorbed on the cathode surface still surrounded by their ionic cloud and then become embedded by the reduction of some of the adsorbed ions.

Using this mechanism a model for the calculation of the weight percent of embedded particles was developed. The basic hypothesis of the model is that a certain amount  $x$  of ions adsorbed on the particle  $X$  must be reduced at the cathode for the particle to become incorporated. This takes

---

into account a certain residence time of a particle on the cathode surface necessary for it to be build in as stated before by Bazzard and Boden [21]. So, not all particles present at the cathode surface will be embedded, which was also a basic assumption in Guglielmi's model.

The mass fraction of embedded particles is defined as follows:

$$\beta = \frac{W_p N_p P}{\frac{M_M j}{nF} + W_p N_p P} \quad (2.7)$$

where  $W_p$  is the weight of one particle,  $N_p$  is the number of particles crossing the diffusion layer at the cathode per unit of time and surface area and  $P$  is the chance of a particle to become incorporated. Faraday's law gives the weight of deposited metal. From the basic hypothesis it follows that  $P$  depends on the probability  $P_{(x/X,j)}$  that at least  $x$  out of  $X$  adsorbed ions are reduced. Hence, if  $p_j$  is the chance that one ion is reduced at current density  $j$ :

$$P_{(x/X,j)} = \sum_{z=x}^X C_z^X (1-p_j)^{X-z} p_j^z \quad (2.8)$$

To calculate  $p_j$  a new assumption is made, that is no distinction is made between the adsorbed ions and free ions and thus:

$$p_j = \frac{\frac{j}{nF}}{\frac{(c_M^b + c_M^s)\delta}{2} + \frac{j}{nF}} \quad (2.9)$$

where  $c_M^b$  and  $c_M^s$  are respectively the bulk concentration and the concentration at the cathode surface of the metal ions. It is not clear why in the left term of the denominator of equation (2.9) a time factor, which would make  $p_j$  dimensionless, is neglected. Celis et. al. [42] do not give any explanation for this, while Buelens [39] just states that a negligible error is created. A factor  $H$  is introduced to take into account bath agitation:

$$P = H P_{(x/X,j)} \quad (2.10)$$

Following from the bath agitation experiments,  $H = 1$  under laminar flow conditions,  $0 < H < 1$  under transition flow conditions and  $H = 0$  under turbulent flow conditions.

Finally,  $N_p$  is related to the number of ions crossing the diffusion layer per unit time and surface area  $N_M$  and to the type of overvoltage control:

$$N_p = N_M \frac{C_p^*}{C_M^*} \left( \frac{j_{tr}}{j} \right)^\lambda \quad (2.11)$$

where  $j_{tr}$  is the transition current density from charge transfer to concentration overvoltage control and  $C_p^*$  and  $C_M^*$  are respectively the number of particles and the number of ions in the bulk. Under charge transfer overvoltage control  $\lambda = 0$ , because the ion-reduction is rate determining, while the diffusion rate is high enough for both particles and free ions. However,  $\lambda \neq 0$  under concentration overvoltage control, because diffusion of ions is rate determining, which is obviously much slower for adsorbed ions than for the free ions.

Similar to earlier models this model can not predict the particle content directly from the experimental conditions. The factors  $x$ ,  $X$  and  $\lambda$  need to be determined by fitting the model with experimental results. The authors obtained a good agreement between the model and experimental results for Cu-Al<sub>2</sub>O<sub>3</sub> and Au-Al<sub>2</sub>O<sub>3</sub> codeposition [39,42]. However, the assumption that at  $j_{tr}$  a transition from charge transfer to mass transport overvoltage control occurs can be questioned. For Cu deposition the cathodic overvoltage of this transition corresponds to the value where Degrez and Winand [58] observe a change in the reduction mechanism of Cu<sup>2+</sup>. This indicates that the change in codeposition behaviour at  $j_{tr}$  is associated with a change in the metal deposition mechanism and not with diffusion limitation of the particle deposition as proposed in this model.

### **2.4.3 Recent models**

Hwang and Hwang [43] proposed a more general model than that of Celis and Buelens, in which some of the factors, like  $H$  and  $j_{tr}$ , are interrelated. Based on the model of Guglielmi, for various current density ranges the particle codeposition rate is determined by the electrode reactions for adsorbed species on the particles, whose rates are determined by kinetic and/or diffusion parameters. They investigated Co-SiC codeposition, hence their starting point is the

reduction of  $H^+$  and  $Co^{2+}$  adsorbed on the particles. Three different current density ranges for this reduction of adsorbed ions are distinguished:

- Low current density where only  $H^+$  ions are reduced
- Intermediate current density, where the  $H^+$  reduction rate has reached its limiting value and also  $Co^{2+}$  is reduced.
- High current where for both ions the reduction rate is at its limiting value.

Similar to Guglielmi's model the metal deposition rate  $V_M$  is defined as:

$$V_M = \frac{M_M}{\rho_M n F} j \Gamma_M (1 - \theta) \quad (2.12)$$

where  $\Gamma_M$  is the current efficiency. In the low current density range the particle deposition rate  $V_p$  is determined by the reduction of the adsorbed  $H^+$  ions and it has been deduced that:

$$V_p = k_1 c_{H^+}^s \sigma e^{B_1 \eta} \quad (2.13)$$

where  $c_{H^+}^s$  is the concentration of adsorbed  $H^+$  ions on the particle surface, which decreases with increasing  $H^+$  reduction:

$$c_{H^+}^s = \left( 1 - \frac{V_p}{V_{p,H^+}} \right) c_{H^+}^b \quad (2.14)$$

where  $V_{p,H^+}$  is the maximum particle deposition rate due to  $H^+$  reduction and  $c_{H^+}^b$  is the  $H^+$  ion concentration in the bulk solution.

In the intermediate current density range the particle deposition rate due to  $H^+$  reduction is at its limiting value  $V_{p,H^+}$ , while the contribution of the metal reduction is similar to that of  $H^+$  in the low current density range. Consequently, the equation for  $V_p$  in this range is given by:

$$V_p = V_{p,H^+} + k_2 \left( 1 - \frac{V_p}{V_{p,M}} \right) c_M^b \sigma e^{B_2 \eta} \quad (2.15)$$

where  $V_{p,M}$  is the limiting particle deposition rate due to the metal reduction and  $c_M^b$  is the metal ion concentration in the bulk. Finally, in the high current density range the particle

---

deposition rate is solely determined by diffusion and is independent of the current density and the adsorbed ions concentration. Equation (2.13) is simplified to:

$$V_p = k_3 \sigma \quad (2.16)$$

The volume fraction of embedded particles can now be calculated using equation (12) and depending on the current density range equation (13), (15) or (16).

This model is an improvement of Guglielmi's model. However, inherently the assumption is made that the reduction of adsorbed ions differs completely from that of free ions. The efficiency of the metal deposition, that is the competition between the reduction of free  $H^+$  and  $Co^{2+}$ , is considered to be independent of current density, while for adsorbed ions different regimes are distinguished. The authors do not discuss the validity of this assumption.

The present mechanism can be generalized to a two step process that is transport of the particle to the cathode surface and a particle-cathode interaction [2]. As can be seen from the foregoing discussion the mass transport step was not or just globally treated in the models. From related fields of research, like filtration, detailed descriptions of mass transport of solid particles and particle surface interactions are known [59]. Recently several authors [27,50,60] tried to develop a model for codeposition using such descriptions. In comparison to the earlier models the present models are much more elaborated. They are build up of a lot of often interrelated equations containing an extensive set of parameters. This renders it difficult to get an easy insight into the effect of an experimental parameter and necessitates the use of extensive computer calculations.

Guo et. al. [27] proposed a model based on a description of the mass transport by so-called similitude numbers, which are dimensionless numbers determined by the factors influencing the mass transport. A standard description of the Sherwood number for mass transport of solid particles in a dilute suspension to a fixed plate was modified for codeposition. A factor  $S_x$  was introduced for the effect of the particle concentration in the bath and a factor  $G_q$  for the incorporation process of the particles in the metal matrix.  $G_q$  contains, among others, a time factor describing the earlier-mentioned residence time of a particle at the cathode surface. If certain

parameters, like temperature and bath constituent are considered to be constant, the particle deposition rate can be calculated from the similitude number  $Sh'$ :

$$Sh' = Co Re^c Dm^d Sx^e Gq^f \quad (2.17)$$

where  $Re$  is the Reynolds number and  $Dm$  is the electrical double layer number, while  $Co$ ,  $c$ ,  $d$ ,  $e$  and  $f$  are constants, which have to be determined by fitting the model with experimental data.

Satisfactory agreement with experimental data were obtained for Cu-SiC codeposition in a channel flow. However, because of the limited range of experimental data it is not clear if the model is able to predict important features, like the peak in the particle inclusion versus current density curve.

In 1987 Valdes [60] developed a model for codeposition at a RDE taking into account the various ways in which a particle is transported. As starting point an equation of continuity for the particle number concentration based on a differential mass balance was chosen. In this equation the particle flux is composed of expressions for the different mass transport processes, that is Brownian diffusion and convection. The convection term takes into account all the forces and torques acting on a particle due to hydrodynamic migration, electromigration and diffusionmigration. Together with expressions for the local electrical field and the local electrolyte concentration for a binary electrolyte a highly coupled set of transport equations is obtained.

Next Valdes noticed the difficulties in obtaining a good description of the particle-electrode interaction. For non-electrochemical systems several particle surface interaction models exist of which the 'perfect sink', that is all particles arriving within a critical distance of the electrode are captured, is the most simple one. However, Valdes showed that this model can not be used, because it predicts maximum codeposition at the limiting current density, which contradicts experimental observations. Therefore, he proposed another model based on the generally accepted assumption that the reduction of adsorbed ions is the determining factor for particle deposition. This electrode-ion-particle electron transfer (EIPET) model leads to a Butler-Volmer like expression for the particle deposition rate. With this model the experimentally observed peak in the particle inclusion versus current density curve is predicted. However, the peak is still found at relatively high current densities, that is close the limiting current density.

Due to the fact that no experimental work has been done on this model it's impossible to assess its validity for real codeposition systems. However, it presented a good basis for the more precise theoretical model of codeposition at a RDE reported by Fransaer et. al. [50]. They developed a trajectory description for a particle based on all the forces and torques acting on it. This includes the forces due to fluid convection and particle motion and the forces acting directly on the particle, for example gravity, the electrophoretic force and the London - van der Waals force. Expressions for all these forces were developed and led to a set of equations describing the particle trajectory. Now the particle volume flux can be determined by calculating the limiting particle trajectory, that is the particle trajectory separating the trajectories of particles reaching the electrode from those passing by.

Close to the electrode surface the trajectory description fails, because it leads to the 'perfect sink' condition, which was seen to be wrong. Hence, the authors introduced a reaction term characterizing the particle electrode interaction. A forcebalance on the particle led to an equation for the probability that a particle at the electrode surface will be incorporated. This forcebalance includes an adhesion force, which was determined from Cu-polystyrene codeposition experiments. Using this adhesion force the trajectory model gives a good description of the variation of the particle content in the deposit as function of the particle concentration in the bath. In contrast to the earlier models the assumption of a necessary reduction of ions adsorbed onto the particles is rejected.

The trajectory model does not predict the maximum in the particle inclusion versus current density curve. Experiments indicate that this maximum is related to the potential of zero charge of the copper electrode, which suggests that the double layer force is responsible for the maximum. Calculations of the adhesion force dependence on the current density from experimental data do not support this last suggestion. A strong repulsive force between the particle and the electrode has to be present at short distances. Therefore, the structural or hydration force was introduced, which is a short range repulsive force due to the ordering of solvent molecules at interfaces in concentrated electrolytes. This hydration force will be minimal if the electric field at the electrode is minimal, that is at the potential of zero charge. So the maximum in the particle inclusion versus current density curve could be caused by changes in the ordering of the



water dipoles due to changes in electrode charge. Plausible explanations for the effect of particle type, monovalent cations and surfactants on the codeposition rate can also be given using the hydration force. Experiments will have to show if a hydration force is actually present.

The trajectory model offers a good mathematical description for gaining a better theoretical insight into the codeposition process. In contrast to earlier models it is based on widely accepted descriptions of particle mass transfer and particle-substrate interactions. It does not heavily rely on assumptions, like the reduction of adsorbed ions, for which only indirect evidence exists. However, experimental investigations into the actual nature of the particle-electrode interaction are still necessary to get a better understanding and consequently a better modelling of the codeposition process.

The trajectory model, just as all earlier models, does not consider the growth behaviour of the metal deposit. As already said before the maximum in the particle occlusion versus current density curve for Cu-matrix codeposition occurs at the same overpotential as a kink in the  $E/\ln i$  curve measured by Degrez and Winand [58]. From this curve they concluded that the cathodic charge transfer coefficient is 0.5 in the low overpotential region and 0.1 in the high overpotential region. This change in charge transfer coefficient is accompanied by a morphological change of the Cu deposit. Such a dramatic change in the charge transfer coefficient suggests a strong change in the nature of the electrode surface. Possibly in the case of Cu deposition the presence of a Cu hydride compound at high overpotential.

## **2.5 Concluding remarks**

Electrochemical codeposition of inert particles in a metal matrix proves to be a suitable technique to produce composite materials. Especially in the field of coatings it offers a good alternative to other techniques and enables the production of composites with unique properties. A lot of often interrelated experimental parameters were seen to influence the codeposition process. A clear picture of the exact effect of each parameter is difficult to obtain, because often different or even contradicting results are reported by different authors. Particle concentration in the bath, current density and bath agitation seem to be the most important parameters.

The mechanism for codeposition, which is generally accepted, involves particle transport to the cathode surface by bath agitation and incorporation in the metal by reduction of adsorbed ions. Attempts to develop models, which are able to predict the amount of incorporated particles from the experimental conditions have failed until now. Good results were obtained with models that need to be fitted first with experimental results to determine some unknown factors. However, these models often have only a limited validity and contain questionable assumptions. Presently, models involving detailed descriptions of particle transport and particle-cathode interactions offer a promising perspective. Though, the exact nature of the particle-electrode interaction has still to be elucidated. Several investigations imply that here the metal growth behaviour, which is mostly neglected, plays an important role.

## References

- [1] J.R. Roos, J.P. Celis, J. Fransaer and C. Buelens, *J. Metals* **42** (1990) 60.
- [2] J.P. Celis, J.R. Roos, C. Buelens and J. Fransaer, *Trans. Inst. Met. Finish.* **69** (1991) 133.
- [3] C. Buelens, J. Fransaer, J.P. Celis and J.R. Roos, *Bull. Electrochem.* **8** (1992) 371.
- [4] J. Fransaer, J.P. Celis, J.R. Roos, *Met. Finish.* **91** (1993) 97.
- [5] V.P. Greco and W. Baldauf, *Plating* **55** (1968) 250.
- [6] N. Periene, A. Cesuniene and L. Taicas, *Plat. Surf. Finish.* **80** (1993) 73.
- [7] Y.S. Chang and J.Y. Lee, *Mater. Chem. Phys.* **20** (1988) 309.
- [8] A.E. Grazen, *The Iron Age* (1959) 94.
- [9] F. Mathis, B. Pierragi, B. Lavelle and B. Criqui, *Proceedings 24<sup>th</sup> ISATA*, Florence (1991) 171.
- [10] J.R. Roos, *Proceedings INCEF'86*, Bangalore (1988) 382.
- [11] T.W. Tomaszewski, R.J. Clauss and H. Brown, *Proc. Am. Electroplaters Soc.* **50** (1963) 169.
- [12] G.N.K. Ramesh Babu and M. Mohammed Yusuf, *Mat. Chem. Phys.* **36** (1993) 134.
- [13] R. Bazard and P.J. Boden, *Trans. Inst. Met. Finish.* **50** (1972) 207.

- [14] G.R. Smith, J.E. Allison and W.J. Kolodrubetz, *Electrochem. Soc. Ext. Abstr.* **85-2** (1985) 326.
- [15] C.G. Fink and J.D. Prince, *Trans. Am. Electrochem. Soc.* **54** (1928) 315.
- [16] R.V. Williams and P.W. Martin, *Trans. Inst. Met. Finish.* **42** (1964) 182.
- [17] M. Keddam, S. Senyarich, H. Takenouti and P. Bernard, *J. Appl. Electrochem.* **24** (1994) 1037.
- [18] A. Anani, Z. Mao, S. Srinivasan and A.J. Appleby, *J. Appl. Electrochem.* **21** (1991) 683.
- [19] F.K. Sautter, *J. Electrochem. Soc.* **110** (1963) 557.
- [20] N. Guglielmi, *J. Electrochem. Soc.* **119** (1972) 1009.
- [21] R. Bazard and P.J. Boden, *Trans. Inst. Met. Finish.* **50** (1972) 63.
- [22] J.P. Celis, Phd-thesis, KU Leuven (1976).
- [23] J.P. Celis and J.R. Roos, *J. Electrochem. Soc.* **124** (1977) 1508.
- [24] R. Narayana and B.H. Narayana, *J. Electrochem. Soc.* **128** (1981) 1704.
- [25] R. Narayan and S. Chattopadhyay, *Surf. Technol.* **16** (1982) 227.
- [26] Y. Suzuki and O. Asai, *J. Electrochem. Soc.* **134** (1987) 1905.
- [27] H. Guo, Q. Qin and A. Wang, *Proc. Electrochem. Soc.* **88-18** (1988) 46.
- [28] J.W. Graydon and D.W. Kirk, *J. Electrochem. Soc.* **137** (1990) 2061.
- [29] M. Verelst, J.P. Bonino and A. Rousset, *Mat. Sci. Eng.* **A135** (1991) 51.
- [30] H. Hayashi, S. Izumi and I. Tari, *J. Electrochem. Soc.* **140** (1993) 362.
- [31] P.K.N. Bartlett, Industrial training report AKZO, Arnhem, (1980) pp. 10-39.
- [32] E.A. Brandes and D. Goldthorpe, *Metallurgia* **76** (1967) 195.
- [33] O. Berkh, S. Eskin, S. Berner and A. Zahavi, *Plat. Surf. Finish.* **82** (1995) 55.
- [34] B. Bozzini, G. Giovannelli, L. Nobili and P.L. Cavallotti, *AIFM Galvanotecnica e Nuove Finiture* **5** (1995) 92.
- [35] T.W. Tomaszewski, L.C. Tomaszewski and H. Brown, *Plating* **56** (1969) 1234.
- [36] C.C Lee and C.C. Wan, *J. Electrochem. Soc.* **135** (1988) 1930.
- [37] A.M.J. Kariapper and J. Foster, *Trans. Inst. Met. Finish.* **52** (1974) 87.
- [38] G.R. Lakshminarayanan, E.S. Chen and F.K. Sautter, *Plat. Surf. Finish.* **63** (1976) 38.
- [39] C. Buelens, Phd-thesis, KU Leuven (1984).
-

- [40] S.H. Yeh and C.C. Wan, *J. Appl. Electrochem.* **24** (1994) 993.
- [41] C. Buelens, J.P. Celis and J.R. Roos, *J. Appl. Electrochem.* **13** (1983) 541.
- [42] J.P. Celis, J.R. Roos, C. Buelens, *J. Electrochem. Soc.* **134** (1987) 1402.
- [43] B.J. Hwang and C.S. Hwang, *J. Electrochem. Soc.* **140** (1993) 979.
- [44] S.W. Watson and R.P. Walters, *J. Electrochem. Soc.* **138** (1991) 3633.
- [45] S.W. Watson, *J. Electrochem. Soc.* **140** (1993) 2235.
- [46] Y. Suzuki, M. Wajima and O. Asai, *J. Electrochem. Soc.* **133** (1986) 259.
- [47] P.J. Sonneveld, W. Visscher and E. Barendrecht, *J. Appl. Electrochem.* **20** (1990) 563.
- [48] D.W. Gibbons, R.H. Muller and C.W. Tobias, *J. Electrochem. Soc.* **138** (1991) 3255.
- [49] P.R. Webb and N.L. Robertson, *J. Electrochem. Soc.* **141** (1994) 669.
- [50] J. Fransaer, J.P. Celis and J.R. Roos, *J. Electrochem. Soc.* **139** (1992) 413.
- [51] J.W. Graydon and D.W. Kirk, *Can. J. Chem. Eng.* **69** (1991) 564.
- [52] K. Helle, *Advances in Organic Coating Science and Technology*, Vol.II, (1979) 264.
- [53] K. Helle, Report AKZO Research, Arnhem (1993).
- [54] K. Meguno, T. Ushida, T. Hiraoka and K. Esumi, *Bull. Chem. Soc. Jpn.* **60** (1987) 89.
- [55] R.A. Tacke, P. Jiskoot and L.J.J. Janssen, *J. Appl. Electrochem.* **26** (1996) 129.
- [56] J.C. Whithers, *Prod. Fin.* **26** (1962) 62.
- [57] R.S. Saifullin and R.G. Khalilova, *J. Appl. Chem. USSR.* **43** (1970) 1274.
- [58] M. Degrez and R. Winand, *Electrochim. Acta* **29** (1984) 365.
- [59] Z. Adamczyk, *Colloids and Surfaces* **35** (1989) 283.
- [60] J.L. Valdes, *J. Electrochem. Soc.* **134** (1987) 223C.

### 3. Electrochemical deposition and heat treatment of Fe-Fe<sub>x</sub>Si composites

#### 3.1 Introduction

Applications of electrochemically deposited composites are generally related to a specific property exhibited by the particles dispersed in the metal matrix. In contrast it is the alloy prepared from an electrochemically deposited Fe-Si composite, which is of practical interest. The deposited composite has to be homogenized to obtain applicable silicon rich iron foil. This is done by annealing the composite at a temperature, which allows interdiffusion of iron and silicon. A similar method has been reported by Bazzard and Boden for the preparation of Ni-Cr alloys [1] and by Smith et. al. for Fe-Ni-Cr alloys [2].

Interdiffusion between two solid materials of different composition is a standard diffusion process arising from concentration gradients of the components [3]. Under equilibrium conditions interdiffusion leads to the formation of regions with a composition in between that of the initial materials and corresponding to thermodynamically stable phases. In a binary system, like Fe-Si, only single phase regions, separated by straight boundaries, are formed. If the overall composition of the system corresponds to a stable phase prolonged annealing eventually leads to complete homogenization. In the Fe-Si phase diagram (Figure 3.1) it can be seen that the desired 6 wt% Si alloy is a stable phase in the Fe(Si) solid solution region.

The surface of silicon particles is covered with a siliconoxide layer, which could act as a diffusion barrier against Fe-Si interdiffusion. Moreover the ternary Fe-Si-O diffusion system could behave very different from the binary Fe-Si system. Although even Fe<sub>3</sub>Si particles are covered with a 50 nm oxide layer consisting of 70 at% siliconoxide [4,5] the use of ferrosilicide, that is Fe<sub>x</sub>Si with  $x > 0$ , instead of Si particles could be advantageous. Also because a shorter annealing time is required to homogenize a Fe-Fe<sub>x</sub>Si composite than a Fe-Si composite. However, a larger amount of Fe<sub>x</sub>Si than Si particles has to be codeposited to produce a 6 wt% Si

alloy. In this chapter the annealing of electrochemically prepared Fe-Si and Fe-Fe<sub>x</sub>Si composites will be discussed.

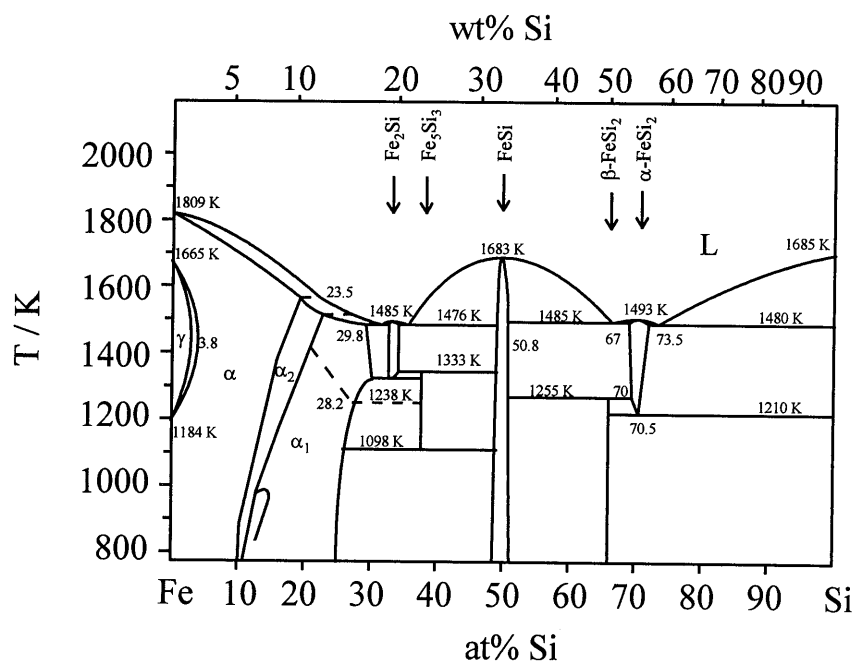


Figure 3.1: Fe-Si phase diagram [6].

### 3.2 Experimental details

Composites were deposited at 363 K from a 3 kmol m<sup>-3</sup> FeCl<sub>2</sub> solution of pH 1 containing a volume fraction Fe<sub>x</sub>Si particles of 0.002. The type, density and conductivity of the Fe<sub>x</sub>Si particles used are given in Table 3.1. The average particle diameter of the Si and Fe<sub>3</sub>Si particles was measured using a Coulter LS 130, whereas that of the FeSi and FeSi<sub>2</sub> particles was

estimated from microscopical investigation of the powders. The density and conductivity of silicon are those specified by the supplier (Goodfellow) and those of the ferrosilicides were obtained from [7]. It was noticed that the FeSi<sub>2</sub> particles are inhomogeneous. EDX-analysis shows islands of FeSi in a matrix with a composition intermediate between stoichiometric β-FeSi<sub>2</sub> and non-stoichiometric α-FeSi<sub>2</sub> (Figure 3.1). Similar inhomogeneity of FeSi<sub>2</sub> was reported by Vijn et. al. [8]. This is probably due to the incongruent melting of β-FeSi<sub>2</sub>, which leads to the formation of FeSi and α-FeSi<sub>2</sub> when a melt of composition β-FeSi<sub>2</sub> is cooled down.

Table 3.1: Properties of the Fe<sub>x</sub>Si particles.

particle type	Average diameter / μm	density / kg m <sup>-3</sup>	conductivity / S m <sup>-1</sup>
Fe <sub>3</sub> Si	5	7.18·10 <sup>3</sup>	7.7·10 <sup>5</sup>
FeSi	50	6.16·10 <sup>3</sup>	3.8·10 <sup>5</sup>
β-FeSi <sub>2</sub>	80	4.93·10 <sup>3</sup>	1.5·10 <sup>2</sup>
Si	1	2.33·10 <sup>3</sup>	43

In order to ensure sufficient particle incorporation, that is close to 6 wt% Si, composites were prepared using the set-up, which is schematically shown in Figure 3.2. The electrolyte suspension was contained in a 700 cm<sup>3</sup> thermostated glass vessel. The cathode, with its active area facing upward, was placed near the bottom of the vessel and the anode was positioned just below the electrolyte surface. During deposition the suspended particles were allowed to settle onto the cathode, where they were incorporated in the growing iron layer.

The 7 cm<sup>2</sup> Ti disc cathode was successively degreased, rinsed, pickled in 4 M HCl and rinsed. The low-alloy steel plate anode was wrapped in filter paper to prevent insoluble anodic reaction products from settling into the bulk solution. Before each experiment the electrolyte was stirred for at least 90 minutes to obtain a homogeneous suspension. To maintain a continuous flow of settling FeSi, FeSi<sub>2</sub> and Fe<sub>3</sub>Si particles the suspension was stirred continuously during deposition. Due to their comparatively large diameter and high density (Table 3.1) these

particles will have settled completely immediately after the stirrer is switched off. The small and low density Si particles settle very slowly and additional stirring is not necessary. In fact stirring reduces Si particle incorporation significantly. A net charge of  $3.9 \cdot 10^6 \text{ C m}^{-2}$  was supplied to the cathode in all experiments.

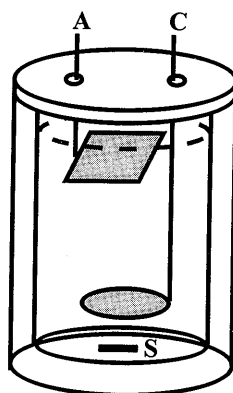


Figure 3.2: Schematic picture of the composite deposition set-up; A = anode, C = cathode and S = stirrer; the broken line indicates the electrolyte surface.

After deposition the composite deposits were stripped from the Ti-substrate, thoroughly rinsed with water and ethanol and stored under vacuum. From each composite several samples were cut of which one was characterised using X-ray diffraction (XRD). From preliminary experiments [9] it was decided to anneal samples of each composite at 1173 and 1423 K for 24 hours. Additionally one Fe-Si composite was annealed at 1273, 1373 and 1423 K. The samples were annealed in flowing  $\text{H}_2$  to prevent oxidation of iron. Cross-sections of the annealed and as-plated samples were embedded in Cu-Perspex and polished. The cross-sections were studied with a light microscope and a scanning electron microscope (SEM). Standardless composition analysis of the samples was performed using the SEM, which is equipped with an energy dispersive X-ray (EDX) Analyser. In the composition analysis only Fe and Si were taken into account and the overall composition was normalized to 100%.



### 3.3 Results

XRD-spectra of the as-plated composites indicate the presence of particles in the iron matrix. Peaks at angles characteristic for  $\alpha$ -Fe and the incorporated particle were detected. In Figures 3.3 - 3.5 cross-sections of as-plated Fe-Si, Fe-FeSi<sub>2</sub> and Fe-Fe<sub>3</sub>Si composites are shown. The Fe-FeSi composite is similar to Fe-Si (Figure 3.3). From the photographs it can be estimated that composites with a volume fraction particles up to 0.5 were obtained. However, the particles were not always homogeneously dispersed through the iron matrix. Differences in particle content within a sample or between samples prepared under equal conditions were noticed. On the average the composites contain 5 - 15 wt% of Si. It follows from the phase diagram (Figure 3.1) that this is within the Fe(Si) solid solution region. Annealing of these composites will give insight into the homogenization treatment of the desired 6 wt% Si composite.

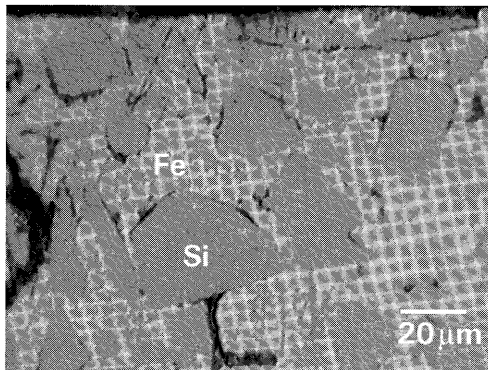


Figure 3.3: Cross-section of an as-plated Fe-Si composite.

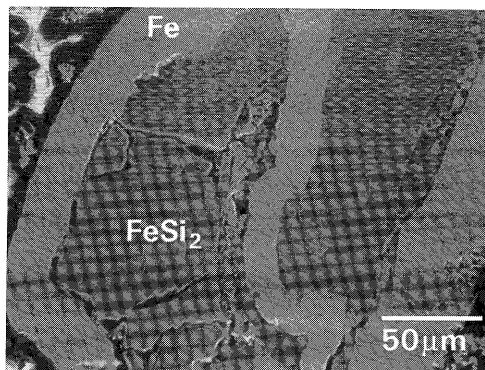


Figure 3.4: Cross-section of an as-plated Fe-FeSi<sub>2</sub> composite.

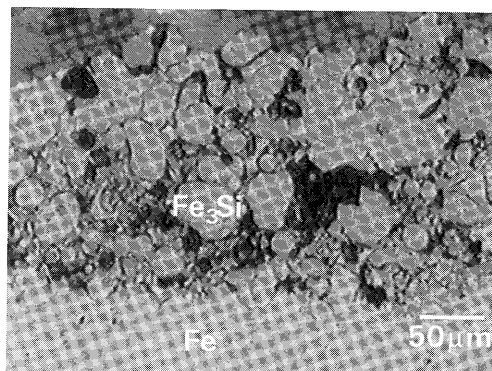


Figure 3.5: Cross-section of an as-plated Fe-Fe<sub>3</sub>Si composite.

On the photographs differences in adherence to the iron matrix between different particles and between different faces of a particle can be seen. Some particles or particle faces are perfectly adhered to the surrounding iron matrix, whereas others exhibit pores and cracks at the interface with the iron matrix. Part of the pores are due to removal of incorporated particles during

sample polishing. Except for Fe<sub>3</sub>Si no differences in adherence to the iron layer between the different particle types can be seen. Even FeSi<sub>2</sub> particles with a diameter comparable to the deposit thickness are covered with a well-adhering iron layer. The Fe-Fe<sub>3</sub>Si deposit shows a very high degree of porosity (Figure 3.5).

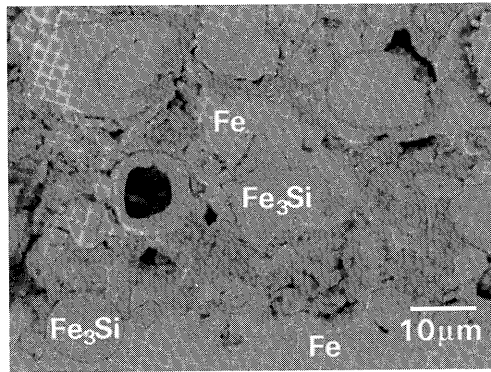


Figure 3.6: Cross-section of a Fe-Fe<sub>3</sub>Si composite annealed at 1173 K.

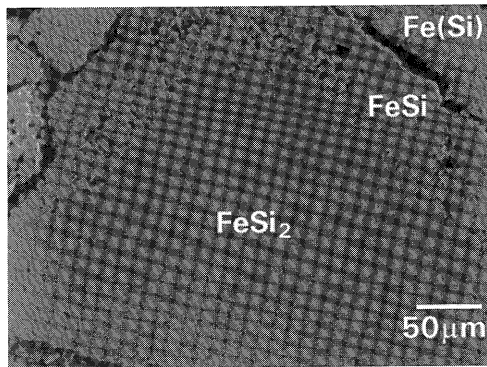
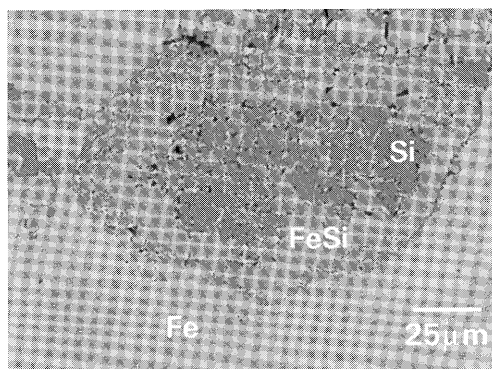
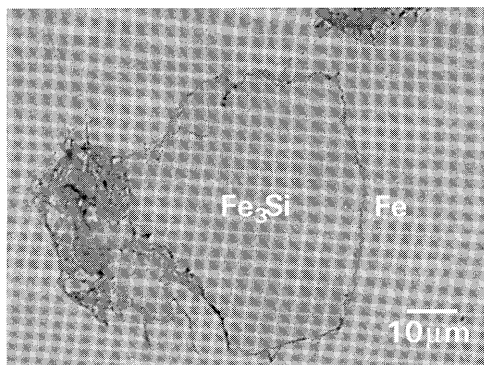


Figure 3.7: Cross-section of a Fe-FeSi<sub>2</sub> composite annealed at 1173 K.



(a)



(b)

Figure 3.8: Cross-sections of a Fe-Si composite annealed at 1373 K.

In Figures 3.6 - 3.10 cross-sections and the composition of annealed composites are presented. With exception of the Fe-Fe<sub>3</sub>Si composites (Figure 3.6) interdiffusion has occurred at all temperatures in all samples. The particles have either partially or completely interdiffused with the iron matrix to new phases. The inhomogeneity of the FeSi<sub>2</sub> particles is gone after annealing (Figure 3.7). It follows from the phase diagram (Figure 3.1) that the detected compositions

---

correspond to thermodynamically stable phases, but that not all possible phases were formed. Irrespective of particle type the only interdiffusion products are FeSi, Fe<sub>3</sub>Si and Fe(Si). In Figure 3.7 an FeSi layer of approximately equal thickness has formed between Fe(Si) and FeSi<sub>2</sub>. In contrast in Figure 3.8 (a) FeSi is separated from Fe by a straight boundary, but islands of Si in FeSi are found in the centre of the particle.

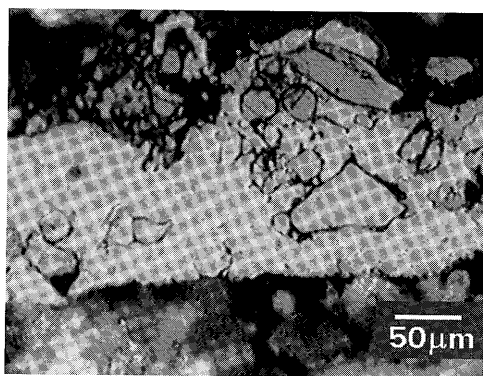


Figure 3.9: Cross-section of a Fe-FeSi composite annealed at 1423 K.

Figures 3.8 and 3.9 show that different phases together with unreacted particles can be found in the same sample. For all temperatures and particle types it was found that different particles in the same sample had reacted differently. Owing to this the effect of temperature on the interdiffusion is difficult to assess. Roughly more iron-rich phases were found with increasing temperature. None of the composites was completely homogenized, but some samples were partially homogenized (Figure 3.10). Despite the homogenization the position of the original particles can still be distinguished due to the presence of pores. Note that the area inside the pores does not necessarily correspond to the cross-section of the original particle. Also around particles which have only partially reacted pores or cracks are seen (Figures 3.6 - 3.10). In comparison to the as-plated composites the amount of pores and cracks has increased implying that they were formed during annealing.

---

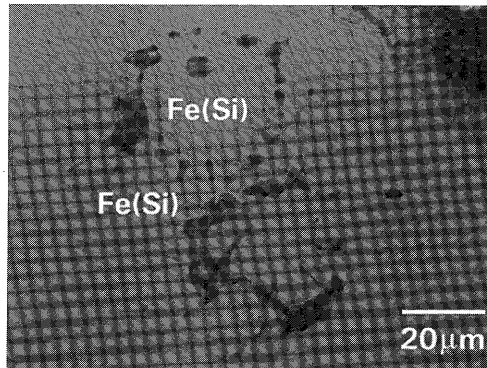


Figure 3.10: Cross-section of a Fe-Si composite annealed at 1273 K.

### 3.4 Discussion

The theoretical diffusion behaviour of a Fe-Si composite with an overall mole fraction Si,  $Y_{Si} = 0.1$  (6 wt%), during a homogenization treatment of time  $t_h$  is depicted in Figure 3.11. For three stages during the annealing the change in  $Y_{Si}$  along a one-dimensional cross-section of the composite is given. The top drawing (a) shows the as-plated composite, where monodisperse particles, homogeneously dispersed through the matrix, are assumed. Immediately after annealing has started a concentration profile consisting of all thermodynamically stable phases between Fe and Si develops at the interface between a particle and the matrix (b). It is assumed that  $FeSi_2$ ,  $FeSi$ ,  $Fe_3Si$  and  $Fe(Si)$  solid solution are the stable phases that can be formed. This corresponds to an annealing temperature below 1100 K (Figure 3.1). Although  $Fe_3Si$  is just the upper limit of the  $Fe(Si)$  solid solution it has a highly ordered structure and it generally behaves as a stoichiometric silicide phase [10,11]. During annealing all phases grow at the expense of their neighbouring phases and the Si-rich phases will gradually disappear (c). Eventually the

whole composite will have interdiffused to a Fe(Si) solid solution with  $Y_{Si} = 0.1$ , represented by the dotted lines in Figure 3.11.

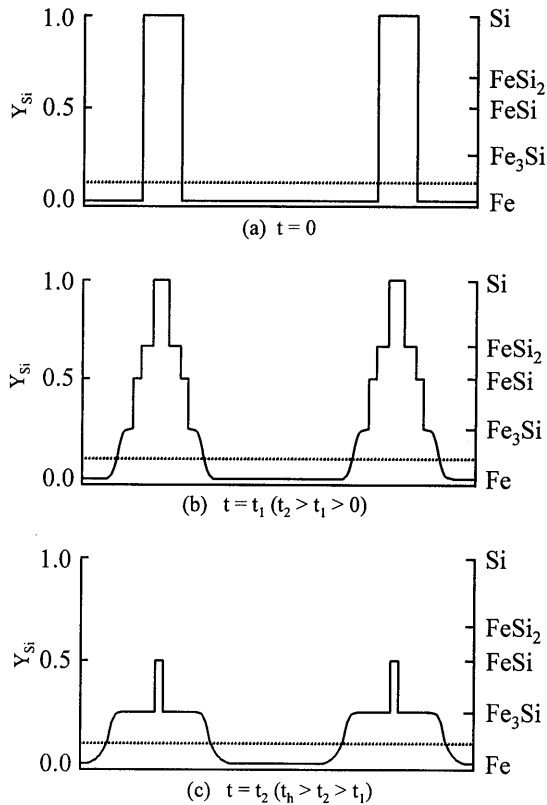


Figure 3.11: Mole fraction Si,  $Y_{Si}$ , along a one-dimensional cross-section of a Fe-Si composite at three stages during a homogenization treatment of time  $t_h$ ; The dotted lines represents the composition at homogenization.

The obtained results clearly deviate from this theoretical behaviour. Different particles in the same composite form different phases and not all possible phases are found. There are several possible reasons for these discrepancies. The missing phases in partially reacted particles could have formed, but in such thin layers that they were not detected [3]. The samples were not

instantaneously cooled down to room temperature. During cooling the high-temperature phase  $\text{Fe}_5\text{Si}_3$  or  $\text{FeSi}_2$  could have completely reacted to phases, which are stable at ambient temperature. Figures 3.3 - 3.5 show that a range of particle sizes are incorporated in the composites. It can easily be understood from Figure 3.11 that after a certain annealing time a small particle can have reacted completely to another phase, while a large particle has only partially reacted to that phase. In this respect the use of the settling method is disadvantageous, because it favours the incorporation of large particles. This is evident when the average particle diameters of the incorporated particles in Figures 3.3 - 3.5 are compared to those of the suspended particles in Table 3.1.

Another disadvantage of the settling method is the formation of pores and cracks in the composite. During deposition particles can settle on top of other particles creating a space in which Fe can not be deposited. Although the electrical conductivity of the particle materials (Table 3.1) is orders lower than that of iron, namely  $1 \cdot 10^7 \text{ S m}^{-1}$  [12], it can not be excluded that electrochemical reactions occur on partially incorporated particles. It has been reported that  $\text{FeSi}$  and  $\text{FeSi}_2$  electrodes are quite active for  $\text{H}_2$  evolution in  $1 \text{ kmol m}^{-3} \text{ H}_2\text{SO}_4$  [13]. Taking into account the lower conductivity and different surface composition of the particles compared to iron it is possible that  $\text{H}_2$  evolves on the particles during deposition resulting in bad adherence of the iron layer on the particles.

As stated in section 3.3 pores and cracks were also formed during annealing. Pore formation during solid state diffusion is due to the Kirkendall effect [14]. The difference in diffusion fluxes of the interdiffusing components is compensated for by a flux of vacancies in the direction of the fastest diffusing component. These vacancies can condensate to pores at nucleation sites like impurities, cracks or existing pores [14-16]. The location of the pores after annealing is indicative for the relative diffusion fluxes of the components. In investigations on  $\text{Fe}(\text{Si})/\text{Fe}$  [17,18] and thin film  $\text{Fe}/\text{Si}$  [11,19] diffusion couples Si is reported to be the faster diffusing component. In contrast for  $\text{Fe}/\text{SiC}$  [20] and  $\text{Fe}-\text{Fe}_x\text{Si}$  [9] diffusion couples Fe was found to be the only diffusing component. In Figures 3.7 - 3.10 pores are found near Fe or  $\text{Fe}(\text{Si})$ , that is close to the original interface between particle and matrix, indicating that Fe is the faster diffusing component. Moreover, homogenized particles are evidenced by a ring of pores



(Figure 3.10). If Si was the faster diffusing component the Kirkendall vacancies would have condensed to one large pore at the centre of the original particle [16,21].

Pore formation is often more extensive in diffusion couples with radial symmetry, like metal matrix composites, than in planar diffusion couples. In all investigations on the heat treatment of electrochemically deposited composites pore formation during annealing was reported [1,22,23]. For some composites this presents hardly a problem [1,23], but it can lead to complete detachment of the particle from the matrix [24]. If one component diffuses much faster than the other the movement of vacancies builds up stresses [16,21]. In diffusion couples with radial symmetry relaxation of these stresses is difficult and pores or cracks occur at the original interface between particle and matrix. In planar couples these stresses can more easily be relaxed and often an external pressure is applied to further reduce pore formation [16].

A good contact between the particles and the matrix is a prerequisite for interdiffusion [3]. Pores act as diffusion barriers, which slow down or totally inhibit interdiffusion. For the Fe-Fe<sub>3</sub>Si composite the absence of interdiffusion is probably due to its high porosity. It can easily be understood that a particle, which is only partly in contact with the iron matrix requires a longer annealing time to interdiffuse to a certain composition than does a well-adhered particle. Porosity can also be responsible for the absence of Fe<sub>3</sub>Si in Figures 3.7 and 3.8 [25,26]. Since, Fe is the faster diffusing species the Kirkendall pores are located near the interface between Fe and Fe<sub>3</sub>Si. The pores slow down Fe diffusion into Fe<sub>3</sub>Si, whereas Fe diffusion from Fe<sub>3</sub>Si into FeSi continues undisturbed. Consequently Fe<sub>3</sub>Si is consumed by FeSi and disappears or does not form at all.

As stated in section 3.1 a siliconoxide layer on Si particles can also act as a diffusion barrier. During a temperature dependent incubation time interdiffusion is inhibited, because the oxide layer has to be broken down for interdiffusion to occur [26]. Break-down of an oxide layer is most likely at imperfections, which results in local interdiffusion through the oxide layer. In Figure 3.8 (a) the formed FeSi layer is not separated from Si by a straight boundary, because Fe has only locally diffused into the Si particle. In agreement with Tu and Mayer [27] it is Fe, which breaks through the siliconoxide layer and diffuses into Si.

Siliconoxide also changes the binary Fe/Si system into a ternary Fe/Si/O system. The results do not yield conclusive evidence for the presence of ternary diffusion, but it can not be excluded. In a ternary system multiphase regions and ternary phases could be formed, but these were not found. Ternary phases could have been mistaken for binary ones, because only Fe and Si were taken into account in composition analysis. However, all detected phases are existing binary phases. The absence of FeSi<sub>2</sub> between FeSi and Si in could be due to ternary diffusion favouring FeSi over FeSi<sub>2</sub> formation. Binary phases, which are formed in the binary couple, can be absent in the ternary couple [3].

The break-through pattern of interdiffusion was not found for the ferrosilicide particles, indicating that the siliconoxide layer is less of a problem on ferrosilicide particles. Despite this difference annealing of ferrosilicide composites does not seem favourable compared to annealing of silicon composites. In all composites partially homogenized areas were found suggesting that complete homogenization is possible. The results imply that composites with a homogeneous dispersion of well-adhering small particles would facilitate homogenization. In this respect Si particles are favoured, because they are available in small particles sizes. The settling method, which yields porous composites of large particles should be avoided. However, preliminary experiments have shown that using a vertical plate or a rotating cylinder electrode composites with less than 0.1 wt% Si particles are obtained. On a rotating disc electrode composites with 6 wt% Si can be obtained (Chapter 4), but this type of electrode is limited to relatively small surface areas and it is not suitable for industrial application.

### **3.5 Conclusions**

During annealing of Fe-Fe<sub>x</sub>Si composites Fe and Si interdiffuse. Thermodynamically stable binary phases are formed, but no complete homogenization is obtained. Not all possible phases were found and different particles in the same composites react differently. This is partly due to the settling method used to produce the composites and partly inherent in Fe-Fe<sub>x</sub>Si interdiffusion. The settling method favours the incorporation of larger particles and introduces pores at the particle metal interface. Because Fe diffuses much faster than Si more pores are

generated during annealing due to the Kirkendall effect. Pores entirely obstruct interdiffusion, as found for the Fe-Fe<sub>3</sub>Si composites, or slow it down. The siliconoxide layer on the Si particles causes an incubation time before undisturbed interdiffusion can occur. Characteristic phenomena of ternary Fe-Si-O diffusion were not found, but could be responsible for the absence of certain phases. No significant difference was found in the diffusion behaviour between the different Fe<sub>x</sub>Si particles.

## References

- [1] R. Bazzard and P.J. Boden, *Trans. Inst. Met. Finish.* **50** (1972) 207.
- [2] G.R. Smith, J.E. Allison and W.J. Kolodrubetz, *Electrochem. Soc. Ext. Abstr.* **85-2** (1985) 326.
- [3] F.J.J. van Loo, *Solid St. Chem.* **20** (1990) 47.
- [4] R.A Williams and G.H. Kellsall, *J. Colloid Interface Sci.* **132** (1989) 210.
- [5] R.A Williams and G.H. Kellsall, *Minerals Eng.* **5** (1992) 57.
- [6] O. Kubaschewski, 'Iron - Binary Phase Diagrams', Springer-Verlag, Berlin (1982) p. 136 - 139.
- [7] G.V. Samsonov and I.M. Vinitskii, 'Handbook of Refractory Compounds', IFI/Plenum, New York (1980) p. 106 and p. 232.
- [8] A.K. Vijh, G. Bélanger and R. Jacques, *Mater. Chem. Phys.* **19** (1988) 215.
- [9] I.S.H. Beate, Graduation report, Eindhoven University of Technology (1993).
- [10] B. Million, *Czech.J. Phys. B* **27** (1977) 928.
- [11] S.S. Lau, J.S.-Y. Feng, J.O. Olowolafe and M.-A. Nicolet, *Thin Solid Films* **25** (1975) 413.
- [12] R.C. Weast (editor), 'Handbook of Chemistry and Physics', 48th Ed., The Chemical Rubber Co., Cleveland (1967) p. F-132.
- [13] A.K. Vijh, G. Bélanger and R. Jacques, *Mat. Chem. Phys.* **20** (1988) 529.
- [14] Y. Adda and J. Philibert, 'La Diffusion dans les Solides', Vol. I, Presses Universitaires de France, Paris (1966) p. 40 - 48 and 574 - 614.

- [15] F.J.J. van Loo, B. Pieraggi and R.A. Rapp, *Acta Metall.* **38** (1990) 1769.
- [16] F. Aldinger, *Acta Metall.* **22** (1974) 925.
- [17] H.Y.M. Mirani and P. Maaskant, *Phys. Stat. Sol.A* **14** (1972) 521.
- [18] R.J. Borg and D.Y.F. Lai, *J. Appl. Phys.* **41** (1970) 5193.
- [19] G. Ottaviani, *Thin Solid Films* **140** (1986) 3.
- [20] R.C.J. Schiepers, PhD Thesis, Eindhoven University of Technology (1991).
- [21] F. Aldinger and M. Kuhn, *Z. Metallkde.* **66** (1975) 260.
- [22] N. Merk, *J. Mat. Sci. Lett.* **14** (1995) 592.
- [23] B.P. Cameron, J. Foster and J.A. Carew, *Trans. Int. Met. Finsish.* **57** (1979) 113.
- [24] W.H. Safranek, 'The Properties of Electrodeposited Metals and Alloys', American Elsevier Publishing Co., Inc., New York (1974) p. 325 - 335.
- [25] J.H. Gülpen, A.A. Kodentsov and F.J.J. van Loo, in 'Applications of Thermodynamics in the Synthesis and Processing of Materials', (edited by P. Nash and B. Sundman), The Minerals, Metals & Materials Society (1995) 127.
- [26] C.H. Anderson and R. Warren, Proc. 9th International Symposium on Reactivity of Solids, Cracow (1980), (edited by K. Dyrek, J. Haber and J. Nowotny), Elsevier, Amsterdam (1982) 820.
- [27] K.N. Tu and J.W. Mayer, in 'Thin Films - Interdiffusion and Reactions', (edited by S.M. Poate, K.N. Tu and J.W. Mayer), John Wiley & Sons, New York (1978) p. 380.

## 4. Iron deposition from a $\text{FeCl}_2$ solution containing suspended silicon particles

(A. Hovestad and L.J.J. Janssen, *J. Appl. Electrochem.* 27 (1997) 756)

### 4.1 Introduction

Although a wide range of particle-metal systems has been investigated, the mechanism of the codeposition process is still not fully understood [1-3]. In all the proposed mechanisms, as discussed in chapter 2, the metal deposition is considered to be unaffected by the presence of particles. However, several researchers have reported marked changes in the metal deposition behaviour on addition of particles, which are closely coupled to codeposition features [4-10]. Among others a shift in the cathodic polarization curve, changes in cathodic Tafel slopes and decreases in metal deposition current efficiency have been observed (see chapter 2). Further investigations on metal deposition in the presence of suspended particles are required to obtain a better understanding of these effects and their relation to the codeposition mechanism. Knowledge of such effects is also necessary for successful industrial application of codeposition systems. In the present work the physical and electrochemical behaviour of a Fe plating bath in the presence of suspended Si particles has been determined.

### 4.2 Experimental details

A 3 M  $\text{FeCl}_2$  solution, operating at 90°C and pH 1, was used as the Fe plating bath. Before each series of experiments a fresh solution was prepared with  $\text{FeCl}_2 \cdot 4\text{H}_2\text{O}$  (Merck, extra pure) and Fe powder (Goodfellow, 99% pure) was added. This solution was allowed to stand in the presence of Fe powder to reduce ferric ions, present as impurity in the salt. Despite this pre-treatment, traces of ferric ions, about 3-5 mM, were still present in the  $\text{FeCl}_2$  solution during the measurements. Two types of anisotropic Si particles were used. Their specifications are given in Table 4.1. Type-I was used to measure all reported parameters. Addi-

tionally, the electrochemical experiments were repeated using type-II. The conductivity of the suspensions was determined under continuous stirring using a conductivity cell (Philips PW9550/60) and a conductivity meter (Radiometer CDM2). A viscosity meter (Ubbelohde, type 0c) was used to measure the viscosity.

Table 4.1: Properties of the Si particles.

type	purity / % Si	Average diameter / $\mu\text{m}$
I	97.5	1.1 (by number)
II	99.3	3.2 (by volume)

The electrochemical experiments were performed in a three-compartment cell consisting of a 150 cm<sup>3</sup> thermostated vessel for the working electrode, a counter electrode compartment and a Luggin capillary compartment for the reference electrode. A gas inlet and outlet were connected to the working electrode compartment. Two types of rotating disc electrodes (RDE), namely a Pt-RDE and a RDE holding interchangeable Ti-cups, were used both having an active surface area of 0.38 cm<sup>2</sup>. A low alloy-steel plate was used as the counter electrode in the experiments involving Fe deposition, while a Pt-plate counter electrode was used in the mass transfer measurements. All potentials given are referred to a saturated calomel electrode (SCE), which was used as the reference electrode.

Before the experiments the electrolyte was saturated with N<sub>2</sub> and electrochemically pre-treated for 90 minutes at -0.1 A using a 10 cm<sup>2</sup> Ti-cathode and a low alloy-steel anode. During the experiments N<sub>2</sub> was passed over the electrolyte to exclude oxygen. In the period between successive measurements a magnetic stirrer was used to maintain the Si particles in suspension. The time scale of the measurements was such that during measurements the electrode rotation was sufficient to prevent particle settlement. All measurements were controlled and registered by a computer coupled to an Autolab/PGSTAT20 (ECO Chemie). Impedance measurements

were carried out with a Solatron 1250 Frequency Response Analyzer and a Solatron Electrochemical Interface 1286.

The current efficiency of Fe deposition,  $\Gamma_{Fe}$ , was obtained by measuring the charge,  $q_-$ , consumed during 30 minutes of cathodic polarization and subsequently the charge,  $q_+$ , necessary for complete anodic dissolution of the deposited Fe. The charge  $q_-$  was corrected for the charge  $q_{-,Fe^{3+}}$  used for reduction of  $Fe^{3+}$  to  $Fe^{2+}$  and  $\Gamma_{Fe} = q_+ / (q_- - q_{-,Fe^{3+}})$  was calculated. It was found that during the potentiostatic deposition a steady current was reached within a few minutes. The dissolution was carried out at 0 V versus SCE to exclude interference of  $H_2$  evolution and  $Fe^{2+}$  oxidation. Side reactions, like the reduction of traces  $Fe^{3+}$ , were negligible at this potential. The Fe deposition was preceded by a conditioning period of 10 minutes at 0 V versus SCE and a short nucleation pulse (1 s) at -0.85 V versus SCE.

Cathodic polarization curves for Fe deposition and limiting currents for  $Fe^{3+}$  reduction were obtained by cyclic voltammetry. Before each measurement a conditioning potential of 0 V versus SCE was applied for 5 minutes. Some irreproducibility was noticed in the cathodic polarization curves and in the  $Fe^{3+}$  reduction limiting currents. Therefore, the effect of particles was investigated by progressively adding fixed quantities of Si powder to the same solution. After each addition of Si powder the solution was magnetically stirred for 5 minutes to obtain a homogeneous suspension. After each measurement of a cathodic voltammogram, potentiostatic impedance spectra were recorded at several cathodic potentials in the frequency range 1 to 65000 Hz to obtain the ohmic solution resistance.

Galvanostatic deposition experiments using the Ti-RDE were performed to determine the Si incorporation in Fe as a function of the current density. The deposits were weighed and dissolved in dilute  $HNO_3$  in a Pt crucible. After evaporation to dryness the Si was dissolved in 1.2 g  $NaCO_3$  and 0.4 g  $NaB_4O_7 \cdot 10H_2O$  at  $1000^\circ C$  for 30 minutes. The resulting mixture was dissolved in 2 M HCl and spectrophotometrically analyzed for Si using the heteropoly blue method [11].

### 4.3 Results and discussion

#### 4.3.1 Conductivity and viscosity

Experiments on suspensions of glass beads containing a broad range of particle sizes carried out by De La Rue and Tobias [12] indicate that Bruggeman's equation, namely:

$$\frac{\kappa_s}{\kappa_c} = (1 - \phi)^{\frac{3}{2}} \quad (4.1)$$

represents the dependence of the suspension conductivity,  $\kappa_s$ , on the particle volume fraction,  $\phi$ , satisfactorily. The conductivity of the continuous phase is indicated by  $\kappa_c$ . The experimental results for the reduced conductivity  $\kappa_r = \kappa_s/\kappa_c$  of the 3 M FeCl<sub>2</sub>-Si suspensions are given in Figure 4.1. The solid line in this figure represents the Bruggeman relation, which fits the experimental values for  $\kappa_s/\kappa_c$  very well. Hence, the 3 M FeCl<sub>2</sub> solution containing Si particles behaves like a suspension of non-conducting particles.

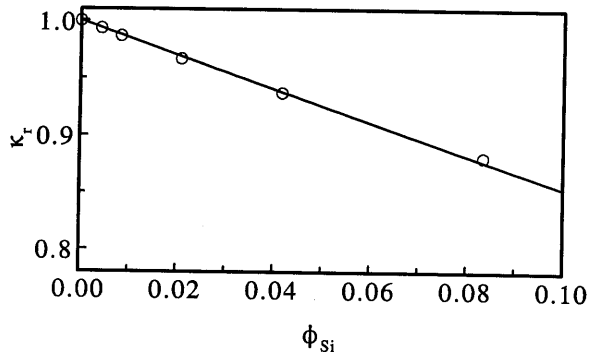


Figure 4.1: Reduced conductivity  $\kappa_r$  of a 3 M FeCl<sub>2</sub> solution at 363 K as a function of Si particle volume fraction; Bruggeman equation (—).

Dispersed particles often cause non-Newtonian viscous behaviour, which influences the hydrodynamics and mass transfer in suspensions. The reduced suspension viscosity ( $\mu_r$ ), that is



the suspension viscosity divided by the viscosity of the continuous phase, is given by the Krieger-Dougherty equation [13]:

$$\mu_r = \left(1 - \frac{\phi}{\phi_m}\right)^{-[\mu]\phi_m} \quad (4.2)$$

where  $[\mu] = \lim_{\phi \rightarrow 0} (\mu_r - 1)/\phi$  is the intrinsic viscosity, which equals 2.5 for spherical particles and  $\phi_m$  is the maximum particle volume fraction. In Figure 4.2 the experimental results for  $\mu_r$  against  $\phi_{Si}$  are given. These results fit the Krieger-Dougherty equation taking  $[\mu] = 3.2$  and  $\phi_m = 1.05$ , which is represented by the full line in Figure 4.2. The value of  $[\mu]$  being higher than 2.5 agrees with the fact that the Si particles are anisotropic [13]. Since the investigated suspensions are relatively dilute the value of  $\phi_m$  can not be determined accurately and has an unrealistic value. It can be concluded that the 3 M FeCl<sub>2</sub>-Si suspension behaves as a Newtonian fluid.

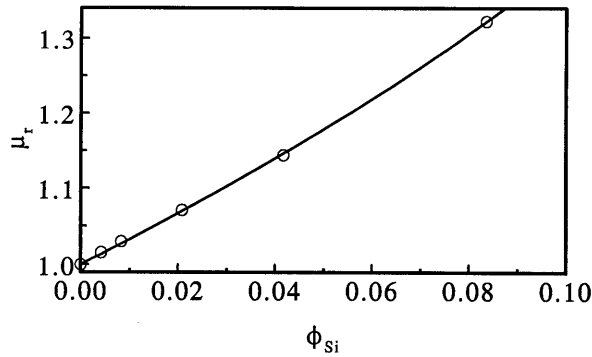


Figure 4.2: Reduced viscosity  $\mu_r$  (○) of a 3 M FeCl<sub>2</sub> solution at 363 K as a function of Si particle volume fraction; (—) fitted Krieger-Dougherty equation.

#### 4.3.2 Particle type

Two types of Si particles were used in the electrochemical experiments (Table 4.1) The type-I particles have a much broader range of particle size than the type-II particles. Both types of particles showed the same effect on the parameters reported below. Therefore, only the results obtained for the type-II particles will be shown.

### 4.3.3 Mass transfer

It is well-known that suspended inert particles can enhance ionic mass transfer to electrodes [14-19]. The mass transfer enhancement could play a role in the effects of particles on metal deposition. The effect of Si particles on the ionic mass transfer in a 3 M FeCl<sub>2</sub> solution was determined using Fe<sup>3+</sup> as indicator ion. In a series of experiments voltammograms at various rotation speeds of a Pt-RDE were measured to determine the limiting current for Fe<sup>3+</sup> reduction in a 3 M FeCl<sub>2</sub> solution containing a small quantity of FeCl<sub>3</sub> and various amounts of Si particles.

Starting with a particle-free 3 M FeCl<sub>2</sub> solution containing 0.037 M FeCl<sub>3</sub>, the open-circuit potential (OCP) of the Pt-electrode became more positive after each addition of Si particles due to a decrease in Fe<sup>3+</sup> concentration. This decrease is caused by the reaction of Fe<sup>3+</sup> with metal Fe, present as an impurity in the Si powder. The Fe<sup>3+</sup> concentration became constant at a lower level soon after addition of Si particles. Hence, to determine the effect of Si particles on the Fe<sup>3+</sup> mass transfer accurately, a correction for the decrease in Fe<sup>3+</sup> concentration,  $c_{Fe^{3+}}^b$ , was taken into account. The relation between the OCP and  $c_{Fe^{3+}}^b$  was determined in a particle-free 3 M FeCl<sub>2</sub> solution and it was found that the OCP was given by the Nernst equation. Hence, the Fe<sup>3+</sup> concentration in the presence of particles was calculated from the measured OCP.

Table 4.2: Exponents of the  $\omega$  dependence of the Fe<sup>3+</sup> limiting current density in a 3 M FeCl<sub>2</sub> solution at 363 K in the presence of various amounts of Si particles.

$\phi_{Si}$	$P\phi$
0	0.50
0.004	0.50
0.009	0.50
0.021	0.51
0.043	0.53
0.086	0.54
0.172	0.60

It was found that the limiting current density,  $j_{\text{L,Fe}^{3+}}$ , for  $\text{Fe}^{3+}$  reduction is proportional to  $\omega^{p_\phi}$ . The values for  $p_\phi$  were obtained from the slope of  $\log j_{\text{L,Fe}^{3+}}$  against  $\log \omega$  curves and are presented in Table 4.2. In the absence of Si particles  $p_\phi = 0.5$ , the same value as for the Levich equation [20]. Applying the Levich equation it was found that  $D_{\text{Fe}^{3+}} = 1.2 \cdot 10^{-9} \text{ m}^2 \text{ s}^{-1}$  in 3 M  $\text{FeCl}_2$  at 363 K.

In Figure 4.3  $j_{\text{L,Fe}^{3+}}/c_{\text{Fe}^{3+}}^b$  is plotted against  $\phi_{\text{Si}}$  for various rotation speeds. This shows that at rotation speeds  $\omega < 100 \text{ s}^{-1}$  the  $\text{Fe}^{3+}$  mass transfer coefficient is practically independent of  $\phi_{\text{Si}}$  and at  $\omega \geq 100 \text{ s}^{-1}$  it increases almost linearly with  $\phi_{\text{Si}}$ . This is the typical behaviour reported for ionic mass transfer in the presence of suspended particles [14-19]. However, the increase in  $\text{Fe}^{3+}$  mass transfer coefficient is clearly smaller compared to values reported in the literature [14-19]. Furthermore, an increase in the exponent  $p_\phi$  with  $\phi$  similar to that shown for  $\phi_{\text{Si}}$  in Table 4.2, was reported by Sonneveld et.al. [17] and Caprani et.al. [14].

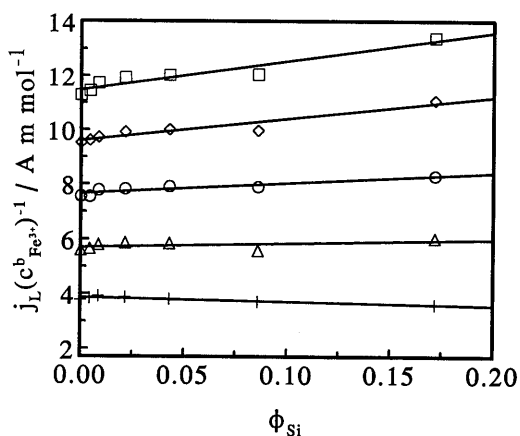


Figure 4.3: Concentration normalized limiting current density for  $\text{Fe}^{3+}$  reduction at a Pt-RDE in a 3 M  $\text{FeCl}_2$  solution at 363 K as a function of  $\phi_{\text{Si}}$  at different RDE rotation speeds,  $\omega$ : 25 (+), 60 ( $\Delta$ ), 100 (O), 160 ( $\diamond$ ) and 225  $\text{s}^{-1}$  ( $\square$ ).

#### 4.3.4 Current efficiency for Fe deposition

Figure 4.4 shows  $\Gamma_{\text{Fe}}$  as a function of the current density for various Si concentrations and a rotation speed of  $100 \text{ s}^{-1}$ . All curves in Figure 4.4 show an increase in efficiency up to  $0.5 \text{ kA m}^{-2}$ . Taking into account the inaccuracy of the results it can be concluded that the Fe deposition current efficiency is practically constant in the current density range  $0.5$  to  $2.5 \text{ kA m}^{-2}$ .  $\Gamma_{\text{Fe}}$  increases slightly with increasing Si concentration. In contrast to the observations for Ni-SiC [7,10] and Ni- $\text{Al}_2\text{O}_3$  [9] the Si particles have no dramatic effect on the Fe deposition current efficiency. Moreover, an increase, rather than a decrease in  $\Gamma$  is observed in the presence of suspended particles.

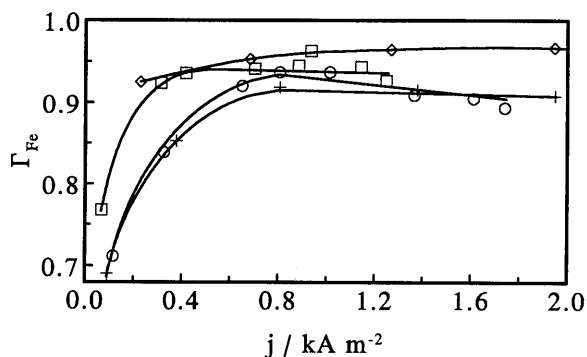


Figure 4.4: Fe deposition current efficiency as function of current density in a  $3 \text{ M FeCl}_2$  solution at  $363 \text{ K}$  containing various amounts of Si particles,  $\phi_{\text{Si}}$ :  $0$  (+),  $0.004$  (O),  $0.086$  ( $\square$ ) and  $0.172$  ( $\diamond$ );  $\omega = 100 \text{ s}^{-1}$ .

#### 4.3.5 Polarization behaviour

Voltammograms on a Pt- and Ti-RDE were measured in a  $3 \text{ M FeCl}_2$  solution with various Si particles contents. The obtained current densities were very high up to about  $10 \text{ kA m}^{-2}$ . A correction for the ohmic potential drop was necessary to acquire correct electrode potentials. It was found that the impedance method was the most reliable to determine this correction.

Corrections obtained with the current interrupt method led to overcompensation at high current densities and were not useful.

Results of impedance measurements were plotted in Nyquist diagrams, which show inclined well-shaped semi-circles with their centres above the real axis. Inclination of semi-circles in impedance plots has often been observed and is attributed to non-uniformity of the electric field at rough electrode surfaces [21,22]. The ohmic solution resistance between working electrode and tip of the Luggin capillary is given by the distance between  $Z_{\text{Re}} = 0$  and the intersection point of a semi-circle with the  $Z_{\text{Re}}$  axis [21,22]. It was found that within experimental accuracy the ohmic solution resistance,  $R_{\Omega}$ , does not change with the potential within the scan range of the voltammograms.

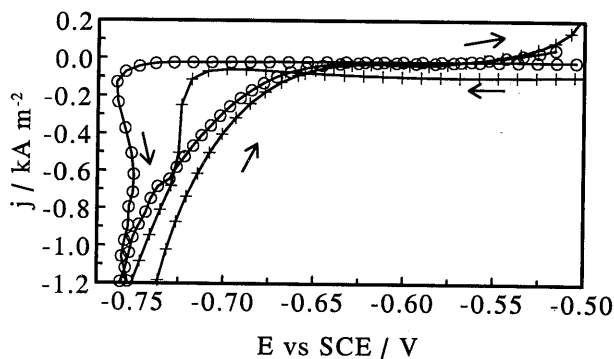


Figure 4.5: Voltammograms for Fe deposition on a Pt-RDE (+) and a Ti-RDE (O) from a particle-free 3 M  $\text{FeCl}_2$  solution at 363 K. Potential scan rate  $2.5 \text{ mV s}^{-1}$ ;  $\omega = 100 \text{ s}^{-1}$ . Arrows indicate scan direction.

Figure 4.5 shows voltammograms on a Ti- and Pt-RDE rotated at  $100 \text{ s}^{-1}$ . For both electrodes the potential was scanned at a rate of  $2.5 \text{ mV s}^{-1}$  from  $-0.5 \text{ V}$  to a more negative potential and back. The ohmic potential drop was taken into account to obtain the correct electrode potentials for the voltammograms. Both voltammograms show a strong hysteresis between the cathodic and anodic scan, indicating the occurrence of a crystallisation overpotential. This is supported by current efficiency measurements. It was found that, at  $-0.75 \text{ V}$ , Fe deposits on Ti with 2.5% current efficiency, while after a nucleation pulse Fe deposits on Fe with 50% current efficiency.

It follows from Figure 4.5 that the current density in the cathodic scan remains constant from -0.50 V to -0.72 V and -0.77 V, for Pt and Ti respectively. At more cathodic potentials the Fe deposition current raises sharply. This shows that there is a clear difference in crystallisation overpotential for Fe deposition on Pt and Ti. Addition of various amounts of Si to the 3 M FeCl<sub>2</sub> solution does not change significantly the value of the crystallisation overpotential for Fe deposition on Pt as well as on Ti. Thus a strong decrease of the crystallisation overpotential as reported for Ni-SiC [7] and Ni-Cr [8] codeposition does not take place in the Fe-Si system.

The anodic scans of the voltammograms measured on Pt at various volume fractions of Si particles are plotted in Figure 4.6. On addition of Si particles the cathodic polarization curve for Fe deposition shifts to slightly lower overpotentials. This was found for both the anodic and cathodic scans on Pt as well as on Ti. A similar depolarisation has been reported for several metal particle systems [4-8]. Taking into account the increase in  $\Gamma_{\text{Fe}}$  with  $\phi_{\text{Si}}$  (Figure 4.4), it can be concluded that the presence of Si particles in the 3 M FeCl<sub>2</sub> solution decreases the overpotential for Fe deposition on Fe compared to the particle-free solution. Since it is unlikely that the Fe deposition reaction is mass transfer controlled in the current density range considered and Si particles hardly affect the mass transfer, the depolarisation is not due to Fe<sup>2+</sup> mass transfer enhancement by Si particles. The decrease in overpotential indicates a slight change in the kinetic parameters for Fe deposition with  $\phi_{\text{Si}}$ .

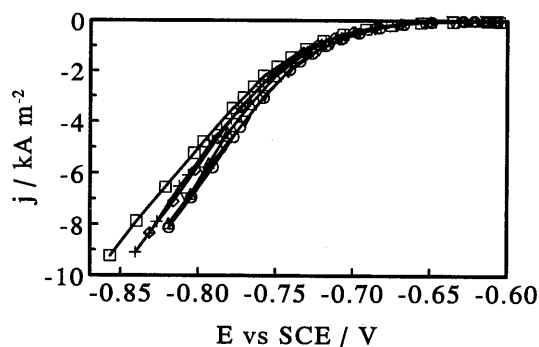


Figure 4.6: Voltammograms for Fe deposition on a Pt-RDE from a 3 M FeCl<sub>2</sub> solution at 363 K containing various amounts of Si particles. Potential scan rate 2.5 mV s<sup>-1</sup>;  $\omega = 100 \text{ s}^{-1}$ .  $\phi_{\text{Si}}$ : 0 ( $\square$ ), 0.004 (+), 0.009 ( $\diamond$ ), 0.043 ( $\Delta$ ), 0.086 ( $\circ$ ) and 0.172 ( $\nabla$ ).

---

To determine the kinetic parameters for Fe deposition on Fe modified Tafel plots were used. By rearrangement of the Butler-Volmer equation it can be shown that:

$$j_{m,Fe} = \frac{j_{Fe}}{1 - \exp\left(-\frac{nF}{RT}|\eta|\right)} = j_{0,Fe} \exp\left(\frac{\alpha_T nF}{RT}|\eta|\right) \quad (4.3)$$

The current density for Fe deposition  $j_{Fe} = \Gamma_{Fe} j$ . In Figure 4.7 the modified Tafel plot of  $\log j_{m,Fe}$  against  $|\eta|$  is given. It shows that the modified Tafel slope increases with increasing overpotential. This dependence may be explained either by the crystallisation potential or the activation polarisation due to the electron transfer reaction. In the latter case a change in the nature of the electrode surface may be occurring, for example caused by the formation of iron hydrides.

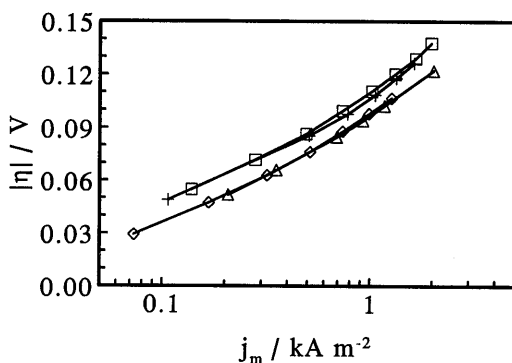


Figure 4.7: Modified Tafel plots for Fe deposition on a Pt-RDE from a 3 M  $\text{FeCl}_2$  solution at 363 K containing various amounts of Si particles.  $\omega = 100 \text{ s}^{-1}$ .  $\phi_{\text{Si}}$ : 0 ( $\square$ ), 0.004 (+), 0.086 ( $\diamond$ ), 0.172 ( $\Delta$ ).

The modified Tafel slope is practically independent of the Si particle content. The observed modified Tafel slope at  $|\eta| < 0.075 \text{ V}$ , namely 0.062 V agrees with the results reported for Fe deposition from  $\text{FeSO}_4$  solutions [23,24]. Assuming  $n = 1$  it can be calculated that  $\alpha_T = 1.1$ ,

which deviates from  $\alpha_T = 0.5$  usually found for a slow one-electron electrode reaction [23,24]. Linear extrapolation of the modified Tafel curve to  $\eta = 0$  gives  $j_{0,Fe}$  if the electron transfer is the rate-determining step. In this case  $j_{0,Fe} = 0.015 \text{ kA m}^{-2}$  for the particle free solution and  $j_{0,Fe}$  increases slightly with increasing  $\phi_{Si}$ . So, Si particles enhance the rate of Fe deposition on Fe, which results in higher deposition current efficiencies and lower overpotentials.

#### 4.3.6 Codeposition

The Si codepositing with Fe in a 3 M  $\text{FeCl}_2$  solution containing 0.086 volume fraction Si particles was determined for various current densities using a Ti-RDE rotating at  $100 \text{ s}^{-1}$ . In Figure 4.8 the amount of Si embedded in the Fe matrix is given as a function of the current density and it is seen to increase with current density. In contrast to various other codeposition systems [1-4,9] no maxima are found for Si incorporation within the investigated current density range. At a current density of  $2 \text{ kA m}^{-2}$  the desired Fe-Si composite containing ~5 wt% Si particles can be obtained.

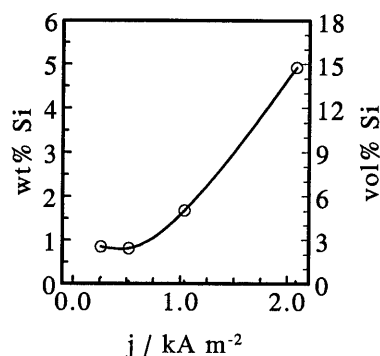


Figure 4.8: Si particle incorporation in Fe deposited on a Pt-RDE from a 3 M  $\text{FeCl}_2$  solution at 363 K with  $\phi_{Si} = 0.086$  as a function of current density;  $\omega = 100 \text{ s}^{-1}$ .

Webb et.al. [9] observed marked changes in the deposition current efficiency and cathodic polarization curves for Ni- $\text{Al}_2\text{O}_3$  codeposition, which depend on the amount of embedded  $\text{Al}_2\text{O}_3$



particles. Taking into account the practically constant value of  $\Gamma_{Fe}$  above  $0.5 \text{ kA m}^{-2}$ , the amount of Si embedded in Fe does not affect the Fe deposition current efficiency. Moreover, there is no effect of the amount of embedded Si particles on the polarization curves for Fe deposition. The observed effects on  $\Gamma_{Fe}$  and the cathodic polarization curves are relatively small and are related to the amount of suspended Si particles.

## References

- [1] C. Buelens, J. Fransaer, J.P. Celis and J.R. Roos, *Bull. Electrochem.* **8** (1992) 371.
- [2] J. Fransaer, J.P. Celis and J.R. Roos, *Met. Finish.* **91** (1993) 97.
- [3] A. Hovestad, L.J.J. Janssen, *J. Appl. Electrochem.* **25** (1995) 519.
- [4] C. Buelens, J.P. Celis and J.R. Roos, *J. Appl. Electrochem.* **13** (1983) 541.
- [5] Y. Suzuki, M. Wajima and O. Asai, *J. Electrochem. Soc.* **133** (1986) 259.
- [6] E.A. Lukashev, *Russ. J. Electrochem.* **30** (1994) 83.
- [7] S.W. Watson, *J. Electrochem. Soc.* **140** (1993) 2235.
- [8] S.W. Watson and R.P. Walters, *J. Electrochem. Soc.* **138** (1991) 3633.
- [9] P.R. Webb and N.L. Robertson, *J. Electrochem. Soc.* **141** (1994) 699.
- [10] S.H. Yeh and C.C. Wan, *J. Appl. Electrochem.* **24** (1994) 993.
- [11] D.F. Boltz, L.A. Trudell and G.V. Potter, in 'Colorimetric Determination of Nonmetals', (edited by D.F. Boltz and J.A. Howell), Chemical Analysis Vol. 8, 2<sup>nd</sup> Edition, J. Wiley & Sons, New York (1978) p. 442.
- [12] R.E. De La Rue and C.W. Tobias, *J. Electrochem. Soc.* **106** (1959) 827.
- [13] H.A. Barnes, J.F. Hutton and K. Walters, 'An Introduction to Rheology', Elsevier, Amsterdam (1989) p. 115.
- [14] M. Marie de Ficquelmont-Loizos, L. Tamisier and A. Caprani, *J. Electrochem. Soc.* **135** (1988) 626.
- [15] A. Caprani, M. Marie de Ficquelmont-Loizos, L. Tamisier and P. Peronneau, *J. Electrochem. Soc.* **135** (1988) 635.
- [16] D.J. Roha, M.S. thesis, University of California, Berkeley (1981).

- [17] P.J. Sonneveld, W. Visscher, E. Barendrecht, *J. Appl. Electrochem.* **20** (1990) 563.
- [18] D.W. Gibbons, R.H. Muller and C.W. Tobias, *J. Electrochem. Soc.* **138** (1991) 3255.
- [19] P.K. Andersen, R.H. Muller and C.W. Tobias, *J. Electrochem. Soc.* **136** (1989) 391.
- [20] R. Greef, R. Peat, L.M. Peter, D. Pletcher and J. Robinson, 'Instrumental Methods in Electrochemistry', Ellis Horwood, Chichester (1985) p. 124.
- [21] S. Iseki, K. Ohashi and S. Nagaura, *Electrochim. Acta* **17** (1972) 2249.
- [22] A.G.C. Kobussen, PhD thesis, University of Utrecht (1981) p. 44-46.
- [23] J.O'M. Bockris, D. Drazic and A.R. Despic, *Electrochim. Acta* **4** (1961) 325.
- [24] K.E. Heusler, in 'Encyclopedia of Electrochemistry of the Elements', Vol. IX part a, (edited by A.J. Bard), Marcel Dekker Inc., New York (1982) p..300.

## 5. Stability of suspensions of polystyrene particles in a zinc deposition electrolyte

### 5.1 Introduction

Particles suspended in an electrolyte are present either as single particles or multiple particle aggregates. The suspension stability is determined by the resistance of a suspension to form aggregates. As discussed in chapter 2, suspension stability affects the codeposition of particles in electrochemical composite plating. Stable suspensions yield composites with a higher particle content [1-6]. Moreover, in industrial practice aggregation is undesired, because it could lead to sedimentation or creaming of particles in storage tanks and clogging of pipelines.

Particle aggregation is determined by the competitive action of attractive and repulsive forces acting between particles. According to the DLVO theory van der Waals attraction and electro-osmotic repulsion are the most important [7,8]. The electro-osmotic force arises from the overlap of the electrical double layers of particles. The electrical double layer is a result of the particle charge and its thickness depends on the electrolyte concentration. In highly concentrated electrolytes the charge of suspended particles is completely shielded by the electrolyte ions resulting in a very thin double layer. Consequently, the electro-osmotic force is negligible and particles aggregate.

Addition of a surfactant can improve suspension stability. Surfactant molecules consist of a hydrophobic and hydrophilic part [9]. When present in a suspension the hydrophobic groups preferentially adsorb on the particles. Mutual repulsion between the hydrophilic groups on different particles stabilizes the suspension. Ionic surfactants augment the electro-osmotic force due to the charge of the hydrophilic group. Alternatively, steric repulsion between large uncharged hydrophilic groups of non-ionic surfactants can prevent particle aggregation.

The physical properties of a suspension, like the conductivity and viscosity, are strongly affected by particle aggregation. Particularly, the rheological behaviour of suspensions is

indicative for their stability [10]. In chapter 6 composite plating from a zinc deposition electrolyte containing suspended polystyrene (PS) particles will be discussed. Since this is a highly concentrated electrolyte it is likely that the PS particles aggregate. The stability of PS particles suspended in a Zn deposition electrolyte was studied using rheological measurements, conductivity measurements and optical microscopy. The effect of several surfactants, in particular cetylpyridinium chloride (CPC), on these properties will be discussed.

## **5.2 Experimental details**

A  $450 \text{ kg m}^{-3} \text{ ZnSO}_4 \cdot 7\text{H}_2\text{O}$ ,  $30 \text{ kg m}^{-3} \text{ H}_3\text{BO}_3$  and  $30 \text{ kg m}^{-3} \text{ Al}_2(\text{SO}_4)_3 \cdot 18\text{H}_2\text{O}$  solution with pH 3 was the zinc deposition electrolyte used. Polystyrene particles with a number average diameter of  $0.8 \mu\text{m}$  were prepared by a surfactant-free emulsion polymerization [11]. After removal of reaction residues by repetitive centrifugation and redispersion, the particles were stored as a 20 wt% suspension in water. Scanning Electron Microscope (SEM) photographs and particle size measurements show that the particles are spherical and practically monodisperse. The degree of polydispersity, that is the volume average diameter divided by the number average diameter, is 1.07. Suspensions were prepared by adding the required amounts of water and the 20 wt% PS suspension to a concentrated zinc deposition electrolyte. Surfactants were added in salt form or as a concentrated solution in water. In all experiments a large excess of surfactant was used (see Chapter 6). The surfactant concentration will be expressed as the amount of moles of surfactant per kg of suspended particles.

The rheological behaviour of the suspensions was studied using a thermostated Brookfield DV II with spindle geometry 00, which is a concentric cylinder type viscometer. An automatic Ubbelohde viscometer containing an 53210/I Ubbelohde capillary was used to measure the viscosity of the particle-free electrolyte. The suspensions were put in an ultrasonic bath for 5 minutes before each measurement. The conductivity of the suspensions was measured using a Philips PW9550/60 conductivity cell with a cell constant of  $87 \text{ m}^{-1}$  connected to a Radiometer CDM2 conductivity meter. A magnetic stirrer was used to prevent particle creaming during the conductivity measurements.

## 5.3 Results

### 5.3.1 Suspension rheology

The viscosity,  $\mu$ , of a fluid is defined as:

$$\mu = \frac{\tau}{\dot{\gamma}} \quad (5.1)$$

where  $\dot{\gamma}$  is the shear rate and  $\tau$  the shear stress [8]. The shear stress was measured at different shear rates in suspensions of various PS volume fractions at three different temperatures. Since the accuracy of the measured shear stress is very low at low shear rates only data at high shear rates are considered. Figure 5.1 shows  $\tau$  against  $\dot{\gamma}$  at various volume fractions  $\phi_{PS}$  at 298 K. At  $\phi_{PS} > 0.01$ , thixotropy, that is a variation in shear stress with time, was observed. The presented data were measured 15 s after a change in shear rate. It was checked that data taken at different times after a change in shear rate give qualitatively similar results.

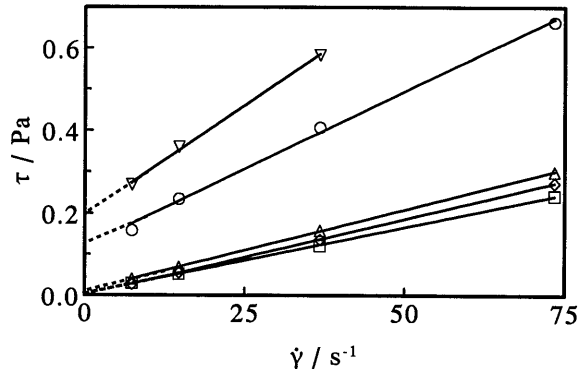


Figure 5.1: Shear stress as a function of the applied shear rate for various amounts of PS particles suspended in Zn deposition electrolyte at 298 K,  $\phi_{PS}$ : 0 ( $\diamond$ ); 0.01 ( $\triangle$ ); 0.05 ( $\circ$ ); 0.08 ( $\nabla$ ); 0.05 + 0.2 mol kg<sup>-1</sup> CPC ( $\square$ ), Lines represent linear fits.

An approximately linear relationship between shear rate and shear stress is observed for all suspensions, but extrapolation to  $\dot{\gamma} = 0$  yields a finite intercept for  $\phi_{PS} > 0.01$ . Defining the slope as  $\mu_\infty$  and the intercept at  $\dot{\gamma} = 0$  as  $\tau_0$  the apparent relation between the shear rate and shear stress can be written as:

$$\tau = \tau_0 + \mu_\infty \dot{\gamma} \quad (5.2)$$

Values of  $\tau_0$  were obtained from  $\tau$  against  $\dot{\gamma}$  curves and are given for various volume fractions PS and at three different temperatures in Table 5.1. At  $\phi_{PS} < 0.01$   $\tau_0$  is approximately equal to 0 when the experimental accuracy is taken into account. An increase in  $\tau_0$  with the amount of suspended particles and with increasing temperature is found. Addition of 0.2 mol kg<sup>-1</sup> CPC reduces  $\tau_0$  to approximately 0 as is shown for  $\phi_{PS} = 0.05$  in Figure 5.1.

Table 5.1: Values of  $\tau_0$  for various  $\phi_{PS}$  in the absence of surfactant and at three different temperatures.

$\phi_{PS}$	$\tau_0 / \text{Pa}$		
	298 K	318 K	333 K
0.001	0.00	0.00	0.00
0.006	0.00	0.00	0.01
0.01	0.01	0.01	0.01
0.05	0.12	0.22	0.31
0.08	0.20	0.31	0.46

From the previous experiments the suspension viscosity can be calculated using equation (5.1), which after substitution of equation (5.2) yields:

$$\mu = \mu_\infty + \frac{\tau_0}{\dot{\gamma}} \quad (5.3)$$

The viscosity of the zinc deposition electrolyte, measured using the Ubbelohde viscometer, is given in Table 5.2 for 3 different temperatures. At 298 K a value of  $3.2 \cdot 10^{-3}$  Pa s is found, which agrees with the value of  $3.7 \cdot 10^{-3}$  Pa s obtained using the Brookfield viscometer. As

required for a particle-free electrolyte the viscosity is independent of the shear rate and it decreases with increasing temperature [8].

Several mathematical equations have been proposed to describe the dependence of the suspension viscosity on the particle volume fraction [12,13]. It is evident from Table 5.1 and equation (5.3) that in the presence of electrolyte the suspension viscosity for  $\phi_{PS} > 0.01$  strongly depends on the shear rate. It has been found that in such cases the reduced suspension viscosity  $\mu_r = \mu_s / \mu_c$ , where  $\mu_s$  is the suspension viscosity and  $\mu_c$  is the viscosity of the continuous phase, in the high shear limit is given by the Krieger-Dougherty equation:

$$\mu_r = \left(1 - \frac{\phi}{\phi_m}\right)^{-[\mu]\phi_m} \quad (5.4)$$

where  $\phi$  is the volume fraction suspended particles,  $\phi_m$  is the maximum particle volume fraction and  $[\mu] = \lim_{\phi \rightarrow 0} (\mu_r - 1)/\phi$  is the intrinsic viscosity [10].

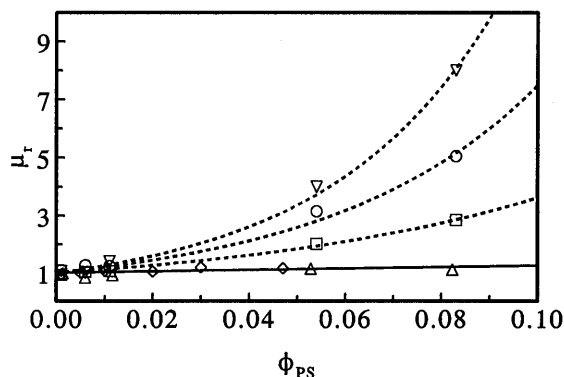


Figure 5.2: Reduced suspension viscosity for various volume fractions of PS particles suspended in: water at 298 K ( $\Delta$ ); electrolyte at 298 K ( $\square$ ); 318 K ( $\circ$ ); 333 K ( $\nabla$ ) and electrolyte + 0.2 mol kg<sup>-1</sup> CPC at 298 K ( $\diamond$ ), solid line represents Einstein equation and broken lines represent fitted Krieger-Dougherty equation.

For a suspension of spherical particles and for  $\phi < 0.05$  the Krieger-Dougherty equation reduces to the Einstein equation:

$$\mu_r = 1 + 2.5\phi \quad (5.5)$$

From equation (5.3) it follows that the viscosity in the high shear limit, that is  $\dot{\gamma} \rightarrow \infty$ , is  $\mu_\infty$ . In Figure 5.2 the reduced viscosity in the high shear limit is shown at various volume fractions PS in water at 298 and in zinc deposition electrolyte at three different temperatures. It shows a good agreement between equation (5.5) and the reduced viscosity measured for suspensions of various volume fractions PS in water.

Table 5.2: Viscosity of Zn deposition electrolyte and intrinsic viscosity of PS suspensions at different temperatures.

T / K	$\mu_c$ / Pa	$[\mu] \dot{\gamma} \rightarrow \infty$
298	$3.2 \cdot 10^{-3}$	$11 \pm 1$
318	$2.5 \cdot 10^{-3}$	$17 \pm 2$
333	$2.0 \cdot 10^{-3}$	$24 \pm 2$

Apparently due to the agglomeration of the particles in the presence of the zinc deposition electrolyte the measured values of the reduced viscosity at  $\dot{\gamma} \rightarrow \infty$  deviate strongly from equation (5.5) even at  $\phi = 0.005$ . These values can be fitted with equation (5.4), although the suspensions are too dilute to determine  $\phi_m$  accurately. The fits are represented by the broken lines in Figure 5.2 and the values obtained for  $[\mu] \dot{\gamma} \rightarrow \infty$  are given in Table 5.2. The intrinsic viscosities are very high compared to those reported by Barnes et.al. [10] for various suspensions. In the presence of  $0.2 \text{ mol kg}^{-1}$  CPC the suspension viscosity is independent of shear rate and varies with the volume fraction PS particles according to the Einstein equation (Figure 5.2).

### 5.3.2 Conductivity

A suspended phase, for example gas bubbles, liquid droplets or solid particles, changes the conductivity of an electrolyte [14-16]. Several mathematical relations have been proposed to describe the change in conductivity of a suspension with the amount of suspended phase. De



La Rue and Tobias [15] have shown that the degree of polydispersity of the suspended phase decides which relation should be used for a particular suspension. The conductivity,  $\kappa_s$ , of a suspension of monodisperse spherical particles is given by the Maxwell equation:

$$\kappa_s = \kappa_c \frac{\left( \frac{\kappa_p}{\kappa_c} + 2 - 2\phi \left( 1 - \frac{\kappa_p}{\kappa_c} \right) \right)}{\left( \frac{\kappa_p}{\kappa_c} + 2 + \phi \left( 1 - \frac{\kappa_p}{\kappa_c} \right) \right)} \quad (5.6)$$

where  $\kappa_c$  is the conductivity of the continuous phase and  $\kappa_p$  is the conductivity of the suspended particles. For a dilute suspension ( $\phi < 0.1$ ) and isolating particles, that is  $\kappa_p \ll \kappa_c$ , this equation reduces to:

$$\kappa_r = \frac{\kappa_s}{\kappa_c} = \left( 1 - \frac{3}{2}\phi \right) \quad (5.7)$$

where  $\kappa_r$  is the reduced suspension conductivity.

Figure 5.3 shows equation (5.7) and the reduced conductivity measured for various volume fractions of PS particles suspended in Zn deposition electrolyte. A deviation from the Maxwell relation is observed. However, strong adsorption of the PS particles on the electrodes of the conductivity cell was noticed. When 0.2 mol kg<sup>-1</sup> CPC is added a good agreement with the Maxwell relation is found (Figure 5.3).

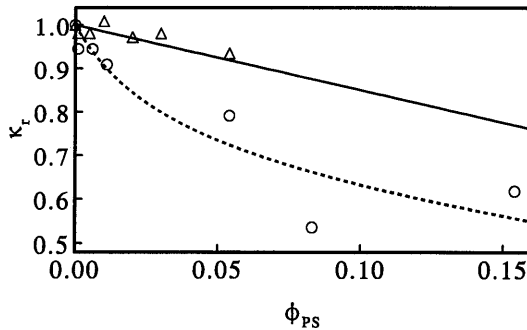


Figure 5.3: Reduced conductivity of Zn deposition electrolyte containing various amounts of PS particles,  $c^*_{cpc} = 0$  (O) and 0.2 mol kg<sup>-1</sup> ( $\Delta$ ), solid line represents Maxwell equation.

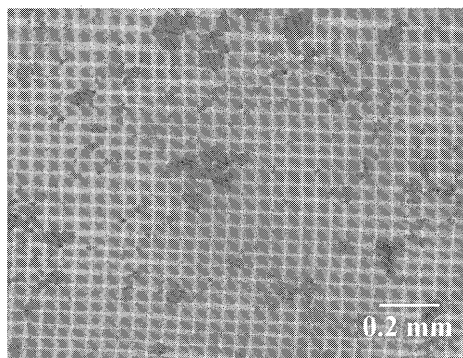
### **5.3.3 Microscopical observation**

Optical microscope photographs of dilute suspension of PS particles ( $\phi_{PS} = 0.004$ ) in the Zn deposition electrolyte without and with addition of  $0.4 \text{ mol kg}^{-1}$  CPC or SDS are shown in Figure 5.4(a)-(c). Figure 5.4(a) shows the presence of large aggregates in the absence of surfactant. Addition of CPC, a cationic surfactant, still yields a suspension containing aggregates, but their size is strongly reduced (Figure 5.4(b)). The same is found on addition of another cationic surfactant, that is cetyltrimethylammonium bromide (CTAB). In the presence of the anionic surfactant sodium dodecylsulphate (SDS) no particle aggregation can be distinguished (Figure 5.4(c)). Finally, a suspension with nonylphenol(ethoxylate)<sub>28</sub> (propoxylate)<sub>13</sub> (NPE1800) [17], a non-ionic surfactant, contains aggregates similar to those seen in the absence of surfactant.

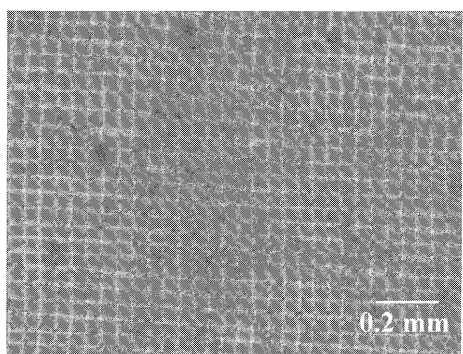
### **5.4 Discussion**

Aggregation of particles in dilute suspensions ( $\phi < 0.3$ ) is evidenced by deviations from Newtonian viscous behaviour [18]. Newtonian fluids have a viscosity independent of the applied shear rate. Hence, the observed changes in viscosity with shear rate for suspensions with  $\phi > 0.01$  signify strong aggregation of the PS particles in the Zn deposition electrolyte. This is supported by the observation of large aggregates. The high electrolyte concentration strongly reduces the electrical double layer thickness of the PS particles leading to a net attraction between particles.

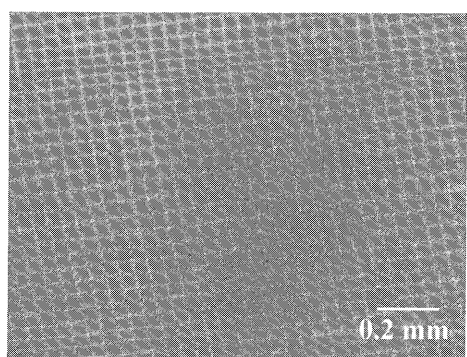
Apart from interaction forces between particles, aggregation is also affected by the Brownian motion of particles and the hydrodynamic conditions [7,10,18]. The equilibrium between aggregate formation due to particle collisions and aggregate break up due to shearing forces determines the aggregate structure. A change in shear rate results in a change in aggregate structure and thus viscosity. The observed thixotropy at  $\phi_{PS} > 0.01$  is a result of the time necessary to establish the new equilibrium after a change in shear rate. The measured viscosity is either too high or too low depending on the shear history of the suspension. From equation (5.3) it can be deduced that the viscosity of the PS suspensions decreases with increasing shear rate. The PS suspensions in Zn deposition electrolyte are shear thinning. The



(a)



(b)



(c)

Figure 5.4: Optical Microscope photographs of PS suspension in the presence of various surfactants,  $\phi_{PS} = 0.004$ ,  $c^*_{surf} = 0.4 \text{ mol kg}^{-1}$ ; (a) Surfactant free; (b) CPC; (c) SDS.

---

empirical equations (5.2) and (5.3) are characteristic for so-called Bingham plastic rheological behaviour, which is often exhibited by aggregating suspensions [18,19]. Here  $\tau_0$  can be identified with an apparent yield stress.

In the high shear rate limit the hydrodynamic forces dominate yielding an approximately disaggregated particle structure, which allows continuous shearing. Here non-Newtonian effects are absent, because aggregate formation is negligible compared to aggregate break-up. However, the strong deviation from the Einstein relation of the reduced  $\mu_\infty$  and the high values of  $[\mu] \dot{\gamma} \rightarrow \infty$  obtained with the Krieger-Dougherty relation indicate that aggregates are still present. It can be concluded that shearing is approximately continuous in the investigated range of shear rates, but higher shear rates are required to completely break-up the PS particle aggregates.

If the shear rate is lowered the Brownian motion and the interaction forces become increasingly important. The aggregate size increases resulting in a larger resistance against shearing, that is a higher viscosity. In the low shear rate limit of the Bingham model this would lead to an infinite viscosity. Here a rigid three-dimensional aggregate structure is formed, which can only be sheared at shear stresses larger than  $\tau_0$ . In reality the suspension can always be sheared to some extent and at low shear rates a finite viscosity is reached. In the dilute PS suspensions,  $\phi_{PS} < 0.01$ , the interparticle distances are so large that a rigid three-dimensional aggregate structure can hardly be formed and  $\tau_0 \approx 0$ . At higher  $\phi_{PS}$  the formation of such a rigid structure becomes increasingly feasible, which is evidenced by increasing values of  $\tau_0$ .

The increase of  $\tau_0$  and  $[\mu] \dot{\gamma} \rightarrow \infty$  with increasing temperature implies that aggregate formation is more effective at higher temperatures. Irrespective of the PS volume fraction the viscosity was found to decrease with temperature. Thus, at a certain value of  $\dot{\gamma}$   $\tau$  decreases with increasing temperature. As a consequence aggregate break up is less effective at higher temperature. Moreover the lower viscosity leads to faster aggregation at higher temperatures. If during the measurements aggregation was not yet complete this yields a higher  $\tau_0$  and  $[\mu] \dot{\gamma} \rightarrow \infty$  at higher temperatures.

The deviation of the reduced conductivity from the Maxwell equation is not solely a result of the particle aggregation. Particle aggregation can be described by taking into account a

---

agglomerate volume fraction, that is the volume fraction of particles in an agglomerate, and a finite agglomerate conductivity [19]. It can be shown that the change in conductivity with particle volume fraction would be different when this is done. The adsorption of PS particles on electrodes of the conductivity cell also decreases the measured conductivity. A particle-rich layer adjacent to the surface of the electrodes is created with a conductivity lower than that of the bulk suspension. This is similar to bubble layers formed adjacent to electrodes of gas-evolving cells [20]. As a result the overall measured conductivity is lower than that of the bulk suspension.

The observed aggregates in the presence of CPC suggests that CPC is not able to stabilize the PS particles suspended in zinc deposition electrolyte. In contrast the variation of the reduced suspension viscosity and conductivity with the volume fraction PS are indicative of a stable suspension. A sheared suspension containing CPC behaves as stable suspension of monodisperse non-conducting spherical particles. The additional charge conferred on the PS particles by adsorbed CPC molecules is still largely shielded by the electrolyte, but a small shear is sufficient to break up the aggregates into single particles.

It was found that also CTAB and SDS can be used to stabilize a suspension of PS particles in Zn deposition electrolyte. The absence of aggregates in the presence of SDS implies that the negative charge conferred on the particles by SDS is less effectively shielded by the electrolyte than the positive charge conferred by CPC or CTAB. In a concentrated electrolyte a non-ionic surfactant is expected to be a better stabilizer than a ionic one. It stabilizes through steric repulsion, which is independent of the electrolyte concentration. However, large aggregates were observed in the presence of NPE1800. Probably steric repulsion is prevented by bridging between the hydrophilic chains of surfactant molecules adsorbed on different particles. Hydroxide species, like  $\text{Al}(\text{OH})_3$  or  $\text{B}(\text{OH})_4$  [21], present in the electrolyte are able to form hydrogen bridges with the propoxylate and ethoxylate chains of NPE1800 [7].

## 5.5 Conclusions

Polystyrene particles strongly aggregate in the Zn deposition electrolyte. Due to the aggregation PS suspensions exhibit a Bingham type of non-Newtonian rheological behaviour. Particularly

---

suspensions with  $\phi_{PS} > 0.01$  show strong changes in viscosity with hydrodynamic conditions and time. Addition of CPC or other ionic surfactants, like CTAB and SDS, stabilizes the PS suspensions. Although particle aggregates are still formed in the presence of CPC a small shear is sufficient to break them up into single particles. The viscosity and conductivity of CPC containing suspensions are characteristic for suspensions of non-interacting monodisperse and spherical particles. Bridging between the hydrophilic chains of different surfactant molecules prevents NPE1800, a non-ionic surfactant, from stabilizing PS suspension.

## References

- [1] K. Helle, Report AKZO Research, Arnhem (1993).
- [2] K. Helle, Proceedings, 4th International Conference in Organic Coating Science and Technology, Athens (1978) 264.
- [3] P.K.N. Bartlett, Industrial training report AKZO, Arnhem (1980) p. 10-39.
- [4] K. Meguro, T. Ushida, T. Hiraoka and K. Esumi, *Bull. Chem. Soc. Jpn.* **60** (1987) 89.
- [5] Y-S. Chang and J-Y. Lee, *Mater. Chem. Phys.* **20** (1988) 309.
- [6] S. Alexandridou, C. Kiparissidis, J. Fransaer and J.P. Celis, *Surf. Coat. Technol.* **71** (1995) 267.
- [7] K. Strenge and K. Mühle, in 'Coagulation and Flocculation', Surfactant Science Series 47, (edited by B. Dobiáš), Marcel Dekker Inc., New York (1993) p 265-320, p 355-390.
- [8] R.F. Probstein, 'Physicochemical Hydrodynamics', 2nd ed., J. Wiley & Sons Inc., New York (1994) p.237-256, 277-302.
- [9] M.R. Porter, 'Handbook of Surfactants', 2nd ed., Blackie Academic and Professional, Glasgow (1994) p 26.
- [10] H.A. Barnes, J.F. Hutton and K. Walters, 'An Introduction to Rheology', Elsevier Science Publishers BV, Amsterdam (1989) p.115-139.
- [11] G. Tuin, A.C.I.A. Peters, A.J.G. van Diemen and H.N. Stein, *J. Colloid Interface Sci.* **158** (1993) 508.

- [12] M. Mooney, *J. Colloid Sci.* **6** (1951) 162.
- [13] D.G. Thomas, *J. Colloid Sci.* **20** (1965) 267.
- [14] R.E. De La Rue and C.W. Tobias, *J. Electrochem. Soc.* **106** (1959) 827.
- [15] R.E. Meredith and C.W. Tobias, *J. Electrochem. Soc.* **108** (1961) 286.
- [16] R.E. Meredith and C.W. Tobias, in 'Advances in electrochemistry and electrochemical engineering', Vol. 2, (edited by P. Delahay and C.W. Tobias), J. Wiley & Sons, New York (1962) p. 15-47.
- [17] A. van den Boomgaard, PhD thesis, Agricultural University of Wageningen (1985).
- [18] J. Laven, F.J. Huisman, L.J. Lalieu and H.N. Stein, *Colloids and Surfaces* **31** (1988) 385.
- [19] P.J. Sonneveld, PhD Thesis, Eindhoven University of Technology (1991) p.76-82.
- [20] L.J.J. Janssen and G.J. Visser, *J. Appl. Electrochem.* **21** (1991) 386.
- [21] C.F. Baes and R.E. Mesmer, 'The Hydrolysis of Cations', J. Wiley & Sons, New York (1976) p. 104-111.





## **6. Effect of surfactants on the electrochemical codeposition of zinc and polystyrene particles**

### **6.1 Introduction**

The codeposition of polystyrene (PS) particles with zinc was investigated as a model system for the electrochemical composite plating of the applicable metal-polymer composites. As shown in the previous chapter PS particles aggregate in zinc deposition electrolyte. Surfactants are needed to obtain a stable suspension. In electrochemical composite plating a cationic surfactant is preferred (section 2.3.5). The positive charge conferred on the particles by a cationic surfactant increases their attraction to the negatively charged cathode, where they codeposit [1-3]. In this chapter the effect of a cationic surfactant, namely cetylpyridinium chloride (CPC), on the codeposition of PS particles and zinc will be presented and compared to that of several other surfactants.

Apart from suspension stability successful industrial application of composite plating requires operation at conditions similar to those used in conventional metal plating. Sufficient particle codeposition should be obtained under turbulent flow conditions and at high current densities, typically  $5\text{-}10\text{ kA m}^{-2}$ . A rotating cylinder electrode (RCE) was used to obtain turbulent flow conditions. The variation in PS incorporation in zinc, both in the absence and presence of CPC, with rotation speed of the RCE, current density and particle electrolyte concentration will be discussed.

### **6.2 Experimental Details**

A  $450\text{ kg m}^{-3}\text{ ZnSO}_4\cdot 7\text{H}_2\text{O}$ ,  $30\text{ kg m}^{-3}\text{ H}_3\text{BO}_3$  and  $30\text{ kg m}^{-3}\text{ Al}_2(\text{SO}_4)_3\cdot 18\text{H}_2\text{O}$  solution operating at pH 3 and 318 K was the electrolyte used for Zn deposition. The PS particles and suspension preparation were described in the previous chapter. A fresh suspension was prepared and stirred for at least 2 hours before every series of experiments. A series of experiments in the

same suspension comprised the variation of only one experimental parameter. When varying surfactant concentration fixed quantities of surfactant were progressively added to the same suspension. The same surfactants as in the previous chapter with addition of cetyltrimethylammonium bromide (CTAB), a cationic surfactant, were used. CPC, CTAB and SDS were added in salt form, while NPE1800 and CTAC were added as a concentrated solution in water. After each addition the suspension was stirred for 45 minutes to allow the surfactant adsorption equilibrium to be established. All surfactant concentrations will be expressed as the amount of moles of surfactant per kg of PS particles.

Zn-PS composites were deposited galvanostatically in a 400 cm<sup>3</sup> thermostated cylindrical glass vessel with a PVC cover. A RCE holding interchangeable Al-cylinders with an active area of 6.7 cm<sup>2</sup> was used as cathode. Zn sheet fitted against the inner vessel wall served as anode. After degreasing and rinsing the RCE was placed in the centre of the vessel concentric with the vessel wall. In the presence of surfactant the required cell voltage was applied before the RCE was lowered into the vessel, to avoid obstruction of Zn deposition by strong surfactant adsorption onto the Al-substrate. At a rotation speed,  $\omega$ , larger than 6 s<sup>-1</sup> the RCE operates under turbulent flow conditions [4].

After deposition the substrate and deposit were rinsed, dried and weighed. Subtraction of the weight of the Al-cylinder before deposition gave the deposit weight. The PS particles were extracted from the deposit by dissolving Zn in 4 M H<sub>2</sub>SO<sub>4</sub> through galvanic coupling the Al-cylinder to Pt-sheet. Occasionally a few drops of 35% H<sub>2</sub>O<sub>2</sub> were needed to dissolve traces of Zn adhering to released particles. The extracted PS particles were recovered over a 0.2  $\mu$ m pore-size filter by vacuum filtration. After drying at 353 K for 90 minutes and cooling down to room temperature under vacuum, the amount of codeposited PS was obtained from the weight difference between the filter before and after filtration. Taking 1050 kg m<sup>-3</sup> and 6500 kg m<sup>-3</sup> for the density of the PS particles and zinc respectively, the volume fraction included PS,  $\alpha_{PS}$ , was calculated. It was found that using this analysis method measurements under the same experimental conditions in the same suspension were reproducible within 15 %. Measurements under the same experimental conditions in different suspensions showed larger discrepancies, but trends were always reproduced.

A few composite deposits were studied using a Cambridge Stereoscan S200 scanning electron microscope (SEM) before composition analysis. Additionally, composites prepared in a 250 cm<sup>3</sup> Hull-cell were investigated. The trapezoidal shape of a Hull-cell allows simultaneous deposition at a range of current densities. A low-alloy steel cathode was placed in the Hull cell at an oblique angle to a zinc anode. After a potential was applied over the electrodes 250 cm<sup>3</sup> electrolyte suspension, preheated to 318 K, was added. The current was adjusted to 3 A and for 900 s a composite was deposited at current densities ranging from 50 to 1500 A m<sup>-2</sup>. During an experiment the continuously stirred electrolyte suspension was not heated. The composite deposit was thoroughly rinsed with water and acetone and dried. A thin Au coating was sputtered on to samples cut from the deposit to enable the observation of the non-conducting PS-particles.

The adsorption of CPC on the PS particles in the zinc deposition electrolyte and in water was studied using the soap titration method developed by Maron et.al. [5-7]. The surface tension of electrolyte suspensions and the conductivity of electrolyte-free suspensions was monitored as a function of the CPC concentration. CPC was added to suspensions as a 0.3 or 17 mol m<sup>-3</sup> solution in steps ranging from 0.01 to 0.5 cm<sup>3</sup>. After CPC addition the suspensions were stirred for 10 minutes before a measurement was done. The surface tension was measured using a Krüss K10T tensiometer equipped with a Pt Wilhelmy-plate. Suspensions were contained in a 50 cm<sup>3</sup> glass vessel, which was repeatedly rinsed with distilled water and acetone and heated in a gas flame before a titration. The Wilhelmy-plate was equally treated before each single measurement. It was allowed to gain thermal equilibrium for 10 minutes before the surface tension was recorded. Conductivity measurements were done using a Philips PW9550/60 conductivity cell connected to a Radiometer CDM2 conductivity meter. During measurements the suspensions were continuously stirred in a 100 cm<sup>3</sup> glass beaker. All titrations were performed at room temperature.

## 6.3 Results

### 6.3.1 Surfactant adsorption

When investigating the effect of surfactant concentration on codeposition the adsorption of the surfactant on the particles has to be considered. Only adsorbed surfactant contributes to suspension stability and particle-cathode interaction. Moreover, free surfactant, that is surfactant not adsorbed on particles, adsorbs on the cathode, which could affect deposit properties. The optimal surfactant concentration for codeposition is the concentration where the adsorption of the surfactant on the particles is maximal [1,3]. Maximum surfactant adsorption is attained at the critical micelle concentration (c.m.c.) of the surfactant.

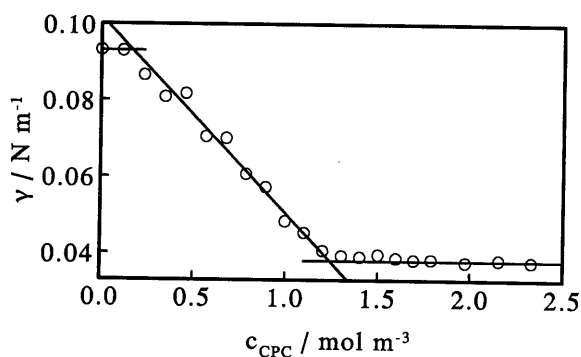


Figure 6.1: Surface tension of zinc deposition electrolyte containing PS particles at various concentrations CPC;  $\phi_{\text{PS}} = 0.054$ . Solid lines are linear fits.

Curves of the surface tension or conductivity of a solution against the total surfactant concentration exhibit a change in slope at the c.m.c. [5-7]. Figure 6.1 shows the surface tension,  $\sigma$ , of the zinc deposition electrolyte containing a volume fraction PS particles,  $\phi_{\text{PS}}$ , of 0.054 on addition of CPC. At  $c = 1.2 \text{ mol m}^{-3}$  the c.m.c. is reached and the surface tension becomes constant. Here the total concentration of surfactant,  $c$ , is equal to the sum of the c.m.c. and the maximum concentration of adsorbed surfactant,  $c_a$ . From equivalent measurements at different volume fractions PS the c.m.c. and the maximum amount of CPC adsorbed per kg of PS particles,  $c_a^*$ , were determined and are given in Table 6.1. Correspondingly values for  $c_a^*$  and

## 6. Effect of surfactants on the electrochemical codeposition of zinc and polystyrene particles

---

the c.m.c. in an electrolyte-free suspension were obtained from conductivity measurements (Table 6.1). The value found for  $c^*_a$  in water is comparable to data reported for adsorption of other surfactants on similar PS particles [8-11]. In the electrolyte  $c^*_a$  is higher and the c.m.c. is lower than in water, because, shielding of the surfactant charge by the electrolyte ions allows surfactant molecules to approach each other more closely.

Table 6.1: Parameters obtained for the adsorption of CPC on PS particles suspended in zinc deposition electrolyte and water.

	$c^*_a / \text{mol kg}^{-1}$	c.m.c. / $\text{mol m}^{-3}$	$c^*_{a,\text{dis}} / \text{mol kg}^{-1}$
electrolyte	0.021	$4 \cdot 10^{-4}$	0.003
water	0.015	0.99	0.005

It is clear from Figure 6.1 and Table 6.1 that at  $\phi_{\text{PS}} = 0.054$  the c.m.c. in the zinc deposition electrolyte is negligible compared to the total concentration of CPC. In fact for all volume fractions PS of interest, that is  $\phi_{\text{PS}} > 0.001$ , the c.m.c.  $\ll c$  and consequently  $c \approx c_a$ . It can be concluded that to obtain maximum CPC adsorption a total amount of  $c^* = 0.021 \text{ mol CPC kg}^{-1}$  of PS particles has to be added. From [8-10] it may be deduced that  $c^*$  for CTAB, CTAC and SDS will be close to that of CPC, while for NPE1800 [11] it will be a factor of 2 to 5 lower. Besides at the c.m.c. in Figure 6.1 another change in slope can be seen at  $c = 0.16 \text{ mol m}^{-3}$ . A discontinuity at very low concentration is found in the presence of suspended particles at all volume fractions both in water and in the electrolyte. The total CPC concentration at the discontinuity increases linearly with the amount of suspended particles. The amount of CPC adsorbed on the particles at the discontinuity,  $c^*_{a,\text{dis}}$ , was calculated and is given in Table 6.1. The discontinuity results from the compensation of the negative charge of the particles by the positively charged CPC molecules [8,10]. The PS particles are negatively charged due to sulphate surface groups formed during particle synthesis. Tuin and Stein [9] measured a value of  $0.0863 \text{ C m}^{-2}$  for the charge density of PS particles in water prepared with the same method. If it is assumed that each sulphate group is compensated for by one CPC molecule it can be calculated that  $0.006 \text{ mol CPC kg}^{-1}$  is required to compensate for this charge. This is

very close to the  $c_{a,d}^*$  obtained in water. In the electrolyte  $c_{a,d}^*$  is lower, because the particle charge is lowered by complexation of the sulphate groups with cations from the electrolyte.

### 6.3.2 Surfactant type and concentration

The amount of PS codepositing from suspensions with  $\phi_{PS} = 0.02$  was determined as a function of concentration of various surfactants. The results are shown in Figure 6.2 for CPC, SDS and NPE1800 and in Figure 6.3 for CPC, CTAB and CTAC.

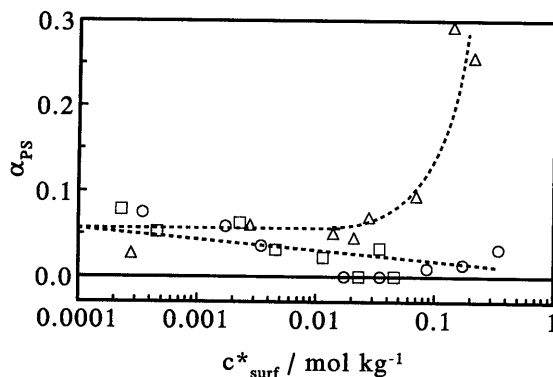


Figure 6.2: Volume fraction of codeposited PS particles against the concentration of various surfactants at  $j = 0.5 \text{ kA m}^{-2}$ ,  $\omega = 100 \text{ s}^{-1}$  and  $\phi_{PS} = 0.02$ ; CPC ( $\Delta$ ); SDS( $\circ$ ) and NPE1800 ( $\square$ ).

At surfactant concentrations lower than  $0.005 \text{ mol kg}^{-1}$  the volume fraction of codeposited PS is equal to that without surfactant, namely  $0.06 \pm 0.03$ , independent of surfactant type and concentration. In the presence of CPC codeposition remains constant up to the concentration at maximum adsorption. At higher concentrations CPC a strong increase, up to a factor of 3, in PS codeposition with  $c_{CPC}^*$  is found. On further addition of SDS or NPE1800 codeposition is reduced and for  $c^* > 0.01 \text{ mol kg}^{-1}$  no significant codeposition can be detected. A similar trend is found for CTAB and CTAC although the decrease in codeposition is less dramatic and occurs at slightly higher concentrations.

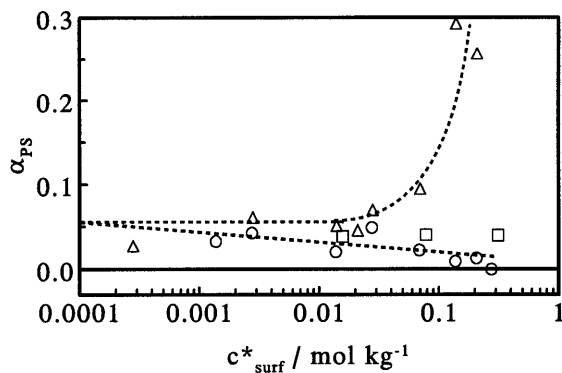


Figure 6.3: Volume fraction of codeposited PS particles against the concentration of three cationic surfactants at  $j = 0.5 \text{ kA m}^{-2}$ ,  $\omega = 100 \text{ s}^{-1}$  and  $\phi_{\text{PS}} = 0.02$ ; CPC ( $\Delta$ ); CTAB( $\circ$ ) and CTAC ( $\square$ ).

### 6.3.3 Particle concentration

In Figure 6.4 the effect of the amount of suspended PS particles on their codeposition with Zn is given at three different CPC concentrations. In accordance with Figure 6.2 and Figure 6.3 practically no difference in codeposition is found between a CPC-free suspension and one containing  $0.02 \text{ mol kg}^{-1}$  CPC. In the presence of  $0.2 \text{ mol kg}^{-1}$  CPC considerably higher codeposition is obtained. At all three CPC concentrations an increase in codeposition with the amount of suspended particles is found. As discussed in Chapter 2 usually the relation between  $\alpha$  and  $\phi$  resembles an Langmuir adsorption isotherm [12-14]. A Langmuir type adsorption isotherm can indeed be fitted through the data in Figure 6.4 as shown by the dotted lines. In the presence of  $0.2 \text{ mol kg}^{-1}$  CPC a very good fit is obtained if the measurements at  $\phi_{\text{PS}} > 0.035$  are neglected. At  $\phi_{\text{PS}} > 0.035$  the amount of codeposited PS is higher than expected from the Langmuir isotherm at lower  $\phi_{\text{PS}}$ . For  $c^*_{\text{CPC}} = 0$  and  $0.02 \text{ mol kg}^{-1}$  the use of a Langmuir isotherm is somewhat ambiguous due to the lower accuracy of these data.

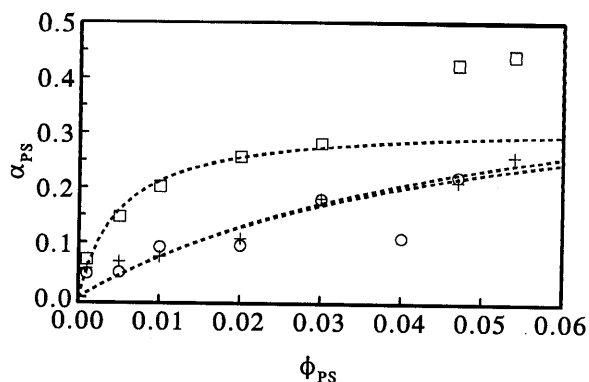


Figure 6.4: Volume fraction of codeposited PS particles against the volume fraction of suspended particles at several concentrations of CPC at  $j = 0.5 \text{ kA m}^{-2}$ ,  $\omega = 100 \text{ s}^{-1}$  and  $c_{CPC}^*$  is 0 (O);  $0.02 \text{ mol kg}^{-1}$  (+) and  $0.2 \text{ mol kg}^{-1}$  (□); Dotted lines are fits with a Langmuir isotherm.

### 6.3.4 Current density

The variation in PS codeposition with current density at  $\omega = 100 \text{ s}^{-1}$  is shown in Figure 6.5 with and without CPC addition. In the presence of  $0.2 \text{ mol kg}^{-1}$  CPC for  $j < 0.5 \text{ kA m}^{-2}$  on certain parts of the electrodes Zn deposition was inhibited by the deposition of a presumably organic material. In all cases PS codeposition is practically unaffected by the current density from  $j = 0.5$  to  $7.5 \text{ kA m}^{-2}$ . It can be concluded that considerable PS codeposition is obtained at current densities suitable for industrial application. For  $c_{CPC}^* = 0$  and  $0.02 \text{ mol kg}^{-1}$  a peak in the curve of  $\alpha_{PS}$  against current density is observed at  $0.05$  and  $0.2 \text{ kA m}^{-2}$  respectively. Similar peaks have been reported for various codeposition systems (see Chapter 2).

From the weight of deposited zinc and the applied current density the current efficiency for zinc deposition,  $\Gamma_{Zn}$ , was calculated using Faraday's law. Practically for all experimental conditions it was found that  $0.90 < \Gamma_{Zn} < 1$ . Taking into account the experimental accuracy this is close to the value of 1 generally reported for zinc deposition [15,16]. A change in  $\Gamma_{Zn}$  with the amount of suspended particles as observed for  $\Gamma_{Fe}$  in Chapter 4 is not found. Even on addition of surfactants no significant change in zinc deposition current efficiency was observed. Some



experiments showed a decrease in current efficiency at high PS codeposition, but no overall correlation between  $\Gamma_{Zn}$  and  $\alpha_{PS}$  is found.

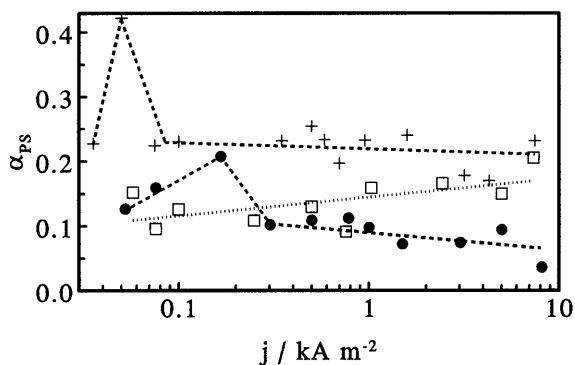


Figure 6.5: Volume fraction of codeposited PS particles against current density at  $\omega = 100 \text{ s}^{-1}$ ,  $\phi_{PS} = 0.02$  and  $c^*_{CPC} = 0$  (O);  $\phi_{PS} = 0.054$  and  $c^*_{CPC} = 0.02 \text{ mol kg}^{-1}$  (+);  $\phi_{PS} = 0.02$  and  $c^*_{CPC} = 0.2 \text{ mol kg}^{-1}$  (□).

### 6.3.5 Electrode rotation speed

Since all results presented so far were obtained with the RCE operating in the turbulent regime, it can be concluded that PS particles codeposit appreciably under turbulent flow. The effect of the electrode rotation speed on PS codeposition at  $j = 0.5 \text{ kA m}^{-2}$  is presented in Figure 6.6. PS codeposition in the presence of  $0.2 \text{ mol kg}^{-1}$  CPC does not vary with rotation speed up to  $\omega = 225 \text{ s}^{-1}$  and decreases with  $\omega$  at higher rotation speeds. On the other hand the amount of codeposited PS rises almost continuously with  $\omega$  in the presence of  $0.02 \text{ mol kg}^{-1}$  CPC. It has to be remarked that here at very low rotation speeds, that is  $\omega < 25 \text{ s}^{-1}$ , the RCE is not able to keep the aggregated particles suspended. This results in depletion of particles from the bulk of the suspension and lower codeposition.

In the absence of surfactant creaming of the electrolyte suspension at high rotation speeds was observed. On top of the suspension a layer of particle foam was formed, which could hardly be resuspended. The amount of PS codepositing at a certain rotation speed was seen to depend on

the experimental sequence. Codeposition from a suspension with  $\phi_{PS} = 0.04$  increased continuously in successive experiments despite the fact that the rotation speed was varied randomly. Moreover the volume fraction codeposited PS at  $\omega = 100 \text{ s}^{-1}$  was 3 times as high at the end of a series of experiments as at the start. Therefore, measurements at alternately high and low rotation speed,  $\omega = 400$  and  $25 \text{ s}^{-1}$  respectively, were performed in a  $\phi_{PS} = 0.02$  suspension. After 4 experiments a steady state is reached, where codeposition at both rotation speeds is constant. It was found that codeposition is highest at  $\omega = 400 \text{ s}^{-1}$ .

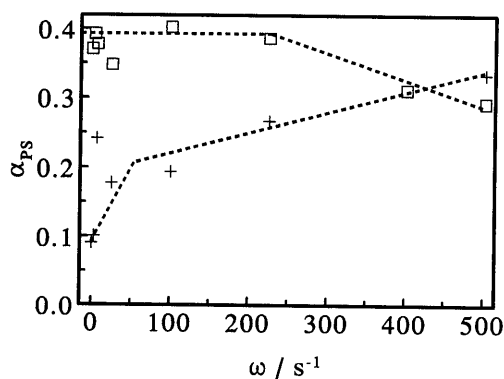


Figure 6.6: Volume fraction of codeposited PS particles against the electrode rotation speed at  $j = 0.5 \text{ kA m}^{-2}$ ,  $\phi_{PS} = 0.054$  and  $c^*_{CPC} = 0.02 \text{ mol kg}^{-1}$  (+);  $\phi_{PS} = 0.02$  and  $c^*_{CPC} = 0.2 \text{ mol kg}^{-1}$  (□).

### 6.3.6 Surface appearance and morphology

SEM photomicrographs of the surface of composites prepared in the Hull cell and the RCE are presented in Figure 6.7 - 6.9 and Figure 6.10 - 6.12 respectively. Zinc deposited in the current density range  $500 - 900 \text{ A m}^{-2}$  from a particle-free electrolyte appears dull light grey. Stacks of platelets orientated at random angles to the substrate, characteristic for zinc deposited from acidic  $\text{ZnSO}_4$  electrolytes [17,18] are produced (Figure 6.7). The platelets are several micrometers in size and are approximately hexagonally shaped. The disadvantage of

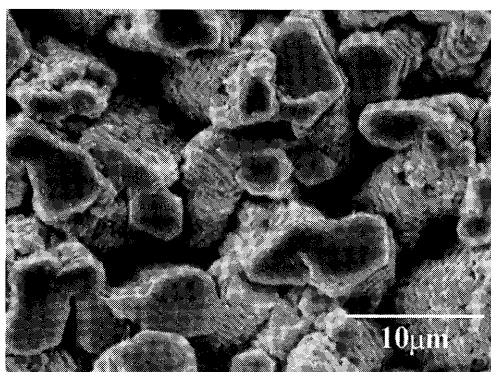


Figure 6.7: SEM photomicrograph of zinc surface morphology at  $500 < j < 900 \text{ A m}^{-2}$  (Hull cell).

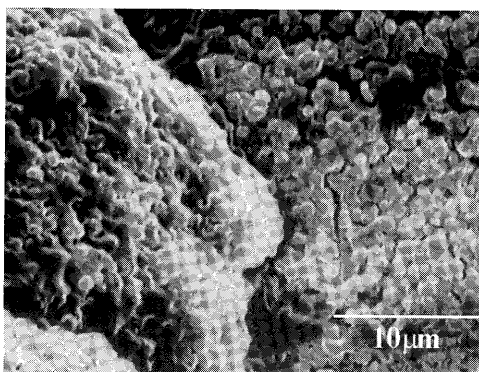


Figure 6.8: SEM photomicrographs of composite surface morphology;  $\phi_{\text{PS}} = 0.013$ ,  $c^*_{\text{CPC}} = 0.3 \text{ mol kg}^{-1}$  and  $500 < j < 900 \text{ A m}^{-2}$  (Hull cell).

using CPC is the reduced deposit quality. In the presence of  $0.3 \text{ mol kg}^{-1}$  CPC and  $\phi_{\text{PS}} = 0.013$  a black and brittle composite consisting of nodules of  $10 - 100 \mu\text{m}$  in diameter is formed (Figure 6.8). In between the nodules areas covered with the organic material mentioned in section 6.3.4 are present. PS particles can be observed in both areas, but zinc platelets can not be distinguished.

---

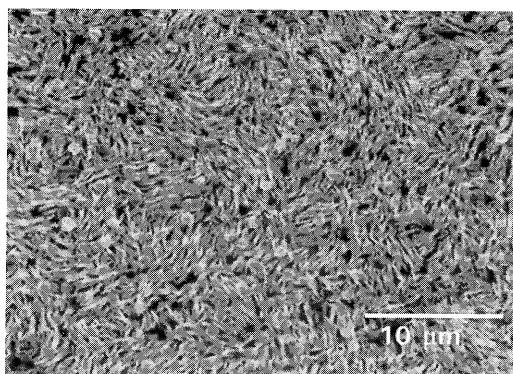


Figure 6.9: SEM photomicrograph of composite surface morphology;  $\phi_{PS} = 0.02$ ,  $c^*_{CTAC} = 0.3 \text{ mol kg}^{-1}$  and  $500 < j < 900 \text{ A m}^{-2}$  (Hull cell).

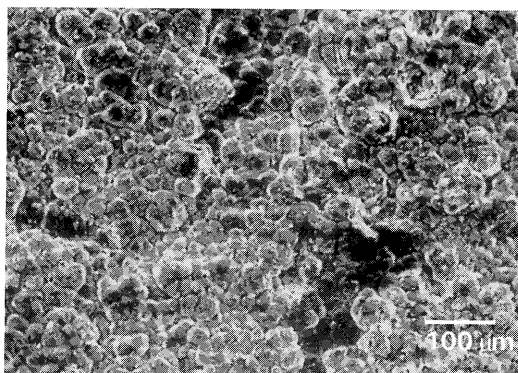


Figure 6.10: SEM photomicrograph of composite surface morphology;  $\phi_{PS} = 0.054$ ,  $c^*_{CPC} = 0.2 \text{ mol kg}^{-1}$ ,  $j = 500 \text{ A m}^{-2}$  and  $\omega = 100 \text{ s}^{-1}$ .

Addition of  $0.3 \text{ mol kg}^{-1}$  CTAC to a  $\phi_{PS} = 0.02$  suspension yields a network of needle-like crystallites with a diameter smaller than  $1 \mu\text{m}$  (Figure 6.9). The deposit is smooth and slightly shiny, but darker than in the absence of surfactant. Surprisingly, a large number of particles can be seen on the deposit surface. In section 6.3.2 it was found that PS codeposition is negligible under these conditions (Figure 6.3). At CTAC concentrations around  $0.02 \text{ mol kg}^{-1}$

---

6. *Effect of surfactants on the electrochemical codeposition of zinc and polystyrene particles*

---

striated deposits are produced. A pattern of ridges separated by valleys appears as alternating dark grey and light grey bands concentric with the cylindrical electrode. The changes in appearance on addition of CTAB, SDS and NPE1800 are similar to that on CTAC addition.

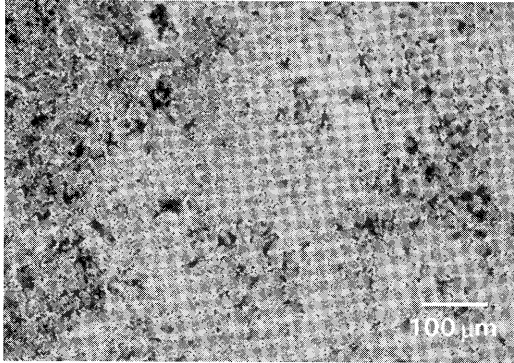


Figure 6.11: SEM photomicrographs of composite surface morphology;  $\phi_{PS} = 0.047$ ,  $\omega = 100$   $s^{-1}$  and  $c^*_{CPC} = 0.02$   $mol\ kg^{-1}$ ;  $j = 500$   $A\ m^{-2}$ .

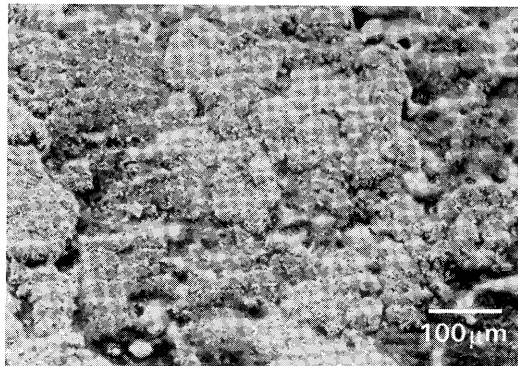


Figure 6.12: SEM photomicrograph of composite surface morphology;  $\phi_{PS} = 0.054$ ,  $\omega = 100$   $s^{-1}$  and  $c^*_{CPC} = 0.02$   $mol\ kg^{-1}$ ;  $j = 50$   $A\ m^{-2}$ .

Composites deposited on a RCE from a  $\phi_{PS} = 0.047$  suspension containing  $0.2 \text{ mol kg}^{-1}$  CPC also shows nodular growth (Figure 6.10) at  $j = 500 \text{ A m}^{-2}$ . The same suspension containing  $0.02 \text{ mol kg}^{-1}$  in contrast exhibits a morphology and appearance comparable to that obtained from the particle-free and surfactant-free electrolyte (Figure 6.11). At lower current density,  $j = 50 \text{ A m}^{-2}$ , a so-called mossy zinc deposit is obtained (Figure 6.12). Mossy deposits consists of spongy nodules made up of very small zinc crystallites and are characteristic for zinc deposited at low current densities [16,19]. In between the nodules PS particle agglomerates are present. Note that under these conditions PS particles codeposition is very high (Figure 6.5).

## **6.4 Discussion**

Several mechanisms and models to describe electrochemical codeposition of particles in a metal matrix were discussed in chapter 2. It was concluded that the mechanism can be generalized to a two step-process, that is transfer of the particles from the bulk to the electrode surface and a particle-electrode interaction leading to particle incorporation [12,13,20]. The exact nature of the particle-electrode is the main point of discussion. The model proposed by Fransaer [12,13] is the most advanced and will be used to discuss the incorporation of polystyrene particles in zinc. A quantitative description of polystyrene incorporation in zinc using this model will not be given. This would require adaptation of the model to the RCE geometry, which is much more complex than the RDE geometry used by Fransaer, due to the turbulent flow conditions. Further complications arise from the aggregation of the polystyrene particles. The older models are not suited to quantitatively describe zinc-polystyrene codeposition, because of their limited validity. For example, the field-assisted Langmuir type adsorption mechanism proposed by Guglielmi [14] can only partly describe the  $\alpha$  against  $\phi$  relation (section 6.3.3), whereas the peaks in Figure 6.5 can not be explained at all (section 2.4.1). Moreover, the fit parameters in these models can not be determined accurately due to the relatively large experimental error.

The practically constant codeposition over a wide range of current densities implies that the particle-electrode interaction is rate-determining in the PS codeposition with zinc. In the presence of  $0.2 \text{ mol kg}^{-1}$  CPC this explanation is supported by the negligible effect of the electrode

rotation speed on codeposition. In the model of Fransaer [12,13] the particle-electrode interaction is described by a force balance on a particle at the electrode surface (Figure 6.13). Forces tending to remove particles from the electrode,  $F_d$ , are counteracted by a friction force,  $F_f$ , which results from forces responsible for particle adhesion,  $F_a$ . The change in PS codeposition with  $\phi_{PS}$  according to a Langmuir adsorption isotherm indicates that the particle adhesion is a simple adsorption process.

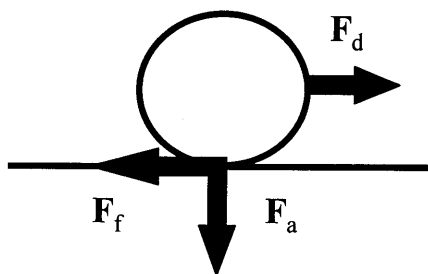


Figure 6.13: Force balance on particle adsorbed on the electrode;  $F_f$  is the friction force,  $F_a$  is the adhesion force and  $F_d$  is the removal force [12].

The particle-electrode interaction forces are the same as the particle-particle interaction forces used in chapter 5. It then follows from the DLVO theory that one of the adhesion forces is the electro-osmotic force, which is related to the charge of the particles and the electrode. As described in section 2.3.5 adsorption of ionic surfactants on particles is therefore expected to affect particle codeposition. [1-3]. It is obvious that this effect is optimal at the concentration, where surfactant adsorption on the particles is maximal. However, no change in codeposition with any of the surfactants at concentrations lower than the concentration at maximum adsorption was observed. Moreover, particle incorporation should be minimal at the surfactant concentration, where the particle charge is completely compensated for by adsorbed surfactant. From Figure 6.2 and 6.3 and the value reported for  $c_{a,dis}^*$  in Table 6.1 it is clear that this is not the case.

In Chapter 5 it was already found that the electro-osmotic force acting between particles is negligible in the zinc deposition electrolyte even in the presence of  $0.4 \text{ mol kg}^{-1}$  surfactant. Shielding of the charge of the surfactant molecules adsorbed onto the PS particles by the electrolyte ions cancels the electro-osmotic force. It can be concluded that even in the presence of surfactants the electro-osmotic force does not affect PS codeposition. This confirms the conclusion of Franssaer that the particle charge has negligible effect on particle adhesion to the electrode. The absence of aggregates in the presence of SDS (Chapter 5) suggest that here electro-osmotic repulsion may be significant and responsible for the reduction of PS codeposition on SDS addition.

Surprisingly, at higher concentrations the surfactants do affect PS codeposition. The increase in suspension stability going from  $0.02$  to  $0.2 \text{ mol kg}^{-1}$  CPC suggests that additional adsorption occurs. Additional adsorption of cationic surfactants on PS particles above the c.m.c. has been observed in electrolytes [10]. The extent of the extra adsorption is quite small and can not explain the difference in behaviour between CPC on the one hand and CTAC and CTAB on the other hand. Furthermore, influence of the counterion of the surfactant can be excluded, because CTAC behaves different from CPC. Above  $0.02 \text{ mol kg}^{-1}$  the free surfactant concentration becomes significant as exemplified by changes in the appearance and morphology of the composites. Therefore, it seems likely that the effect of the surfactants on the PS codeposition is caused by the free surfactant.

Electrochemical investigations on the adsorption of CTAB and CPC on mercury show that CPC is electrochemical reducible at potentials more negative than  $-0.71 \text{ V vs. SHE}$  [21,22]. Since the equilibrium potential of the  $\text{Zn}^{2+} / \text{Zn}$  couple is  $-0.76 \text{ V vs. SHE}$  [23], reduction of CPC, adsorbed on the cathode, can occur during Zn deposition. CPC reduces to a dimeric species, which remains adsorbed onto the electrode [22,24]. This explains the organic material observed on the electrodes. The dimeric species will be the sites where PS particles strongly adsorb, resulting in enhanced PS codeposition. Moreover it is possible that the dimeric species are formed from a monomer adsorbed on the zinc electrode and another monomer adsorbed on the PS particles. The decrease in PS codeposition with increasing concentration found for other surfactants could then be explained by adsorption of free surfactant on the growing Zn layers, which blocks PS particle attachment.



Alternatively, the change in growth behaviour of zinc, due to the change in the free surfactant concentration, is responsible for the differences in PS codeposition. The effect of CPC on the surface morphology and codeposition is very different from the other surfactants, which have a similar effect. Changes in deposit appearance and surface morphology correlate with changes in PS codeposition. Figure 6.14 shows a generalized picture of the main types of growth morphologies which can be encountered for zinc deposition [17,18]. Zinc deposits as hexagonal platelets, which are oriented at different angles to the substrate depending on the plating conditions. At intermediate current densities the platelets are stacked at random angles to the substrate as observed for deposition from a particle-free electrolyte (Figure 6.7). At high current densities a vertical type of deposit is formed where the platelets make an angle of  $90^\circ$  with the electrode surface. A basal type of deposit characterised by the platelets lying parallel to the electrode surface is formed at low current densities.

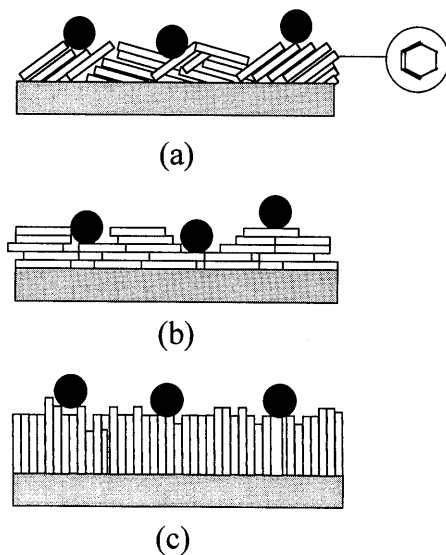


Figure 6.14: Growth morphologies of zinc deposits; (a) intermediate type, (b) basal type, (c) vertical type [17]; Black spots represent particles.

---

A basal type of deposit is also obtained in the presence of impurities like Co, Ni and Sb, which deposit in between the stacks of platelets resulting a nodular structure [17,18,25,26]. Figure 6.8 and 6.10 show such a morphology in the presence of high concentrations CPC. The dimeric product of CPC reduction also deposits in between the nodules. Addition of organics, like glue, changes the morphology to the vertical type [17,18,25,26]. Comparison of Figure 6.9 with 6.14 shows that CTAC has a similar effect on the composite deposits, although the platelets are changed into needle-like crystallites. In the presence of PS particles and up to  $c^*_{\text{surf}} = 0.02 \text{ mol kg}^{-1}$  the intermediate type of growth is observed (Figure 6.11).

It is obvious that there is a difference in surface roughness between the different morphology types. For example, the vertical type morphology yields smooth deposits. The friction force, which prevents a particle from being removed from the surface before being incorporated depends on the local surface roughness around the particle. Particles are depicted in Figure 6.14 to show how they can be adsorbed onto the deposit. A particle adsorbed in a recessed area has a much larger probability of becoming included than one adsorbed on a flat surface. Particularly if particles are able to move along the surface due to shearing forces or Brownian rotation to recessed areas, a rough surface leads to higher amounts of embedded particles. Comparing the roughness associated with the growth morphologies of zinc particle incorporation will decrease in the order: basal, intermediate and vertical type. Correspondingly PS codeposition is the largest at high concentrations of CPC, the lowest with high concentrations of CTAC or the other surfactants and in between for suspensions containing up to  $0.02 \text{ mol kg}^{-1}$  surfactant.

A similar reasoning could explain the peaks at low current density in the  $\alpha_{\text{PS}}$  against  $j$  curves (Figure 6.5). A deposit consisting of mossy nodules was found at the peak in the presence of  $0.02 \text{ mol kg}^{-1}$  CPC (Figure 6.12). Similar to composites prepared at high CPC concentrations this is a basal type of morphology, where particles deposit in between nodules. Consequently increased codeposition compared to the intermediate type of morphology obtained at higher current densities is expected [17]. For Au- $\text{Al}_2\text{O}_3$  codeposition Buelens [27] reported an equivalent correlation between the orientation of Au crystallites and peaks with current density. Moreover, these peaks in  $\text{Al}_2\text{O}_3$  codeposition occur at the same current density as kinks in the Au polarisation curve. In fact, it has often been reported that a peak in codeposition is associated with a kink in the polarisation curve [12,13,28,29]. Similarly, the peaks in PS codeposition

---

appear around the current density, where Wiart et. al. [15,16] found a 'S'-type kink in galvanostatic polarisation curves for Zn deposition from acidic ZnSO<sub>4</sub> electrolyte. Here the morphology changes from the mossy basal type to the compact intermediate type.

The changes in  $\alpha_{PS}$  with  $\omega$  affirm that hydrodynamics have to be considered too. The shear field due to the electrode rotation exerts a force on particles at the electrode surface [13,20]. If this force becomes larger than the friction force, particles will be swept away from the electrode surface. Due to surface heterogeneity this condition will not be reached by all adsorbed particles at the same shear rate [20]. At high rotation speeds the rate of PS particle removal becomes larger than that of attachment at certain sites on the electrode. As a result PS codeposition in the presence of 0.2 mol kg<sup>-1</sup> CPC is reduced at  $\omega > 225$  s<sup>-1</sup> (Figure 6.6).

In aggregated suspensions, that is without surfactant or with 0.02 mol kg<sup>-1</sup> CPC, the effect of  $\omega$  on PS codeposition is more complex. Apart from aggregate removal, changes in aggregate size with shear rate play a role. Generally, the size of aggregates decreases with shear rate, which varies with position in the gap between RCE and wall [30]. If it is assumed that smaller aggregates codeposit more readily than larger ones, the increase in PS codeposition with  $\omega$  can be understood. Though it should be noted that reports on the effect of particle size on codeposition show exactly the opposite behaviour [31]. Preferential codeposition can also take place [32,33]. In suspensions of polydisperse particles, such as aggregated PS suspensions, only particles smaller than a certain size are able to codeposit. A reduction in the average aggregate size with shear rate results in a larger fraction of particles that are able to codeposit. In the absence of surfactant the situation is further complicated by thixotropy, which was found during rheological measurements (Chapter 5). The time necessary to reach a steady state between aggregate break up and formation, after the changes in shear rate explains the dependence of PS codeposition on the experimental sequence.

Also the enhanced codeposition at  $\phi_{PS} > 0.035$  when  $c^*_{CPC} = 0.2$  mol kg<sup>-1</sup> as compared to the extrapolated Langmuir behaviour at lower  $\phi_{PS}$  could be due to hydrodynamic effects. Fransaer [12,13] observes a similar increase in PS codeposition with Cu at higher amounts of suspended particles. This is explained by hydrodynamic interactions of suspended particles with other either suspended or adsorbed particles. In adsorption theory additional adsorption at higher

adsorbate concentration is usually attributed to a second adsorption process [34]. At  $\phi_{PS} > 0.035$  PS particles could adsorb on top of particles already adsorbed at the electrode surface or onto less active electrode surface sites. For example incorporation of PS particles in zinc and in the CPC reaction product could take place simultaneously. The latter would be similar to electropainting processes where pigment particles are included in a depositing organic polymer [35].

## **6.5 Conclusions**

It was shown that polystyrene particles codeposit with zinc in volume fraction as large as 0.4 under turbulent flow conditions. Up to current densities of  $8 \text{ kA m}^{-2}$  composites containing an appreciable amount of PS particles can be obtained. In contrast to expectation cationic surfactants do not have a beneficial effect on PS codeposition. In fact with the exception of CPC all surfactants strongly diminish codeposition at high concentrations. CPC does enhance codeposition, but this is related to its reduction at the cathode and subsequent deposition on the growing zinc layer. Unfortunately, the deposit quality is strongly reduced in the presence of CPC.

The effect of most parameters can be explained by assuming that PS codeposition with zinc is governed by the interaction between particles and the electrode. Competition between particle adhesion through Langmuir type adsorption and particle removal governs PS codeposition. There is a correlation between changes in deposit morphology and PS codeposition. Differences in particle removal and adherence for different deposit morphologies could play a role in the effect of surfactants on codeposition. In aggregated suspensions, changes in aggregate size with hydrodynamics strongly affect codeposition.

## **References**

- [1] K. Helle, Report AKZO Research, Arnhem (1993).
- [2] K. Helle, Proceedings, 4th International Conference in Organic Coating Science and Technology, Athens (1978) 264.
- [3] P.K.N. Bartlett, Industrial training report AKZO, Arnhem (1980) p. 10-39.
- [4] D.R. Gabe, *J. Appl. Electrochem.* **13** (1983) 3.

- [5] S.H. Maron, M.E. Elder and M.E. Ulevitch, *J. Colloid Interface Sci.* **9** (1954) 89.
- [6] S.H. Maron, M.E. Elder and M.E. Ulevitch, *J. Colloid Interface Sci.* **9** (1954) 104.
- [7] K.J. Abbey, J.R. Erickson and R.J. Seidewand, *J. Colloid Interface Sci.* **66** (1978) 203.
- [8] P. Conner and R.H. Ottewill, *J. Colloid Interface Sci.* **37** (1971) 642.
- [9] G. Tuin and H.N. Stein, *Langmuir* **10** (1994) 1054.
- [10] J. Zhao and W. Brown, *Langmuir* **11** (1995) 2944.
- [11] A. van den Boomgaard, PhD thesis, Agricultural University of Wageningen (1985).
- [12] J. Fransaer, J.P. Celis and J.R. Roos, *J. Electrochem. Soc.* **139** (1992) 413.
- [13] J. Fransaer, Phd Thesis, Catholic University of Leuven (1994).
- [14] N. Guglielmi, *J. Electrochem. Soc.* **119** (1972) 1009.
- [15] I. Epelboin, M. Ksouri and R. Wiaart, *J. Electrochem. Soc.* **122** (1975) 1206.
- [16] J. Bressan and R. Wiaart, *J. Appl. Electrochem.* **9** (1979) 43.
- [17] R.C. Kerby, in 'Application of polarization measurements in the control of metal deposition', Process metallurgy 3, (edited by I.H. Warren), Elsevier Science Publishers B.V., Amsterdam (1984) p.111.
- [18] D.J. MacKinnon, J.M. Brannen and P.L. Fenn, *J. Appl. Electrochem.* **17** (1987) 1129.
- [19] J.N. Jovičević, D.M. Dražić and A.R. Despić, *Electrochim. Acta* **22** (1977) 589.
- [20] Z. Adamczyk, *Colloids and Surfaces* **35** (1989) 283.
- [21] A. Pappa-Lousi, P. Nikitas and Ph. Andonoglou, *Electrochim. Acta* **39** (1994) 375.
- [22] P. Nikitas, A. Pappa-Lousi and S. Antoniou, *J. Electroanal. Chem.* **367** (1994) 239.
- [23] 'Encyclopedia of Electrochemistry of the elements', Vol V, ed. A.J. Bard, Marcel Dekker Inc., New York (1982) p. 1.
- [24] L.N. Nekrasov, H. Almualla, T.N. Khomchenko, Yu.D. Smirnov and A.P. Tomilov, *Russ. J. Electrochem.* **30** (1994) 73.
- [25] D.J. MacKinnon and J.M. Brannen, *J. Appl. Electrochem.* **7** (1977) 451.
- [26] R. Sato, *J. Electrochem. Soc.* **106** (1959) 206.
- [27] C. Buelens, Phd Thesis, Catholic University of Leuven (1984) p.169-183.
- [28] P.R. Webb and N.L. Robertson, *J. Electrochem. Soc.* **141** (1994) 669.
- [29] C. Buelens, J.P. Celis and J.R. Roos, *J. Appl. Electrochem.* **13** (1983) 541.

- [30] 'Coagulation and Flocculation', Surfactant Science Series 47, ed. B. Dobiáš, Marcel Dekker Inc, New York (1993) .
- [31] G. Maurin and A. Lavanant, *J. Appl. Electrochem.* **25** (1995) 1113.
- [32] O. Berkh, S. Eskin, S. Berner and A. Zahavi, *Plat. Surf. Finish.* **82** (1995) 55.
- [33] B. Bozzini, G. Giovannelli, L. Nobili and P.L. Cavallotti, *AIFM Galvanotecnica e Nuove Finiture* **5** (1995) 92.
- [34] C.H. Giles and D. Smith, *J. Colloid Interface Sci.* **47** (1974) 755.
- [35] B.A. Cooke, N.M. Ness and A.L.L. Palluel, in 'Industrial Electrochemical processes', (edited by A.T. Kuhn), Elsevier Publishing Company, Amsterdam (1971) p. 417-465.

---

## List of symbols

A	constant in Tafel equation for metal deposition ( $V^{-1}$ )
B, B <sub>1</sub> , B <sub>2</sub>	constant in Tafel equation for particle deposition ( $V^{-1}$ )
<b>B</b>	maximum induction (T)
c <sub>i</sub>	concentration of species i ( $\text{mol m}^{-3}$ )
c* <sub>i</sub>	amount of surfactant i per unit weight of particles ( $\text{mol kg}^{-1}$ )
C*	number of ions or particles per unit volume in the bulk bath ( $\text{m}^{-3}$ )
Co	dimensionless constant (-)
C <sub>z</sub> <sup>x</sup>	binomial constant (-)
d	thickness (m)
D <sub>i</sub>	diffusion coefficient of species i ( $\text{m}^2 \text{s}^{-1}$ )
Dm	double layer dimensionless number
E	electrode potential (V)
f	frequency ( $\text{s}^{-1}$ )
F	Faraday constant ( $\text{C mol}^{-1}$ )
<b>F</b>	force (N)
g	acceleration due to gravity constant ( $\text{m s}^{-2}$ )
Gq	particle incorporation dimensionless number (-)
H	hydrodynamic coefficient (-)
j	current density ( $\text{A m}^{-2}$ )
j <sub>0</sub>	exchange current density ( $\text{A m}^{-2}$ )
j <sub>L,i</sub>	limiting current density of species i ( $\text{A m}^{-2}$ )
j <sub>m</sub>	modified current density, $j / (1 - \exp(\alpha n F   \eta   / RT))$ ( $\text{A m}^{-2}$ )
j <sub>tr</sub>	transition current density ( $\text{A m}^{-2}$ )
k	Langmuir adsorption constant (-)
k <sub>1</sub> , k <sub>2</sub> , k <sub>3</sub>	rate constants for particle deposition ( $\text{m}^4 \text{mol}^{-1} \text{s}^{-1}$ )
m	weight (kg)

---

M	molecular weight ( $\text{kg mol}^{-1}$ )
n	number of electrons transferred for the oxidation or reduction of an ion (-)
N	flux of ions or particles crossing the diffusion layer ( $\text{m}^{-2} \text{s}^{-1}$ )
P	particle incorporation probability (-)
$P_j$	probability for an ion to be reduced at current density $j$ (-)
$P_\phi$	exponent to $\omega$ for particle volume fraction $\phi$ (-)
q	charge (C)
Re	Reynolds number (-)
R	gas constant ( $\text{J K}^{-1} \text{mol}^{-1}$ )
$R_\Omega$	ohmic resistance ( $\Omega$ )
r	radius (m)
$Sh'$	modified Sherwood number (-)
$S_x$	dimensionless number for particle bath concentration (-)
T	temperature (K)
V	deposition rate ( $\text{m s}^{-1}$ )
v	particle settling speed ( $\text{m s}^{-1}$ )
$v_0$	constant for particle deposition ( $\text{m s}^{-1}$ )
$W_p$	particle weight (kg)
X	amount of ions adsorbed on a particle (-)
x	amount of ions adsorbed on a particle that need to be reduced (-)
$Z_{Re}$	real part of electrode impedance ( $\Omega$ )

*Greek letters*

$\alpha$	volume fraction of incorporated material (-)
$\alpha_T$	cathodic transfer coefficient (-)
$\beta$	mass fraction of incorporated material (-)
$\gamma$	surface tension ( $\text{N m}^{-1}$ )
$\dot{\gamma}$	shear rate ( $\text{s}^{-1}$ )



$\delta$	diffusion layer thickness (m)
$\phi$	volume fraction of suspended particles (-)
$\phi_m$	maximum volume fraction of suspended particles (-)
$\Gamma$	current efficiency (-)
$\eta$	overpotential (V)
$\kappa$	conductivity ( $\text{S m}^{-1}$ )
$\lambda$	measure of interaction between free and adsorbed ions due to current density (-)
$\mu$	viscosity (Pa s)
$\mu_\infty$	viscosity at infinite shear rate (Pa s)
$[\mu]$	intrinsic viscosity (-)
$\Pi$	dimensionless parameter (-)
$\theta$	strong adsorption coverage (-)
$\rho$	density ( $\text{kg m}^{-3}$ )
$\sigma$	loose adsorption coverage (-)
$\tau$	shear stress (Pa)
$\tau_0$	yield stress (Pa)
$\omega$	angular velocity of rotating electrode ( $\text{s}^{-1}$ )

*Subscripts*

a	adsorbed
c	continuous phase
d	detachment
dis	discontinuity
f	friction
M	metal
p	particle
r	reduced
s	suspension

---

*Electrochemical deposition of metal matrix composites*

---

surf	surfactant
-	cathodic
+	anodic

*Superscripts*

b	bulk
s	surface

## Summary

When inert particles are suspended in a metal plating electrolyte these particles are incorporated in the growing metal layer during deposition. This way composites consisting of a dispersion of particles in a metal matrix can be prepared. These composites exhibit unique properties compared to metal deposits. On the basis of two possible applications electrochemical composite deposition was investigated. Homogenized composites of silicon particles in iron, that is silicon-rich iron foil, could be used as transformer sheet. Furthermore, there is an interest in producing metal-polymer composites on industrial scale.

The production of silicon-rich iron foil requires homogenization of the electrochemically prepared iron-silicon composites by a heat-treatment. Here the use of iron silicide particles instead of silicon particles could be advantageous. Composites of silicon particles and different iron silicide particles in iron were heated at various temperature. Iron and silicon interdiffuse during the heat-treatment, but the composites are not homogenized to the desired alloy. The formation of voids during composite deposition and during heat-treatment impede fast and unobstructed interdiffusion. Practically no differences between silicon particles or iron silicide particles can be seen.

Suspended particles can have strong effects on metal deposition, which are correlated to changes in the concentration of incorporated particles. In order to obtain a better understanding of these correlations, some physical and electrochemical properties of the iron deposition electrolyte in the presence of suspended silicon particles were investigated. A suspension of silicon particles in iron deposition electrolyte behaves as an aggregate-free suspension of anisotropic non-conducting particles. The particles slightly increase iron(III) ion mass transfer to the cathode. Furthermore, the particles enhance iron deposition resulting in a higher current efficiency and a depolarization for iron deposition. These effects are related to the amount of suspended and to the amount of incorporated particles.

As model system for the electrochemical deposition of metal-polymer composites the incorporation of polystyrene particles in zinc was investigated. Industrial application of

electrochemical composite plating requires an aggregate-free suspension, from which composites can be deposited at high current densities and under turbulent flow conditions. A rotating cylinder electrode was used to obtain turbulent flow conditions. Rheological measurements on suspension of polystyrene particles in zinc deposition electrolyte show that the particles strongly aggregate. Therefore it was decided to use cetylpyridinium chloride (CPC), a cationic surfactant, to stabilize the suspension. A cationic surfactant is preferred, because it could create an additional attraction between the particles and the cathode.

Incorporation measurements show that the incorporation of polystyrene particles in zinc is high both in the presence and absence of CPC. At high concentrations CPC strongly enhances polystyrene incorporation. The current density and flow conditions hardly affect the amount of incorporated polystyrene. It can be concluded that the incorporation of polystyrene particles in zinc is governed by the competition between particle adsorption on the electrode surface and particle removal from the electrode surface due to solution flow. In contrast to expectation all other surfactants strongly reduce polystyrene incorporation. The beneficial effect of CPC is not related to its positive charge, but to the electrochemical reduction of CPC at the cathode. It seems that the changes in morphology of the zinc deposit, due to the surfactants, are responsible for the differences in polystyrene incorporation.

## Samenvatting

Als in een metaaldepositie-elektrolyt inerte deeltjes gesuspenderd zijn dan worden deze deeltjes tijdens de depositie ingebouwd in de groeiende metaallaag. Op deze manier kunnen composieten bestaande uit een dispersie van deeltjes in een metaalmatrix bereid worden. Deze composieten hebben bijzondere eigenschappen in vergelijking met metaaldeposieten. Aan de hand van twee mogelijke toepassingen is de elektrochemische composietdepositie onderzocht. Gehomogeniseerde composieten van siliciumdeeltjes in ijzer, siliciumrijk ijzerfolie, kunnen gebruikt worden als transformatorplaat. Daarnaast bestaat er interesse om metaal-polymeer composieten te produceren op industriële schaal.

Om siliciumrijk ijzerfolie te maken moeten elektrochemisch bereide ijzer-siliciumcomposieten gehomogeniseerd worden door een warmtebehandeling. Hierbij zou het gebruik van ijzersilicide deeltjes in plaats van siliciumdeeltjes voordelen kunnen hebben. Composieten van siliciumdeeltjes en verschillende ijzersilicidedeeltjes in ijzer zijn verhit bij verschillende temperaturen. IJzer en silicium interdiffunderen gedurende deze warmtebehandeling, maar de composieten worden niet gehomogeniseerd tot de gewenste legering. De vorming van gaten tijdens composietdepositie en tijdens de warmtebehandeling bemoeilijken snelle ongehinderde interdiffusie. Het maakt vrijwel geen verschil of siliciumdeeltjes of ijzersilicidedeeltjes zijn ingebouwd.

Gesuspenderde deeltjes kunnen grote effecten hebben op de metaaldepositie, die correleren met veranderingen in de concentratie ingebouwde deeltjes. Om meer inzicht te krijgen in deze correlaties zijn enkele fysische en elektrochemische eigenschappen van het ijzerdepositie-elektrolyt in de aanwezigheid van gesuspenderde siliciumdeeltjes onderzocht. Een suspensie van siliciumdeeltjes in ijzerdepositie-elektrolyt gedraagt zich als een aggregaatvrije suspensie van anisotrope niet-geleidende deeltjes. De deeltjes verhogen in geringe mate het massatransport van ijzer(III)ionen naar de kathode. Daarnaast versnellen de deeltjes de ijzerdepositie, wat leidt tot een groter stroomrendement en een depolarisatie voor ijzerdepositie. Deze effecten zijn gerelateerd aan de hoeveelheid gesuspenderde en niet aan de hoeveelheid ingebouwde deeltjes.

Als modelsysteem voor de elektrochemische depositie van metaal-polymeercomposieten is de inbouw van polystyreendeeltjes in zink onderzocht. Industriële toepassing van elektrochemische composietdepositie vereist een aggregaadvrije suspensie, waaruit bij hoge stroomdichtheden en onder turbulente stromingsomstandigheden composieten kunnen worden neergeslagen. Om de turbulente stromingsomstandigheden te verkrijgen is een roterende cilinder elektrode gebruikt. Reologische metingen aan suspensies van polystyreendeeltjes in zinkdepositie-elektrolyt wijzen uit dat de deeltjes sterk aggregeren. Daarom is er voor gekozen om cetylpyrrolidinium chloride (CPC), een kationische oppervlakte-actieve stof, te gebruiken om de suspensie te stabiliseren. Een kationische oppervlakte-actieve stof geniet de voorkeur, omdat deze een extra aantrekking tussen de deeltjes en kathode zou kunnen geven.

Inbouwmetingen laten zien dat de inbouw van polystyreendeeltjes in zink hoog is zowel in de aanwezigheid als afwezigheid van CPC. In hoge concentraties verhoogt CPC de polystyreeninbouw sterk. De stroomdichtheid en de stromingsomstandigheden hebben nauwelijks invloed op de hoeveelheid ingebouwd polystyreen. Hieruit kan geconcludeerd worden dat de inbouw van polystyreendeeltjes in zink bepaald wordt door de competitie tussen deeltjesadsorptie aan het elektrode-oppervlak en deeltjesverwijdering van het elektrode-oppervlak door de vloeistofstroming. In tegenstelling tot de verwachtingen blijken alle andere oppervlakte-actieve stoffen de polystyreen inbouw sterk te verlagen. Het effect van CPC is daarom niet gerelateerd aan zijn positieve lading, maar aan de elektrochemische reductie van CPC aan de kathode. Het lijkt erop dat veranderingen in de morfologie van het zinkdepositiet door de oppervlakte-actieve stoffen de verschillen in polystyreeninbouw veroorzaken.

## **Curriculum Vitae**

De schrijver van dit proefschrift werd op 30 januari 1969 geboren te Zevenaar. In mei 1987 behaalde hij het Atheneum diploma aan de Gemeentelijke Scholen Gemeenschap Doetinchem. In september van dat jaar begon hij de studie Scheikunde aan de Katholieke Universiteit Nijmegen, waarvan het propedeutisch examen werd behaald in Juni 1988. In de vakgroep Vaste Stof Chemie verrichtte hij zijn afstudeeronderzoek naar de groei van (in)commensurabel gemoduleerde calaveriet- en sylvanietkristallen. Na een onderzoeksstage op het gebied van lage temperatuur Röntgendiffractie aan de Università degli Studi di Milano in Italië, werd in Augustus 1993 het doctoraal examen afgelegd. Aansluitend begon hij als assistent in opleiding binnen de subgroep Elektrochemie van de vakgroep Instrumentele Analyse aan de Technische Universiteit Eindhoven. Onder leiding van dr. L.J.J. Janssen is een onderzoeksproject verricht, gefinancierd door Hoogovens B.V. IJmuiden. De resultaten van dit onderzoek zijn beschreven in dit proefschrift.



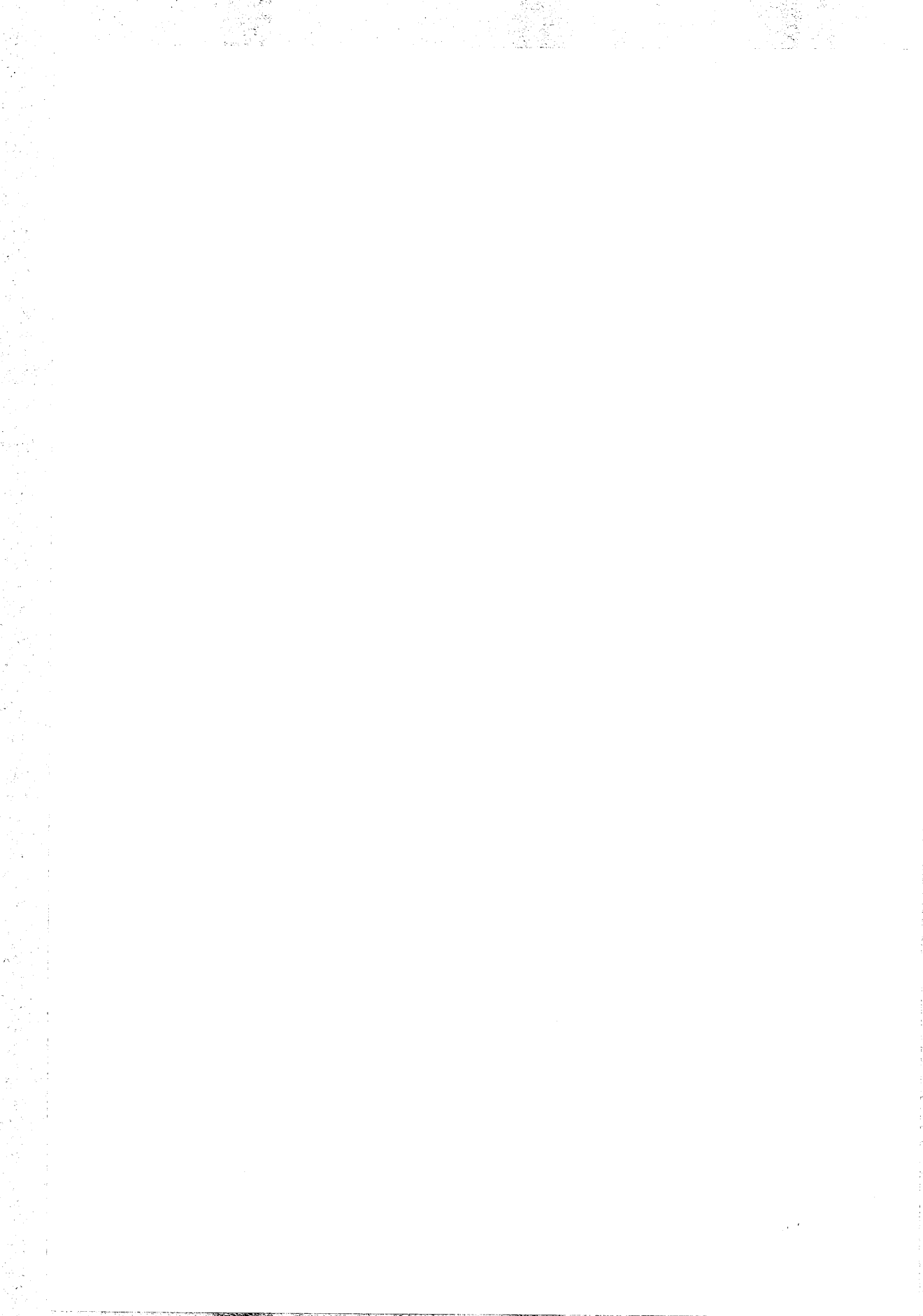


---

## Dankwoord

Graag wil ik iedereen bedanken, die op enige manier bijgedragen heeft aan de totstandkoming van dit proefschrift. Met name bedank ik Jos Janssen voor het in goede banen leiden van dit onderzoek zonder de nodige zelfstandigheid te beperken en Marlène Blijlevens voor haar onmisbare hulp bij het experimentele deel van het onderzoek. Verder is een belangrijk gedeelte van dit proefschrift mede het resultaat van het afstudeerwerk van Ruud Ansink en Ruud Heesen. Jacques Wijenberg en Henny Schram van Hoogovens R&D leverden een waardevolle bijdrage door de voortgangsbijeenkomsten, die altijd in een aangename sfeer verliepen. Medewerkers van de vakgroepen TCT en TVM ben ik erkentelijk voor hun hulp bij respectievelijk de colloïdchemische en de vastestofdiffusie experimenten. De discussies met Roland, Karoli en Ilja over mijn onderzoek, hun eigen onderzoek en elektrochemie in het algemeen waren erg nuttig. Zij en de overige medewerkers, TWAIO's, KIPen en afstudeerders van de subgroep elektrochemie zorgden voor een plezierige werksfeer. Tenslotte bedank ik mijn promotoren en de promotiecommissie.

---



STELLINGEN

behorende bij het proefschrift

**“Electrochemical deposition of metal matrix composites”**

van

Arjan Hovestad

**1**

Voor een goede mathematische beschrijving van composietdepositie moet gebruik gemaakt worden van de deeltjesflux en de aantalconcentratie deeltjes in plaats van de inbouwfractie en de volume- of gewichtconcentratie deeltjes.

(Z. Adamczyk, *Colloids and Surfaces* **35** (1989) 283)

**2**

In hun Ni-Al<sub>2</sub>O<sub>3</sub> codepositie-experimenten hadden Webb en Robertson rekening moeten houden met de aanwezigheid van oppervlakte-actieve stoffen in de nikkeldepositie-elektrolyt.

(P.R. Webb, N.L. Robertson, *J. Electrochem. Soc.* **141** (1994) 669)

**3**

Het opstellen van een voorspellende model voor de inbouw van deeltjes in metaallagen is onmogelijk zolang de groei van metaaldeposieten niet exact beschreven kan worden.

**4**

Het gebruik van de Bruggeman dan wel de Bruggemann vergelijking is een goede indicatie voor de aandacht, die een auteur aan zijn citaties besteedt.

(o.a. I. Roušar, K. Micka and A. Kimla, 'Electrochemical Engineering I Parts A-C', Elsevier Science, Amsterdam (1986) p.170 en 225)

**5**

Het opheffen van unieke en in eigen behoeften voorzienende onderzoeksgroepen op universiteiten is in strijd met zowel 'de ondernemende universiteit' als het 'HOOP' ter verbetering van het universitair onderwijs en onderzoek.

**6**

Het meer en meer uitbesteden van onderzoek door bedrijven aan universiteiten in de vorm van promotieprojecten leidt tegelijkertijd tot een toename van het aantal gepromoveerden en een afname van de behoefte aan gepromoveerden in de bedrijven.

**7**

Aangezien (universitair) onderwijs en sport fundamenteel andere uitgangspunten hebben dan commerciële ondernemingen, leidt een verre gaande commercialisering van beide onherroepelijk tot belangenconflicten.

**8**

Alle landen binnen de huidige EU zijn het er over eens, dat het verenigde Europa er net zo uit moet zien als het eigen land op dit moment.

**9**

Ondanks dat vaak het tegendeel wordt beweerd, behoort het Nederlands voetbal tot het sterkste van Europa en is dit vooral het gevolg van de overheersing door Ajax, Feyenoord en PSV in de competitie.

**10**

Het juist toepassen van de buitenspelregel in het voetbal is inherent onmogelijk, omdat de grensrechter of scheidsrechter naar twee of meer spelers tegelijk moet kijken.